Self-regulation and the stability of large ecological networks

György Barabás[1,2], Matthew J. Michalska-Smith[2], Stefano Allesina[2,3,4]

1: Division of Theoretical Biology, Dept. IFM, Linköping University, SE-58183 Linköping, Sweden

2: Dept. of Ecology & Evolution, University of Chicago, 1101 E. 57th Chicago, IL 60637, USA

3: Computation Institute, University of Chicago, 1101 E. 57th Chicago, IL 60637, USA

4: Northwestern Institute on Complex Systems, Northwestern University, Evanston, IL 60208, USA

Abstract

Stability of complex ecological networks depends both on the interactions between species and the direct effects of the species on themselves. These self-effects are known as "self-regulation" when an increase in a species' abundance decreases its per capita growth rate. Sources of self-regulation include intraspecific interference, cannibalism, time scale separation between consumers and their resources, spatial heterogeneity, and nonlinear functional responses coupling predators with their prey. The influence of self-regulation on network stability is understudied; worse, the empirical estimation of self-effects poses a formidable challenge. Here we show that empirical food web structures cannot be stabilized unless the majority of species exhibit substantially strong self-regulation. We also derive an analytic formula predicting the effect of self-regulation on network stability with high accuracy, and show that even for random networks, as well as networks with cascade structure, stability requires negative self-effects for a large proportion of species. These results suggest that the aforementioned potential mechanisms of self-regulation are likely more important in contributing to the stability of observed ecological networks than previously thought.

What keeps the exponential growth capacity of natural populations in check? Some regulatory mechanism is required, a feedback decreasing growth rates when abundance is high and increasing them when abundance is low. Common regulating factors include resource shortage, predation pressure, pathogen load, refuge availability, etc. Sometimes, however, the per capita growth rate of a species has a direct negative dependence on its own abundance—this is called "self-regulation"[1,2]. Self-regulation may be caused by direct mechanisms such as intraspecific interference or certain forms of cannibalism. Also, it is sometimes possible to eliminate from consumer-resource relationships the explicit dependence of the consumer on the resource (or vice versa) via a separation of time scales, leading to "effective" self-regulation, as was done by MacArthur in deriving the Lotka–Volterra equations from an underlying consumer-resource system[3]. Finally, immigration from outside sources and nonlinear functional responses coupling predators and prey can give rise to self-regulatory effects. The important commonality across all of these mechanisms is that they can cause per capita growth rates to directly depend on the abundance of the species in question.

How important is self-regulation in natural systems? To further specify what we mean by "important", in this work we will focus on the property of local asymptotic stability, i.e., whether

small perturbations of species' abundances away from an equilibrium point tend to be dampened, with the system returning to the equilibrium. Local asymptotic stability is assessed using the the community matrix (Jacobian evaluated at the equilibrium point)[4]. This matrix having its rightmost eigenvalue in the left half of the complex plane signals the stability of the system; otherwise the system is unstable. Self-regulatory effects appear in the community matrix as negative entries along its diagonal (Supplementary Information [SI], Section 1).

We ask what fraction of species in large ecological networks must exhibit self-regulation for the system to be (locally asymptotically) stable, and how strong this self-regulation must be. In two simple reference cases, the answer is known: first, a system completely devoid of any self-regulation cannot be stable; second, sufficiently strong simultaneous self-regulation of all species always leads to stability (SI, Section 1.2). The difficult question is whether stability can be achieved by something between these extremes. It is known that some ecological networks can be stabilized by just a single well-chosen self-regulating species[5]. However, such systems have especially simple topologies, and it is unclear whether empirical networks with more complex structure could be stabilized in the same way.

Views on this question differ strongly between ecologists: some believe most species must experience at least weak self-regulation at least some of the time[2,6,7], while others maintain that only primary producers and maybe top predators self-regulate to an appreciable degree[8–11]. To some extent, this disagreement is undoubtedly fueled by the unfortunate fact that the empirical study of self-regulation is a formidable challenge. While it is true that measuring a population's growth rate as a function of its abundance typically yields a negative relationship between the two[12], this will in general not be due to direct self-effects but rather to depletion of consumables, greater parasitic load at high abundance, or increased predation pressure[10]. Though disentangling causes is not impossible[13–16], it is still a difficult task from an empirical point of view.

For this reason, here instead we look at the importance of self-regulation by assessing its theoretical consequences, and seeing if they are consistent with certain broad empirical patterns. Since one such pattern is the relative stability of ecological communities at certain spatiotemporal scales, one can inquire what levels of self-regulation would be required to confer stability to large ecological communities.

Results

Self-regulation in empirical food webs

To answer the question of how common and how strong self-regulation must be to achieve stability, we analyzed empirical food webs. First, we used published parameterizations obtained by Jacquet et al.[17] using the Ecopath modeling framework[18] (Table 1). Since these have already been parameterized, they can be used out of the box. Their disadvantage is that they are highly aggregated networks, containing between 39 and 51 species. To see also what results one might obtain from more species-rich communities, we also parameterized 12 well-resolved food webs (see Methods) containing between 170 and 484 species (Table 2). The two approaches also make it possible to compare their results for consistency.

Initially, none of the webs and parameterizations included self-effects. For each web, we gradually increased the fraction of self-regulating species P from 0 to 1. For each P, the identities of the self-regulating species were randomly assigned 1000 times, and the fraction of cases which ended up stable was tallied. This procedure was then repeated for different strengths of self-regulation.

Name	Species	Links
Chesapeake Present[51]	41	167
Mid Atlantic Bight[50]	51	515
Moorea Barrier Reef[52]	39	267
Newfoundland Grand Banks (1900)[53]	48	519
Newfoundland Grand Banks (mid-1980s)[53]	48	519
Newfoundland Grand Banks (mid-1990s)[53]	48	525
Tampa Bay[54]	48	340

Table 1: Information on the seven largest Ecopath networks parameterized by Jacquet et al.[17], with each row corresponding to a different web. Columns indicate, respectively, the name of the web (with a reference for the source of the original data), its number of species and the number of links.

Name	Species	Links	Structural rank
Carpinteria Salt Marsh[55]	272	3878	197
Flensburg Fjord[46]	180	1567	128
Kongs Fjorden[56]	268	1632	164
Little Rock Lake[47]	181	2316	150
Lough Hyne[57]	349	5088	287
Otago Harbour[48]	180	1856	158
Punta Banda[55]	355	5291	234
Caribbean Reef[58]	249	3293	204
San Quintin[55]	289	3934	179
Serengeti[49]	170	585	54
Sylt Tidal Basin[59]	230	3298	215
Weddell Sea[60]	484	15435	448

Table 2: As Table 1, but for the twelve highly resolved empirical food webs. An additional column shows the structural rank[45] of each web (maximum possible rank the matrix of the web can attain assuming its nonzero entries are arbitrary).

For the Ecopath webs, at least 50% of species must exhibit substantially strong self-regulation if the community is to have a realistic chance of being stable (Figure 1**a**). Instead of just primary producers and top predators, it is in fact a majority of species that must self-regulate. This result is even stronger in the well-resolved food webs (Figure 1**b**). The qualitative pattern is the same as before, but there is a large quantitative difference: instead of over half, now over 90% of species must exhibit self-regulation for the network to be stable. This was true regardless of which particular well-resolved network we analyzed, or which particular parameterization we applied to them (SI, Section 7).

Although we have performed the analysis for several different values of the strength of self-regulation, one might wonder whether imposing extremely strong self-effects on just a few species could stabilize the networks. Our results yield a counterintuitive answer to this question: given a set of self-regulating species, the most stabilized configurations are not those with the strongest self-interactions, but those with intermediate ones (Figure 1). Beyond a point, increasing the strength of self-regulation actually destabilizes the system. Though this may seem strange at first, it can be
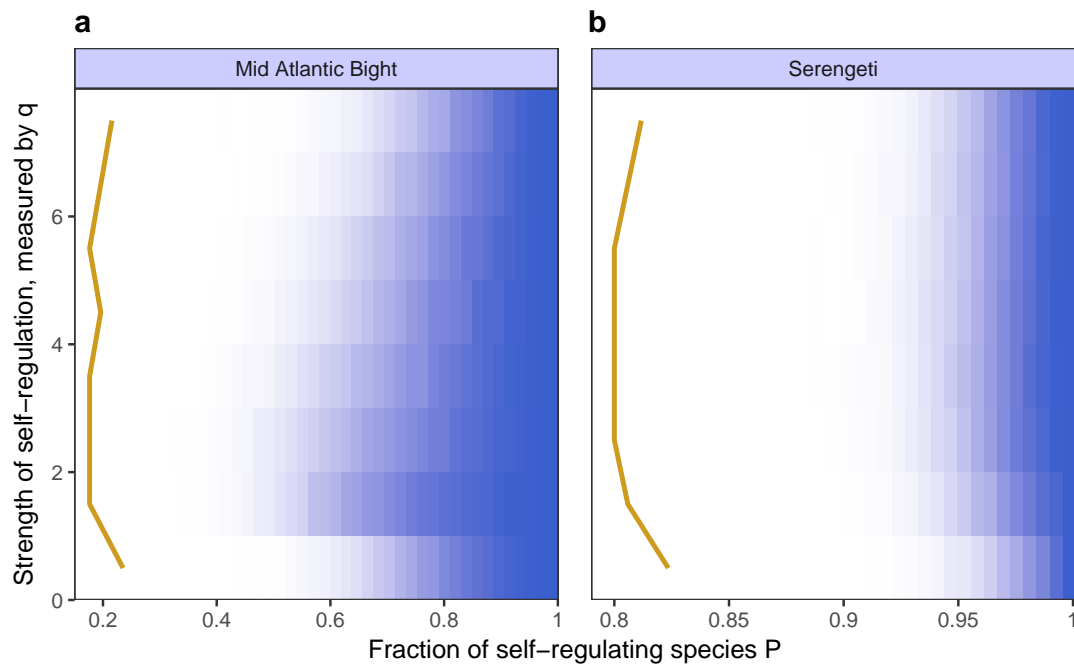
Figure 1: The fraction of self-regulating species required for stability, in (**a**) the Ecopath-modeled Mid-Atlantic Bight[50] web, and (**b**) the Serengeti[49] food web parameterized with $g = -0.95$ and no indirect effects (see Methods). Each grid of the heat-map represents the probability of stability given q and the fraction of self-regulating species P, ranging from white (0% chance of stability) to blue (100% chance). The yellow line is the lowest fraction of self-regulating species compatible with stability for the given strength of self-regulation, found using a stochastic search algorithm. Notice that the highest overall probability of stability is always obtained for an intermediate value of self-regulation strength.

understood by considering an example where all but one single species are self-regulating. Very weak self-effects will not be able to stabilize any system in the first place. On the other hand, for prohibitively strong self-regulation, the one single species without the burden of a negative self-effect has such an overwhelming advantage over all the others that it will drive them extinct. If the system is to be stable for at least some self-regulation strengths, it then must happen at intermediate ones (SI, Sections 2.4 and 5).

One could also ask whether, by choosing very carefully which particular species self-regulate, their fraction could be considerably lowered while still achieving stability. To test this, we searched for the minimal value of P compatible with local stability (Figure 1, yellow lines). This was done by choosing the identities of the self-regulating species to be the most conducive to stability via a stochastic search algorithm (SI, Section 7.4). As seen, P is indeed reduced this way, especially in the case of the Ecopath webs, where it drops to about 20-30% of the species. In the case of the well-resolved webs, P reduces only to about 80% of all species, which is still a large majority. That is, there is no way of targeting particular species with self-regulation which would alleviate the need for the majority of species to be self-regulated.

Moreover, contrary to ecological intuition, there is no obvious trophic pattern to the minimal set of self-regulating species: it is not true that primary producers or top predators are more likely to be included than species from other trophic levels. Instead, the self-regulating species are more or

less uniformly distributed across trophic levels. Additionally, it is impossible to stabilize any of the large networks by having only basal and top species self-regulate: by assigning self-regulation to all species within these two trophic groups only, the webs turned out unstable in all cases (SI, Section 7.7).

Theoretical analysis

Despite all the different empirical food webs and parameterizations considered above leading to the conclusion that the majority of species must be self-regulating, food web data is always incomplete no matter how well-resolved, and any finite set of parameterizations will fall short of the infinitely many possible ones. Furthermore, it is unclear whether food webs possess some peculiar structure which has lead us to find this result, or if they pertain to a much wider class of networks. To answer these questions, we conducted a theoretical analysis in two steps.

First, we considered random network ensembles such that the pairwise effects of species i on species j and that of of j on i are drawn from a bivariate distribution with given marginal means, marginal variances V, and correlation ρ [19–23]. Using a new result in the mathematical theory of such systems [24], we show that even a handful of species lacking self-regulation are sufficient to destabilize them (SI, Section 2). Moreover, we obtained an analytical formula for the distance of such networks from stability using the recently proposed quaternionic resolvent method [25] (SI, Sections 3-5). From this it turns out that just two relevant quantities determine the minimum fraction of self-regulating species P required for network stability: the correlation ρ, and the scaled strength of self-regulation $d/\sqrt{SV}$ where d is the self-regulation strength and S the number of species (Figure 2). The results show that local stability is unattainable without either the majority of species strongly self-regulating, or ρ being close to -1.

Second, real food webs have markedly nonrandom structure, and one may wonder if the above random network results are sensitive to incorporating realistic network topology. One well-known structural feature of real food webs is that they are close to a cascade pattern [26,27]: species may be ordered such that those lower in the hierarchy may be eaten by species higher up, but not vice versa ("big fish eat small fish"). Performing the analysis on such webs (SI, Sections 2.5 and 6), we find the following result: Figure 2 is still valid as long as one replaces the original ρ with a new effective correlation ρ_{eff}, and the original V with an effective variance V_{eff}. Both ρ_{eff} and V_{eff} can be straightforwardly calculated using the original data. Since our results are derived in the limit of a very large number of species, they are not well suited to analyzing the Ecopath webs, which had only between 39 and 51 species. However, our analytical formula does predict the stability of the well-resolved empirical networks with high accuracy (SI, Section 7.5). The accuracy is sufficiently high not to leave much room for improvement by including further structural properties of real food webs in the theoretical analysis. For instance, real food webs, apart from possessing an approximate cascade structure, are also close to being interval, and have broader degree distributions than expected by chance. Incorporating these other properties into a model is an unsolved theoretical problem—but, since the approximation is accurate even in their absence, doing so is not expected to yield any substantial improvement.

One question is where empirical systems tend to be located in the parameter space of Figure 2. Previous studies [17] suggest a slight but positive correlation between ρ and $\sqrt{SV}$, imposing a negative correlation between the two axes of the plot. It is not yet known whether a significant relationship is retained between ρ_{eff} and $\sqrt{SV_{\text{eff}}}$ though; furthermore, the empirical difficulty in determining d means we do not know where real-world communities lie exactly. However, we calculated the
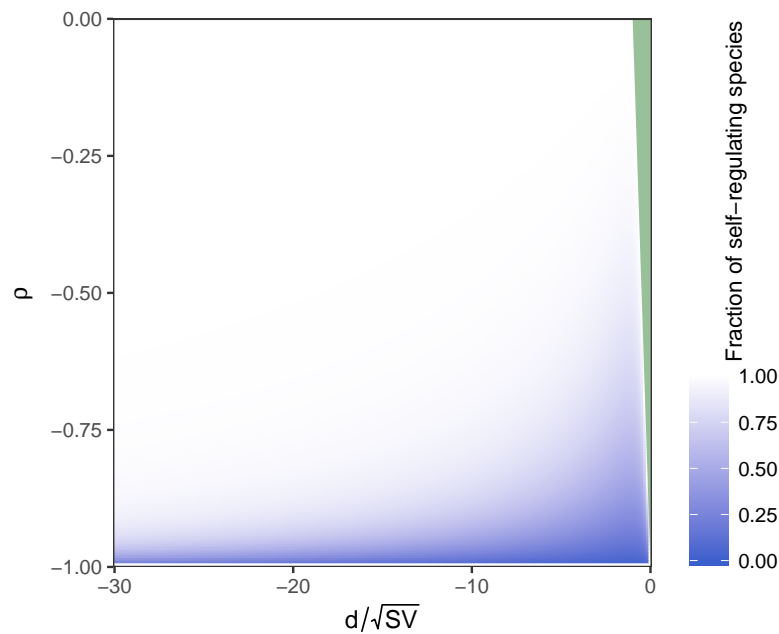
Figure 2: The minimum fraction of self-regulating species required for stability, as a function of the average pairwise correlation ρ and normalized self-regulation strength $d/\sqrt{SV}$ (where d is the raw strength of self-regulation, S is the number of species, and V is the variance of all interaction strengths excluding self-effects). In the green shaded region the system is unstable regardless of the value of P. This theoretical map may correspond either to elliptic random networks or networks with cascade structure (in which case the effective parameters ρ_{eff} and V_{eff} must be used instead of ρ and V; see SI, Section 6). Self-effects are sampled from a distribution equal to d with probability P and to zero with probability $1 - P$. Stability can only ever be achieved for $P \approx 1$, except for correlation values close to -1. Note that only negative values of ρ are shown, even though $-1 \leq \rho \leq 1$ in principle—this is because stability cannot ever be achieved for $\rho > 0$, except when P is strictly equal to 1.

effective correlation ρ_{eff} for all our food webs and parameterizations. Having done so, this quantity was never found to be lower than about -0.35. Then one can say, based on Figure 2, that a large fraction of species must self-regulate for stability, regardless of the particular value of $d/\sqrt{SV_{\text{eff}}}$. This is consistent with our results from analyzing the empirical webs.

Discussion

Our two main results are an analytical method for predicting the stability properties of large ecological networks with high accuracy, and the conclusion that local asymptotic stability cannot be achieved without the majority of the diagonal entries in the community matrix being strongly negative.

In light of this, it would seem that even the most ardent proponents of the "self-regulationist" view[2,6,7] have been overly cautious in assessing the prevalence of negative self-effects. Yodzis[2] concluded, based on an analysis of relatively low-resolution food webs, that "it appears that at least one-tenth and perhaps as much as one-half of the consumer species [in these communities] need to exhibit some degree of intraspecific interference if the equilibrium viewpoint is to apply".

Sterner et al.[6], after finding it difficult to stabilize small ecological networks without widespread self-regulation, state that "in the absence of sufficient data on the prevalence of self-damping in different trophic levels, it seems best to allow for self-damping in all trophic levels in community models"—with the fraction of species having to self-regulate at each level being left as an open question. The closest it comes to the results expounded here can be found in an almost off-hand remark by Moore and de Ruiter[7], who state that "arguably, most, if not all, populations are subject to intraspecific competition and self-regulation to some degree" (p. 36). Based on the results presented here, at least half and possibly more than 90% of species must be subject to self-regulation to a substantial degree.

It is important to emphasize what our results do *not* say. First, they do not imply that a large P means all species have an equally high probability of self-regulation. For instance, if all basal species self-regulate, then reaching the required fraction of self-regulating species is in principle possible with species at higher trophic levels having a lower frequency of self-regulation: if a fraction $P = 0.7$ of 100 species need to be self-regulating but half of the species are basal, then only 40% of consumers may need self-regulation. Second, they do not imply that intraspecific aggression, cannibalism, or other forms of direct interference are overwhelmingly important in stabilizing communities. As pointed out earlier, self-regulatory terms may appear in the community matrix via indirect mechanisms such as time scale separation between consumers and their resources, nonlinear functional responses, or spatial dynamics. Since our treatment of self-regulation was phenomenological, one cannot say what mechanism brought about the self-regulatory terms. All we can say is that *something* must be providing them if the system is to be stable. In fact, this is in line with several recent empirical studies of coexistence which have found not only that intraspecific effects are ubiquitous, but also that their magnitude is overwhelmingly larger than those of the interspecific ones[28–32]. As these studies are phenomenological, they say nothing about the mechanisms behind this pattern. Let us therefore reflect on some of the possibilities for where self-effects may originate from.

Direct self-regulation via predator interference or cannibalism are, in a sense, the simplest candidate mechanisms from a conceptual point of view. The only problem is that we do not know how important they are—though it has been argued that predator interference is quite common in nature[14,16]. Cannibalism is often important in marine systems, and cannibalism may act in a self-regulatory way under many circumstances (exceptions include the case when the fraction of individuals consumed is proportional to the total population size, or when only postreproductive individuals are eaten).

Nonlinear functional responses can also generate self-regulatory terms; moreover, though functional responses in nature may be more complicated than we tend to think[33], one may be quite sure that they will by and large be nonlinear. To explore their effect, we studied two different dynamical food web models (SI, Section 8). In the first model, based on equilibrium biomass distributions obtained from Damuth's Law[34], nonlinear functional responses were unable to stabilize dynamics, and they did not even reduce the required fraction of *directly* self-regulating species if stability was to be achieved. The allometric model of Schneider et al.[35], on the other hand, was occasionally able to produce stable, species-rich networks without any other self-regulation mechanism. Overall, while stabilization via nonlinear functional responses is definitely a possibility, our preliminary exploration suggests that it is not the most typical outcome.

Time scale separation between consumers and resources also results in self-regulation[3], though its importance in stabilizing community dynamics is understudied. However, it may in fact be more important than we think. Marine plankton use resources such as light (with instantaneous

dynamics in comparison to the planktonic life cycle), introducing self-regulatory terms in the plankton. Planktonic dynamics is notoriously complex[36], but probably none of that complexity matters from the point of view of a whale population consuming the plankton, since whales averages over those complexities in time and space due to their incomparably slower life cycle. Thus, planktonic dynamics may be effectively instantaneous from the whales' point of view, introducing effective self-regulation in whale dynamics. In the absence of further information, however, one cannot say how much this mechanism tends to contribute to network stability.

Finally, the fact that communities are distributed in space and are limited in their dispersal ability can impose self-regulation on all species simultaneously, and may have a large role in stabilizing real-world communities. This view is supported by recent theoretical findings[37] based on a random matrix perspective on multipatch dispersal. Spatial structure can stabilize dynamics via 1) the "eigenvalue pushback effect" (the bulk of the eigenvalue distribution moves in the negative direction, very much in analogy with what we see on Supplementary Figures 18 and 32); 2) the "Jacobian averaging effect" (heterogeneous interaction strengths in various patches averaged over the whole metacommunity act to reduce overall variance and thus $\sqrt{SV}$, leading to more stabilized communities), and 3) the "negative feedback effect" (migration can introduce effective self-regulation). We think it is very possible that the large and widespread negative diagonal entries in community matrices, necessary for their stability, are provided by communities' spatial structure. Putting it differently: were it possible to homogenize a community and thus eliminate its spatial aspect, one would predict a severe loss of species diversity due to the disappearance of self-regulation terms alone. Such a prediction is in line with classic experiments[38] demonstrating the stabilizing powers of spatial heterogeneity.

Apart from all the above mechanisms, there is of course an alternative interpretation of our results: that self-regulation is not actually common and therefore real-world ecosystems are inherently locally unstable. The question then becomes whether natural systems tend to reside at fixed point equilibria, or perhaps Mother Nature is indeed a strange attractor[39]. There is some evidence that fixed point behavior is twice as common as having limit cycles[40], with examples of truly chaotic dynamics being extremely rare[36]. However, future research in time series modeling may easily change these figures—therefore, ruling out the option of local instability on the basis of this evidence may be premature. Abandoning the idea of local asymptotic stability would of course also mean losing the mathematical and conceptual advantages it offers, since fixed point analysis is incomparably simpler than the study of nonequilibrium attractors.

We have analyzed two different types of empirical food webs: those based on the Ecopath modeling framework[17,18] which were already parameterized but relatively small in size, and large food webs containing hundreds of species but which were not yet parameterized. The data required to parameterize these webs using Ecopath is not available; we therefore resorted to parameterization based on allometric relationships (see Methods). An advantage of these parameterizations is that they ensure the feasibility[41–43] of the system (all species having positive equilibrium abundances). Regardless of parameterization, the qualitative pattern emerging was the same (Figure 1): a large fraction of species must self-regulate for stability, and the greatest likelihood of stability occurs at intermediate self-regulation strengths. But quantitatively, there was a significant difference between the Ecopath webs and the well-resolved ones: while in the former case, "only" half the species must self-regulate for stability, in the latter, this was closer to 90%. It is not clear at this point whether the difference is due to the different structural properties of the Ecopath and the allometric models, or rather simply due to the considerably lower species richness of Ecopath webs, or to a combination of both. However, even the more conservative Ecopath prediction requires substantially strong and widespread self-regulation for stability.

These results are in line with our theoretical analysis. Since the analysis is quite general, we expect the same conclusions on self-regulation to hold in any network of sufficient size and complexity, not just ecological ones: local stability requires widespread negative self-effects. Despite its generality, the theoretical results are of little relevance to networks where self-regulation appears naturally for every interacting component, such as biochemical or neural networks[1]. Where the source of such "natural" mechanisms is not immediately obvious (as in ecology), the results still compel us to believe either that the overwhelming majority of all populations on this planet experience substantial self-regulation, or else that ecosystems are in fact locally unstable. It may yet be premature to say which is the case—but either way, we are forced to reconsider how we think about the dynamics of large ecological communities.

Methods

For the Ecopath matrices, we used the seven largest ones parameterized by Jacquet et al.[17] (Table 1).

For the well-resolved networks, we took the adjacency matrices of 12 published empirical food webs (Table 2). We first removed all cannibalistic self-loops, and in the few cases two species mutually preyed upon each other, we dropped one of the two feeding links at random. Parameterization then proceeded by assuming appropriate body mass scaling allometries and type I functional responses[27,44] (see also SI, Section 7.1). Three independent parameterizations of each web were created, with the parameter controlling the scaling between body masses and equilibrium abundances, g, being set to either -0.55, -0.75, or -0.95.

Diagonal entries of the parameterized matrices $\mathbf{A}$ were set to d with probability P and to zero with probability $1 - P$. The value of P was varied from 0 to 1 in steps of $1/S$; i.e., the number (as opposed to fraction) of self-regulating species always increased by one at every step. The strength of self-regulation d was -2^q times the leading eigenvalue of the matrix without any self-effects, where $q = 0.5, 1.5, 2.5, \ldots, 7.5$ (i.e., eight different strengths of self-regulation were implemented for each web, measured in units of the leading eigenvalue).

For every combination of P, d, g, and food web identity, the diagonal entries were sampled independently 1000 times. We recorded the number of cases out of these which ended up stable; this number divided by 1000 was interpreted as the probability of achieving stability with the given P, d, g, and food web (Figure 1).

Due to the low structural rank[45] (maximum possible rank a matrix can attain assuming its nonzero entries are arbitrary) of many of the highly resolved empirical food webs, all the above was repeated for four different parameterizations of the webs in Table 2: 1) the original parameterized food webs; 2) the original web plus indirect negative interactions; 3) the original web plus indirect positive interactions; and 4) the original web plus both indirect negative and positive interactions. The indirect interactions modify the offdiagonal entries of the community matrix, contributing to them via apparent competition and indirect mutualisms. Indirect positive interactions were assigned to species sharing a common consumer, while indirect negative interactions were assigned to those sharing a common resource. Their strengths were drawn uniformly between zero and the mean positive (negative) direct interaction strength, divided by a factor f. This factor in turn assumed the values 2, 5, and 10; all simulations were repeated for all three values of f. Results proved insensitive both to the value of f and to whether indirect effects were present at all (SI, Section 7.3).

To find the minimal P compatible with stability (Figure 1**b**, yellow line), we took our parameterized food webs, and starting with $P \approx 1$ tried to find an arrangement of the diagonal entries such that the network was stable. We did this by minimizing the leading eigenvalue via a stochastic

search algorithm (SI, Section 7.4) and stopping the moment a stable solution was found. At that point, P was reduced and the above repeated. We did this until at least one hundred independent runs of the hill climbing and five independent runs of the genetic search algorithm failed to find a stable configuration. The smallest P where a stable configuration was found was then taken to be the minimum fraction of self-regulating species necessary for stability. We have performed this on each Ecopath web in Table 1, and all parameterizations of the Flensburg Fjord[46], Little Rock Lake[47], Otago Harbour[48], and Serengeti[49] food webs in Table 2 (see Supplementary Figures 21, 23, 25, and 29 for the results).

The analytical calculation used to obtain Figure 2 is described in detail in the SI (Sections 3-6). The dynamical models studying self-regulation generated by nonlinear functional responses are described in the SI, Section 8.

Data and code availability

All code and data used in this study are available at https://github.com/dysordys/diagonal.

Author contributions

GB wrote the manuscript and supplement, performed the analytical calculations, and made figures; MJM performed simulations and made figures; SA performed simulations. All authors contributed to devising the study and editing the manuscript.

References

[1] C. J. Puccia and R. Levins. *Qualitative modeling of complex systems*. Harvard University Press, Cambridge, MA, USA, 1985.

[2] P. Yodzis. The stability of real ecosystems. *Nature*, 289:674–676, 1981.

[3] R. H. MacArthur. Species packing and competitive equilibria for many species. *Theoretical Population Biology*, 1:1–11, 1970.

[4] R. M. May. *Stability and Complexity in Model Ecosystems*. Princeton University Press, Princeton, USA, 1973.

[5] A. Wollrab, S. Diehl, and A. M. De Roos. Simple rules describe bottom-up and top-down control in food webs with alternative energy pathways. *Ecology Letters*, 15:935–946, 2012.

[6] R. W. Sterner, A. Bajpai, and T. Adams. The enigma of food chain length: absence of theoretical evidence for dynamical constraints. *Ecology*, 78:2258–2262, 1997.

[7] J. C. Moore and P. C. de Ruiter. *Energetic food webs*. Oxford University Press, Oxford, UK, 2012.

[8] S. L. Pimm and J. H. Lawton. Number of trophic levels in ecological communities. *Nature*, 268:329–331, 1977.

[9] D. Tilman. *Resource Competition and Community Structure*. Princeton, New York, USA, 1982.

[10] S. L. Pimm. *Food webs*. The University of Chicago Press, Chicago, USA, 2002.

[11] P. Chesson. Species Competition and Predation. In R. Leemans, editor, *Ecological Systems: Selected Entries from the Encyclopedia of Sustainability Science and Technology*, chapter 13. Springer Science+Business Media, New York, USA, 2013.

[12] P. Turchin. *Complex population dynamics: a theoretical/empirical synthesis*. Princeton University Press, Princeton, New Jersey, USA, 2003.

[13] J. E. C. Flux. Evidence of self-limitation in wild vertebrate populations. *Oikos*, 92:555–557, 2001.

[14] G. T. Skalski and J. F. Gilliam. Functional responses with predator interference: viable alternatives to the Holling type II model. *Ecology*, 82:3083–3092, 2001.

[15] B. C. Rall, C. Guill, and U. Brose. Food-web connectance and predator interference dampen the paradox of enrichment. *Oikos*, 117:202–213, 2008.

[16] G. Kalinkat, F. D. Schneider, C. Digel, C. Guill, B. C. Rall, and U. Brose. Body masses, functional responses and predator–prey stability. *Ecology Letters*, 16:1126–1134, 2013.

[17] C. Jacquet, C. Moritz, L. Morissette, P. Legagneux, F. Massol, P. Archambault, and D. Gravel. No complexity–stability relationship in empirical ecosystems. *Nature Communications*, 7:12573, 2016.

[18] V. Christensen. ECOPATH II - a software for balancing steady-state ecosystem models and calculating network characteristics. *Ecological Modelling*, 61:169–185, 1992.

[19] V. L. Girko. The circle law. *Theory of Probability and its Applications*, 29:694–706, 1984.

[20] H. J. Sommers, A. Crisanti, H. Sompolinsky, and Y. Stein. Spectrum of large random asymmetric matrices. *Physical Review Letters*, 60:1895–1898, 1998.

[21] Z. Bai and J. W. Silverstein. *Spectral analysis of large dimensional random matrices*. Springer-Verlag, New York, USA, 2009.

[22] S. Allesina and S. Tang. Stability criteria for complex ecosystems. *Nature*, 483:205–208, 2012.

[23] S. Allesina and S. Tang. The stability-complexity relationship at age 40: a random matrix perspective. *Population Ecology*, 57:63–75, 2015.

[24] S. O'Rourke and D. Renfrew. Low rank perturbations of large elliptic random matrices. *Electronic Journal of Probability*, 19:1–65, 2014.

[25] T. Rogers. Universal sum and product rules for random matrices. *Journal of Mathematical Physics*, 51:093304, 2010.

[26] J. E. Cohen, F. Briand, and C. M. Newman. *Community food webs: Data and theory*. Springer-Verlag, Berlin, Germany, 1990.

[27] S. Allesina, J. Grilli, G. Barabás, S. Tang, J. Aljadeff, and A. Maritan. Predicting the stability of large structured food webs. *Nature Communications*, 6:7842, 2015.

[28] J. M. Levine and J. HilleRisLambers. The importance of niches for the maintenance of species diversity. *Nature*, 461:254–258, 2009.

[29] L. S. Comita, H. C. Muller-Landau, S. Aguilar, and S. P. Hubbell. Asymmetric density dependence shapes species abundances in a tropical tree community. *Science*, 329:330–332, 2010.

[30] M. R. Metz, W. P. Sousa, and R. Valencia. Widespread density-dependent seedling mortality promotes species coexistence in a highly diverse Amazonian rain forest. *Ecology*, 91:3675–3685, 2010.

[31] D. J. Johnson, W. T. Beaulieu, J. D. Bever, and K. Clay. Conspecific negative density dependence and forest diversity. *Science*, 336:904–907, 2012.

[32] C. Chu and P. B. Adler. Large niche differences emerge at the recruitment stage to stabilize grassland coexistence. *Ecology*, 85:373–392, 2015.

[33] R. Arditi and L. R. Ginzburg. *How species interact—altering the standard view on trophic ecology*. Oxford University Press, Oxford, New York, USA, 2012.

[34] J. Damuth. Population density and body size in mammals. *Nature*, 290:699–700, 1981.

[35] F. D. Schneider, U. Brose, B. C. Rall, and C. Guill. Animal diversity and ecosystem functioning in dynamic food webs. *Nature Communications*, 7:12718, 2016.

[36] E. Beninkà, K. D. Jöhnk, R. Heerkloss, and J. Huisman. Coupled predator–prey oscillations in a chaotic food web. *Ecology Letters*, 12:1367–1378, 2009.

[37] D. Gravel, F. Massol, and M. A. Leibold. Stability and complexity in model meta-ecosystems. *Nature Communications*, 7:12457, 2016.

[38] C. B. Huffaker. Experimental studies on predation: Dispersion factors and predator-prey oscillations. *Hilgardia*, 27:795–834, 1958.

[39] A. Hastings, C. L. Hom, S. Ellner, P. Turchin, and C. J. Godfray. Chaos in ecology: is Mother Nature a strange attractor? *Annual Review of Ecology and Systematics*, 24:1–33, 1993.

[40] B. E. Kendall, J. Prendergast, and O. N. Bjørnstad. The macroecology of population dynamics: taxonomic and biogeographic patterns in population cycles. *Ecology Letters*, 1:160–164, 1998.

[41] G. Barabás, S. Pigolotti, M. Gyllenberg, U. Dieckmann, and G. Meszéna. Continuous coexistence or discrete species? A new review of an old question. *Evolutionary Ecology Research*, 14:523–554, 2012.

[42] R. P. Rohr, S. Saavedra, and J. Bascompte. On the structural stability of mutualistic systems. *Science*, 345:1253497, 2014.

[43] Jacopo Grilli, Matteo Adorioso, Samir Suweis, György Barabás, Jayanth R. Banavar, Stefano Allesina, and Amos Maritan. Feasibility and coexistence of large ecological communities. *Nature Communications*, 2017.

[44] S. Tang, S. Pawar, and S. Allesina. Correlation between interaction strengths drives stability in large ecological networks. *Ecology Letters*, 17:1094–1100, 2014.

[45] K. J. Reinschke. *Multivariable Control — A Graph-theoretic Approach. Lecture Notes in Control and Information Science 108.* Springer-Verlag, Berlin, Germany, 1988.

[46] C. D. Zander, N. Josten, K. C. Detloff, R. Poulin, J. P. McLaughlin, and D. W. Thieltges. Food web including metazoan parasites for a brackish shallow water ecosystem in Germany and Denmark: Ecological Archives E092-174. *Ecology*, 92(10):2007–2007, 2011.

[47] N. D. Martinez. Artifacts or attributes? Effects of resolution on the Little Rock Lake food web. *Ecological Monographs*, 61:367–392, 1991.

[48] K. N. Mouritsen, R. Poulin, J. P. McLaughlin, and D. W. Thieltges. Food web including metazoan parasites for an intertidal ecosystem in New Zealand: Ecological Archives E092-173. *Ecology*, 92(10):2006–2006, 2011.

[49] E. B. Baskerville, A. P. Dobson, T. Bedford, S. Allesina, T. M. Anderson, and M. Pascual. Spatial guilds in the Serengeti food web revealed by a Bayesian group model. *PLoS computational biology*, 7(12):e1002321, 2011.

[50] T. Okey and R. Pugliese. In S. Guenette, V. Christensen, and D. Pauly, editors, *Fish. Impacts North Atl. Ecosyst. Model. Anal.*, pages 167–181. Fisheries Centre Research Reports, 2001.

[51] V. Christensen, A. Beattie, C. Buchanan, M. Hongguang, S. J. D. Martell, R. J. Latour, D. Preikshot, J. H. Sigrist M.B., Uphoff, C. J. Walters, R. J. Wood, and H. Townsend. Fisheries ecosystem model of the Chesapeake Bay: methodology, parameterization, and model exploration. *NOAA Technical Memorandum*, pages 1–146, 2009.

[52] J. Arias-Gonzalez, B. Delesalle, B. Salvat, and R. Galzin. Trophic functioning of the Tiahura reef sector, Moorea Island, French Polynesia. *Coral Reefs*, 16:231–246, 1997.

[53] J. J. Heymans and T. J. Pitcher. In T. J. Pitcher, J. J. Heymans, and M. Vasconcellos, editors, *Ecosyst. Model. Newfoundl. time periods 1995, 1985, 1900 1450*, volume 10, pages 5–71. Fisheries Centre Research Reports, 2002.

[54] C. J. Walters, V. Christensen, S. Martell, and J. F. Kitchell. Possible ecosystem impacts of applying MSY policies from single-species assessment. *ICES Journal of Marine Science*, 62:558–568, 2005.

[55] R. F. Hechinger, K. D. Lafferty, J. P. McLaughlin, et al. Food webs including parasites, biomass, body sizes, and life stages for three California/Baja California estuaries: Ecological Archives E092-066. *Ecology*, 92:791–791, 2011.

[56] U. Jacob, A. Thierry, U. Brose, et al. The role of body size in complex food webs: A cold case. *Advances In Ecological Research*, 45:181–223, 2011.

[57] J. O. Riede, U. Brose, B. Ebenman, U. Jacob, R. Thompson, C. R. Townsend, and T. Jonsson. Stepping in Elton's footprints: a general scaling model for body masses and trophic levels across ecosystems. *Ecology Letters*, 14:169–178, 2011.

[58] S. Opitz. *Trophic interactions in Caribbean coral reefs*. Number 1085. WorldFish, 1996.

[59] D. W. Thieltges, K. Reise, K. N. Mouritsen, J. P. McLaughlin, and R. Poulin. Food web including metazoan parasites for a tidal basin in Germany and Denmark: Ecological Archives E092-172. *Ecology*, 92(10):2005–2005, 2011.

[60] U. Jacob. *Trophic dynamics of Antarctic shelf ecosystems: food webs and energy flow budgets*. PhD thesis, Bremen, Univ., Diss., 2005.

Self-regulation and the stability of large ecological networks
Supplementary material

György Barabás[1,2], Matthew J. Michalska-Smith[2] & Stefano Allesina[2,3,4]

1: Division of Theoretical Biology, Dept. IFM, Linköping University, SE-58183 Linköping, Sweden

2: Dept. of Ecology & Evolution, University of Chicago, 1101 E. 57th Chicago, IL 60637, USA

3: Computation Institute, University of Chicago, 1101 E. 57th Chicago, IL 60637, USA

4: Northwestern Institute on Complex Systems, Northwestern University, Evanston, IL 60208, USA

Contents

1 Preliminaries

1.1 Dynamical framework

We assume there are S interacting species in an ecological community. The dynamics of the species densities $n_1, \ldots, n_S$ are determined by some unspecified system of ordinary differential equations:

$$\frac{\mathrm{d}n_i(t)}{\mathrm{d}t} = f_i(n_1(t), \ldots, n_S(t); \kappa_1, \ldots, \kappa_L) \qquad (i = 1, \ldots, S), \tag{1.1}$$

where the $f_i(\cdot)$ are functions of the densities and model parameters $\kappa_1, \ldots, \kappa_L$. We assume there is a fixed point $n_1^*, \ldots, n_S^* > 0$ such that

$$f_i(n_1^*, \ldots, n_S^*; \kappa_1, \ldots, \kappa_L) = 0 \tag{1.2}$$

for some values of the parameters. Linearizing around this fixed point and defining

$$A_{ij} = \left. \frac{\partial f_i}{\partial n_j} \right|_{n_1 = n_1^*, \ldots, n_S = n_S^*}, \tag{1.3}$$

we can write the dynamics of small deviations $x_i(t)$ from n_i^* as

$$\frac{\mathrm{d}x_i(t)}{\mathrm{d}t} \approx \sum_{j=1}^{S} A_{ij} x_j(t), \tag{1.4}$$

or, in matrix notation, as

$$\frac{\mathrm{d}\mathbf{x}(t)}{\mathrm{d}t} \approx \mathbf{A}\mathbf{x}(t). \tag{1.5}$$

We call the matrix $\mathbf{A}$, which is the Jacobian evaluated at equilibrium, the community matrix. The solution to Eq. 1.5 can be written explicitly:

$$\mathbf{x}(t) = \mathrm{Exp}(\mathbf{A}t)\,\mathbf{x}(0), \tag{1.6}$$

where $\mathrm{Exp}(\mathbf{A}t)$ is obtained by substituting the matrix $\mathbf{A}t$ into the Taylor series of the exponential function.

Let the eigenvalues of $\mathbf{A}$ be $\lambda_1, \ldots, \lambda_S$. The spectral density function of $\mathbf{A}$ is defined as

$$w(z) = \frac{1}{S} \sum_{i=1}^{S} \delta(\lambda_i - z), \tag{1.7}$$

where $z \in \mathbb{C}$, and $\delta(\cdot)$ is the Dirac delta function. More generally, one can define the expected spectral distribution of an ensemble of matrices as

$$w(z) = \mathbb{E}(\delta(\lambda_i - z)), \tag{1.8}$$

where $\mathbb{E}(\cdot)$ denotes expectation. The spectral density gives a complete description of where the eigenvalues of $\mathbf{A}$ are expected to lie in the complex plane.

Local stability of the equilibrium $\mathbf{n}^* = (n_1^*, \ldots, n_S^*)$ depends on the spectral abscissa $\eta(\mathbf{A})$ of $\mathbf{A}$:

$$\eta(\mathbf{A}) = \sup\{\mathrm{Re}(z) : z \in \mathrm{support}(w)\}, \tag{1.9}$$

where $\sup(\cdot)$ means supremum. As long as $\eta(\mathbf{A}) < 0$, the system is locally stable (small perturbations of the densities away from $\mathbf{n}^*$ eventually decay); otherwise, it is unstable. This condition means that all eigenvalues must have negative real parts for stability.

1.2 Self-regulation

This work is concerned with the role of self-regulation in stabilizing community matrices. The classical definition for self-regulation is that it is a *direct* negative dependence of species i's per capita growth rate on its own density. The per capita population growth rate of species i is defined as

$$r_i = \frac{1}{n_i}\frac{\mathrm{d}n_i}{\mathrm{d}t}. \tag{1.10}$$

From this and Eq. 1.1, it follows that $f_i = n_i r_i$.

The community matrix can be written in terms of the per capita growth rate. Using Eq. 1.3 and $f_i = n_i r_i$, we write

$$A_{ij} = \left.\frac{\partial f_i}{\partial n_j}\right|_{n_1=n_1^*,\ldots,n_S=n_S^*} = \left.\frac{\partial(n_i r_i)}{\partial n_j}\right|_{n_1=n_1^*,\ldots,n_S=n_S^*} = \left[\delta_{ij}r_i + n_i\frac{\partial r_i}{\partial n_j}\right]_{n_1=n_1^*,\ldots,n_S=n_S^*}, \tag{1.11}$$

where δ_{ij} is the Kronecker symbol (equal to 1 for $i = j$ and to 0 otherwise). Assuming a feasible community with all $n_i^* > 0$, the r_i are zero at equilibrium, and so we have

$$A_{ij} = n_i^* \left.\frac{\partial r_i}{\partial n_j}\right|_{n_1=n_1^*,\ldots,n_S=n_S^*}. \tag{1.12}$$

For positive n_i^*, A_{ii} is nonzero precisely when r_i has direct dependence on n_i, and describes self-regulation whenever this dependence is negative around the equilibrium point. We therefore conclude that negative diagonal entries of the community matrix correspond to self-regulation. We will stick to this broad definition of self-regulation until Section 8, where we will examine a narrower version of the concept.

A system completely devoid of self-regulation has $A_{ii} = 0$ for all i. Such a system cannot be locally stable, because the trace of a matrix is also the sum of its eigenvalues, and since this sum is now zero, $\eta(\mathbf{A}) \geq 0$.

Adding a constant diagonal matrix $d\mathbf{I}$ (where $\mathbf{I}$ is the identity matrix) to $\mathbf{A}$ corresponds to each species being self-regulated at the exact same strength. The eigenvalues of $\mathbf{A}$ are then simply shifted in the complex plane by d. This is because the eigenvalues λ of $\mathbf{A}$ satisfy the characteristic equation $0 = \det(\mathbf{A} - \lambda\mathbf{I})$, while the eigenvalues λ' of $\mathbf{A} + d\mathbf{I}$ satisfy the characteristic equation $0 = \det(\mathbf{A} + d\mathbf{I} - \lambda'\mathbf{I}) = \det(\mathbf{A} - (\lambda' - d)\mathbf{I})$. Comparing the two expressions, $\lambda = \lambda' - d$, or $\lambda' = \lambda + d$. Therefore, if λ is an eigenvalue of $\mathbf{A}$, then $\lambda + d$ is an eigenvalue of $\mathbf{A} + d\mathbf{I}$. It follows that any $\mathbf{A}$ can be stabilized by adding sufficiently strong simultaneous self-regulation to all species, i.e., by adding $d\mathbf{I}$ to $\mathbf{A}$ with d being less than $-\eta(\mathbf{A})$.

In case the diagonal entries of $\mathbf{A}$ are nonzero but not constant either, the eigenvalues acquire more spread along the real axis by having greater diagonal variance. Indeed, the variance $\mathbb{V}(\lambda)$ of the eigenvalues of any $S \times S$ matrix $\mathbf{A}$ reads

$$\mathbb{V}(\lambda) = \mathbb{E}(\lambda^2) - \mathbb{E}^2(\lambda) = \frac{\mathrm{trace}(\mathbf{A}^2)}{S} - \left(\frac{\mathrm{trace}(\mathbf{A})}{S}\right)^2 = \frac{1}{S}\sum_{i=1}^{S}\sum_{j=1}^{S}A_{ij}A_{ji} - \left(\frac{1}{S}\sum_{i=1}^{S}A_{ii}\right)^2$$

$$= \frac{1}{S}\sum_{i=1}^{S}\sum_{j\neq i}A_{ij}A_{ji} + \frac{1}{S}\sum_{i=1}^{S}A_{ii}^2 - \left(\frac{1}{S}\sum_{i=1}^{S}A_{ii}\right)^2 = \frac{1}{S}\sum_{i=1}^{S}\sum_{j\neq i}A_{ij}A_{ji} + \mathbb{V}(A_{ii}) \tag{1.13}$$

(Jorgensen et al. 2000). Thus increasing the variance of the diagonal entries increases the variance of the eigenvalues. Furthermore, since for matrices with real entries $\mathbb{V}(\lambda) = \mathbb{V}(\mathrm{Re}(\lambda)) - \mathbb{V}(\mathrm{Im}(\lambda))$,

increasing diagonal variance must act to increase eigenvalue variance in the real direction, possibly destabilizing the system. That is, for a given mean diagonal (strength of self-regulation), a smaller variance of the diagonal entries generally results in a more stabilized configuration.

1.3   Elliptic matrices

Let $\mathbf{M}$ be an $S \times S$ matrix, with diagonal entries M_{ii} zero, and pairs of entries (M_{ij}, M_{ji}) independently sampled from a bivariate distribution with zero marginal means, marginal variances V, and correlation ρ. This leads to $\mathbb{E}(M_{ij}) = 0$, $\mathbb{E}(M_{ij}^2) = V$, and $\mathbb{E}(M_{ij}M_{ji}) = V\rho$. When S is large, matrices constructed in this way are called *large elliptic random matrices* (O'Rourke and Renfrew 2014); here we will call them *elliptic matrices* for short. Rescaling the matrix by dividing each entry with $\sqrt{SV}$ leads to $\mathbb{E}(M_{ij}) = 0$, $\mathbb{E}(M_{ij}^2) = 1/S$, and $\mathbb{E}(M_{ij}M_{ji}) = \rho/S$; these matrices are called *standard elliptic matrices*.

According to the *elliptic law* (Sommers et al. 1998, Allesina and Tang 2012, Tang et al. 2014, O'Rourke and Renfrew 2014, Allesina and Tang 2015, Allesina et al. 2015), when $S \rightarrow \infty$, the eigenvalues of standard elliptic matrices are uniformly distributed in an ellipse in the complex plane centered at zero, with horizontal semiaxis $1 + \rho$ and vertical semiaxis $1 - \rho$. The most important aspect of this theorem is its *universality*: as long as all moments of the bivariate distribution are finite, one obtains the same spectral distribution, regardless of the bivariate probability distribution's shape. The elliptic law also recovers, as a special case, Wigner's semicircle law for the spectral distribution of symmetric matrices, obtained when $\rho = 1$.

Random matrix theorems are derived using standard elliptic matrices in the $S \rightarrow \infty$ limit. Approximations for finite S can be obtained by applying the results for standard elliptic matrices, and then simply rescaling by $\sqrt{SV}$. For instance, the eigenvalues of finite-size, non-standard elliptic matrices are uniformly distributed in an ellipse centered at zero in the complex plane, with horizontal/vertical semiaxes approximately equal to $\sqrt{SV}(1 \pm \rho)$ instead of $1 \pm \rho$. (Supplementary Figure 1). Naturally, the larger S is, the better the approximation will work in practice.

2   Low-rank perturbations of elliptic matrices

Let $\mathbf{M}$ be a standard elliptic matrix and $\mathbf{D}$ be a low-rank $S \times S$ matrix, i.e., one with k nonzero eigenvalues, $S - k$ zero eigenvalues, and $k \ll S$. Let us number the eigenvalues $\lambda_i(\mathbf{D})$ of $\mathbf{D}$ such that $\lambda_i(\mathbf{D}) \neq 0$ for $i = 1, \ldots, k$ and $\lambda_i(\mathbf{D}) = 0$ for $i = k+1, \ldots, S$. We are interested in the eigenvalues $\lambda_i(\mathbf{A})$ of $\mathbf{A} = \mathbf{M} + \mathbf{D}$. The low-rank perturbation theorem for elliptic matrices (O'Rourke and Renfrew 2014) states that in the $S \rightarrow \infty$ limit, the eigenvalues are still distributed in an ellipse with horizontal/vertical semiaxes $1 \pm \rho$, except for at most k eigenvalues. These k eigenvalues $\lambda_i(\mathbf{D})$ $(i = 1, \ldots, k)$ affect the eigenvalues $\lambda_i(\mathbf{A})$ in the following way:

$$\lambda_i(\mathbf{A}) = \begin{cases} \text{unaffected} & \text{if } |\lambda_i(\mathbf{D})| \leq 1, \\[2ex] \lambda_i(\mathbf{D}) + \dfrac{\rho}{\lambda_i(\mathbf{D})} + o(1) & \text{if } |\lambda_i(\mathbf{D})| > 1 \end{cases} \tag{2.1}$$

(we used the standard order notation; further technical conditions of the theorem are found in O'Rourke and Renfrew 2014). For large but finite S and elliptic matrices that are not standardized,
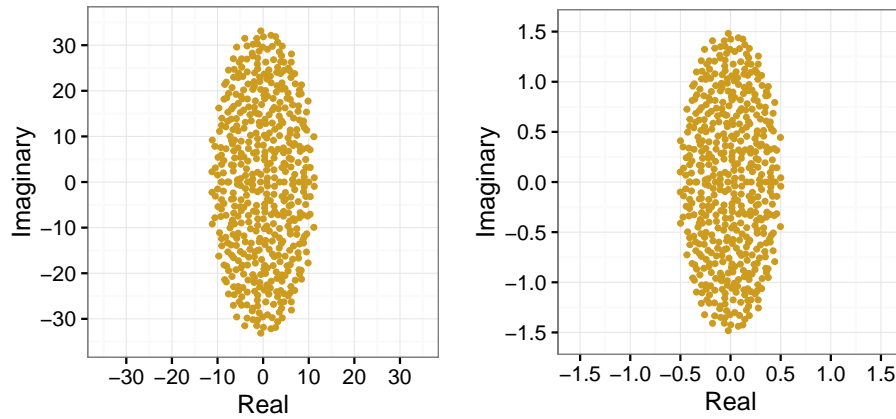
Supplementary Figure 1: Eigenvalues (yellow points) of an elliptic matrix with $S = 500$, $V = 1$, and $\rho = -1/2$ (left). Normalizing its entries by $\sqrt{SV}$, one obtains a standard elliptic matrix and its eigenvalues (right). Since $\rho = -1/2$, the horizontal/vertical semiaxes $1 \pm \rho$ of the standard elliptic matrix are $1/2$ and $3/2$, respectively. This is clearly seen on the right panel. The eigenvalue distribution in the left panel is the same, except both the real and imaginary axes are rescaled by $\sqrt{SV} = \sqrt{500} \approx 22.36$. The horizontal and vertical semiaxes are therefore approximately equal to $\sqrt{SV}(1+\rho) \approx 11.18$ and $\sqrt{SV}(1-\rho) \approx 33.54$.

Eq. 2.1 may be used as

$$\lambda_i(\mathbf{A}) \approx \begin{cases} \text{unaffected} & \text{if } |\lambda_i(\mathbf{D})| \leq \sqrt{SV}, \\[2ex] \lambda_i(\mathbf{D}) + \dfrac{\rho SV}{\lambda_i(\mathbf{D})} & \text{if } |\lambda_i(\mathbf{D})| > \sqrt{SV}. \end{cases} \tag{2.2}$$

Supplementary Figure 2 shows an example of the effect a low-rank perturbation has on the spectrum of an elliptic matrix. The perturbing matrix has rank three; the outlier eigenvalues' positions are accurately predicted by Eq. 2.2.

2.1   Elliptic matrices with nonzero mean

One very important application of the low-rank perturbation theorem is in calculating the spectra of random matrices whose entries are sampled from a distribution with nonzero mean (O'Rourke and Renfrew 2014). Let $\mathbf{M}$ be an $S \times S$ random matrix with $\mathbb{E}(M_{ij}) = \mu$, $\mathbb{E}(M_{ij}^2) = V$, and $\mathbb{E}(M_{ij}M_{ji}) = \rho$. Let $\mathbf{E}$ be the $S \times S$ matrix with each entry equal to 1; $\mathbf{E}$ is a rank-one matrix. First, let us write $\mathbf{M}$ as

$$\mathbf{M} = (\mathbf{M} - \mu\mathbf{E} + \mu\mathbf{I}) + \mu\mathbf{E} - \mu\mathbf{I}. \tag{2.3}$$

The expression in parentheses is now an elliptic matrix, its eigenvalues falling uniformly in an ellipse with horizontal/vertical semiaxes $\sqrt{SV}(1 \pm \rho)$ in the complex plane (we first subtract off the mean, but in the process modify the diagonal; the $\mu\mathbf{I}$ term restores it to zero). Outside the parentheses, the $\mu\mathbf{E}$ term is a rank-one perturbation: $S - 1$ of its eigenvalues are zero, and a single eigenvalue is equal to $S\mu$. By Eq. 2.2, the effect of this matrix is to modify a single eigenvalue, which now will approximately be equal to $S\mu + \rho SV/(S\mu) = S\mu + \rho V/\mu$ (but only if $|S\mu| > \sqrt{SV}$, or, equivalently, $|\mu| > \sqrt{V/S}$). Finally, the effect of $-\mu\mathbf{I}$ is to shift the whole spectrum by subtracting μ from each eigenvalue, so that $S - 1$ eigenvalues fall in an ellipse with horizontal/vertical semiaxes $\sqrt{SV}(1 \pm \rho)$

centered at $-\mu + 0i$ in the complex plane, and there is a single outlier whose position is given by $(S-1)\mu + \rho V/\mu$ (Supplementary Figure 3, left panel).
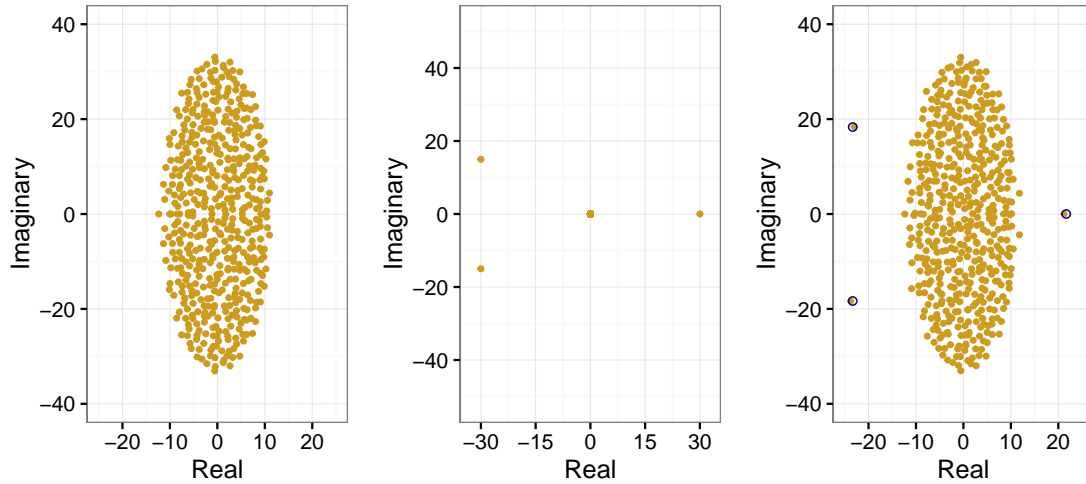
Supplementary Figure 2: Left: spectrum of elliptic matrix $\mathbf{M}$ with $S = 500$, $V = 1$, and $\rho = -1/2$ (yellow points). Center: spectrum of a rank-three 500×500 matrix $\mathbf{D}$ with the three nonzero eigenvalues equal to 30, $-30 + 15i$, and $-30 - 15i$. Right: spectrum of $\mathbf{A} = \mathbf{M} + \mathbf{D}$. The predicted effect of the perturbations from Eq. 2.2 (blue circles) matches the numerical results.
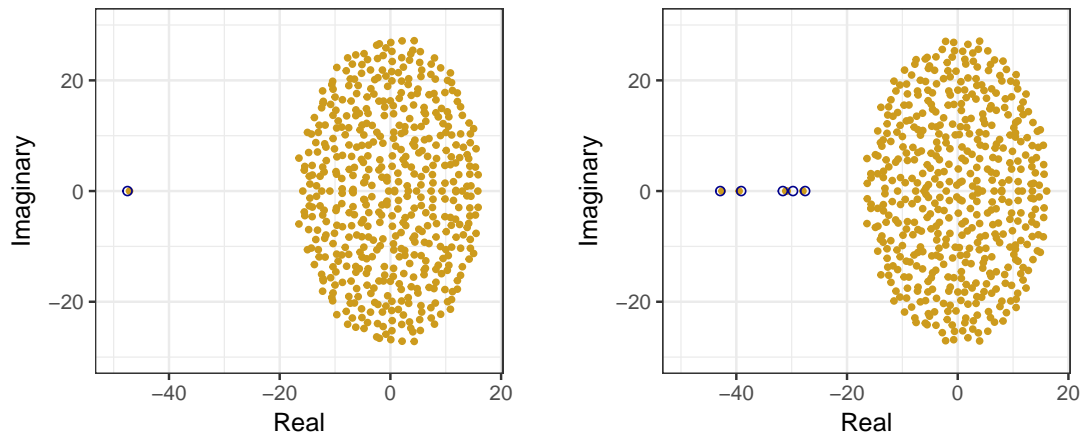
Supplementary Figure 3: Left: Spectrum of elliptic matrix (yellow points) with $S = 500$, $V = 1$, $\rho = -1/4$, and $\mu = -1/10$, i.e., its entries have nonzero mean. Equivalently, the matrix can be decomposed via Eq. 2.3, with $\mathbf{D} = \mu \mathbf{E}$. The outlier's predicted position is $(S-1)\mu + \rho V/\mu = -47.4$ (blue circle). Right: the same elliptic matrix but with $\mu = 0$, and 10 species out of the 500 being self-regulated (yellow points). Blue circles show the predicted positions of the perturbed values based on the low-rank perturbation formula Eq. 2.2. Clearly, the system cannot be stabilized by just a few species exhibiting self-regulation.

2.2   No stabilization when only a few species self-regulate

Since the diagonal entries of any elliptic matrix $\mathbf{M}$ are all zero, no species are self-regulating. Self-regulation can be introduced via $\mathbf{A} = \mathbf{M} + \mathbf{D}$, where $\mathbf{D}$ is the diagonal matrix

$$\mathbf{D} = \begin{pmatrix} d_1 & 0 & 0 & \cdots \\ 0 & d_2 & 0 & \cdots \\ 0 & 0 & d_3 & \cdots \\ \vdots & \vdots & \vdots & \ddots \end{pmatrix} \tag{2.4}$$

In case only $k \ll S$ of the d_i are nonzero, $\mathbf{D}$ is a low-rank perturbation to $\mathbf{M}$ with rank k. The spectral distribution of $\mathbf{A}$ is therefore given by the ellipse defined by $\mathbf{M}$, plus at most k outliers. Since the spectral abscissa $\eta(\mathbf{A})$ is still approximately $\sqrt{SV}(1+\rho) > 0$, the matrix cannot be stabilized by just a few species self-regulating (Supplementary Figure 3, right panel).

Similar results hold when $\mathbb{E}(M_{ij}) = \mu \neq 0$. For simplicity, assume only one species is self-regulating. As discussed above, an elliptic matrix with nonzero mean can be thought of as a standard elliptic matrix plus a rank-one perturbation $\mu\mathbf{E}$, where $\mathbf{E}$ is the matrix of all ones. Adding self-regulation to one single species means that $\mathbf{D}$ is now a matrix of all zeros except for $D_{11} = d$ (we choose the self-regulating species to be species 1 without loss of generality, since $\mathbf{M}$ is a random matrix whose rows have identical statistical properties in the large S limit). Decomposing $\mathbf{M}$ as in Eq. 2.3, $\mathbf{A}$ is an elliptic matrix shifted by $-\mu\mathbf{I}$ plus the perturbation $\mu\mathbf{E} + \mathbf{D}$, which reads

$$\mu\mathbf{E} + \mathbf{D} = \begin{pmatrix} \mu+d & \mu & \mu & \cdots \\ \mu & \mu & \mu & \cdots \\ \mu & \mu & \mu & \cdots \\ \vdots & \vdots & \vdots & \ddots \end{pmatrix}. \tag{2.5}$$

This is a rank-two matrix, so all but two eigenvalues are zero. The eigenvectors belonging to the nonzero eigenvalues must have the structure $(u, v, v, \ldots, v)$. Writing out the eigenvalue equation as

$$\begin{pmatrix} \mu+d & \mu & \mu & \cdots \\ \mu & \mu & \mu & \cdots \\ \mu & \mu & \mu & \cdots \\ \vdots & \vdots & \vdots & \ddots \end{pmatrix} \begin{pmatrix} u \\ v \\ v \\ \vdots \end{pmatrix} = \lambda \begin{pmatrix} u \\ v \\ v \\ \vdots \end{pmatrix}, \tag{2.6}$$

we get

$$(\mu+d)u + (S-1)\mu v = \lambda u, \qquad \mu u + (S-1)\mu v = \lambda v. \tag{2.7}$$

Using the inherent freedom in choosing eigenvector components, we may fix $v = 1$. We then have

$$(\mu+d)u + (S-1)\mu = \lambda u, \qquad \mu u + (S-1)\mu = \lambda. \tag{2.8}$$

The two solutions for λ yield the nonzero eigenvalues:

$$\lambda_{\pm} = \frac{S\mu+d}{2} \pm \sqrt{\left(\frac{S\mu}{2}\right)^2 - \frac{S-2}{2}\mu d + \left(\frac{d}{2}\right)^2}. \tag{2.9}$$

Adding self-regulation to a single species when $\mu \neq 0$ is therefore equivalent to adding a rank-two perturbation to an elliptic matrix. Again, since only two eigenvalues are affected, stability cannot be achieved, regardless of how strongly the species is self-regulating.

More generally, if $k \ll S$ species self-regulate, the low-rank perturbation affects $k+1$ which is still insufficient to alter the matrix's stability properties (Supplementary Figure 4).
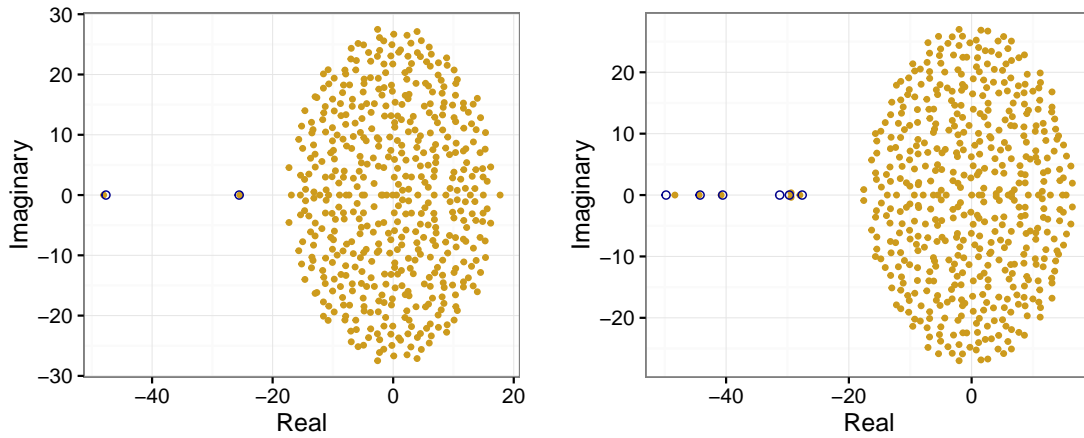
Supplementary Figure 4: Spectra of matrices $\mathbf{A} = \mathbf{M} + \mathbf{D}$, where $\mathbf{M}$ is a random matrix with $S = 500$, $\mu = -1/10$, $V = 1$, and $\rho = -1/4$. On the left, $\mathbf{D}$ is a matrix of all zeros except for $D_{11} = -30$; on the right, the first five diagonal entries of $\mathbf{D}$ are uniformly and independently sampled from $[-50, -30]$. Since the random matrices have nonzero mean, the number of outliers is 2 on the left and 6 on the right; their positions are predicted by the low-rank perturbation formula Eq. 2.2 (blue circles). On the left, the values are given more specifically by Eq. 2.9.

2.3   A handful of non-self-regulating species are sufficient to destabilize

We can approach the same problem from the opposite end: suppose all but $k \ll S$ species are self-regulated. For simplicity, assume the strength of self-regulation, d, is the same for all self-regulating species (this restriction is relaxed in subsequent sections). Such a matrix can be written

$$\mathbf{A} = \mathbf{M} + d\mathbf{I} + \mathbf{D}, \tag{2.10}$$

where $\mathbf{M}$ is elliptic, and $\mathbf{D}$ is given by Eq. 2.4 with $d_i = -d$ for k of the S diagonal entries, and $d_i = 0$ otherwise. The role of $\mathbf{D}$ is to offset the effect of $d\mathbf{I}$ for the k non-self-regulating species. Since $k \ll S$, we can once again apply the low-rank perturbation theorem to obtain the spectrum of $\mathbf{M} + \mathbf{D}$, which then gets shifted by d due to the effect of $d\mathbf{I}$ (Section 1.2). Using Eq. 2.2, the outlier eigenvalues' positions are now

$$\lambda_i(\mathbf{A}) \approx \underbrace{\lambda_i(\mathbf{D})}_{-d} + \underbrace{\frac{\rho SV}{\lambda_i(\mathbf{D})}}_{-d} + d = -\frac{\rho SV}{d} = \frac{\rho SV}{|d|}. \tag{2.11}$$

In the last step, we used $d < 0$, which must be the case if the species self-regulate as opposed to self-enhance.

A consequence of Eq. 2.11 is that, for $\rho \geq 0$, even a single species without self-regulation destabilizes the system. For $\rho < 0$, the system will be stable. However, stripping self-regulation from a few more species will lead to destabilization (Supplementary Figure 5). Extending this analysis to the case of matrices with nonzero mean is a straightforward exercise that does not alter the results (Supplementary Figure 6).

One may wonder whether a single eigenvalue crossing the imaginary axis is of much biological importance. If this corresponds to a transcritical bifurcation whereby a few species go extinct, the rest of the system may still be functional. This, however, is not the case here. Assume all but
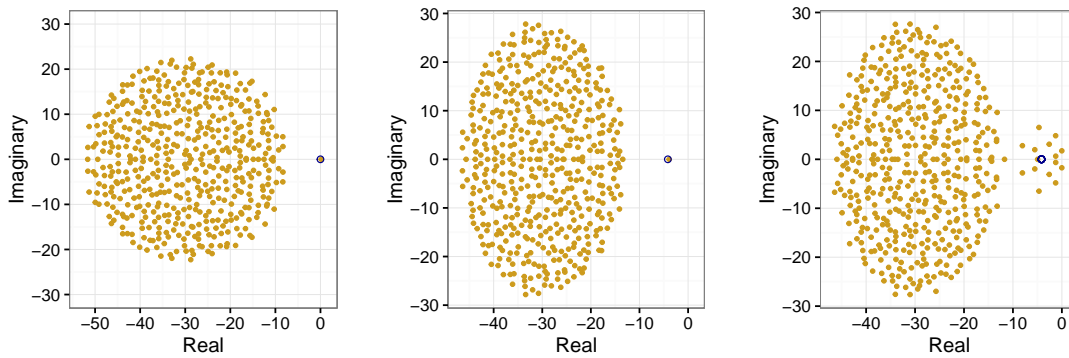
Supplementary Figure 5: Spectrum of elliptic matrices with $S = 500$ and $V = 1$, when all but a handful of species are self-regulated. Left: random matrix with $\rho = 0$. Lifting self-regulation from even a single species destabilizes the system. Center: for a random matrix with $\rho = -1/4$, lifting self-regulation from a single species does not yet destabilize. Right: doing so with $k = 15$ species does destabilize.
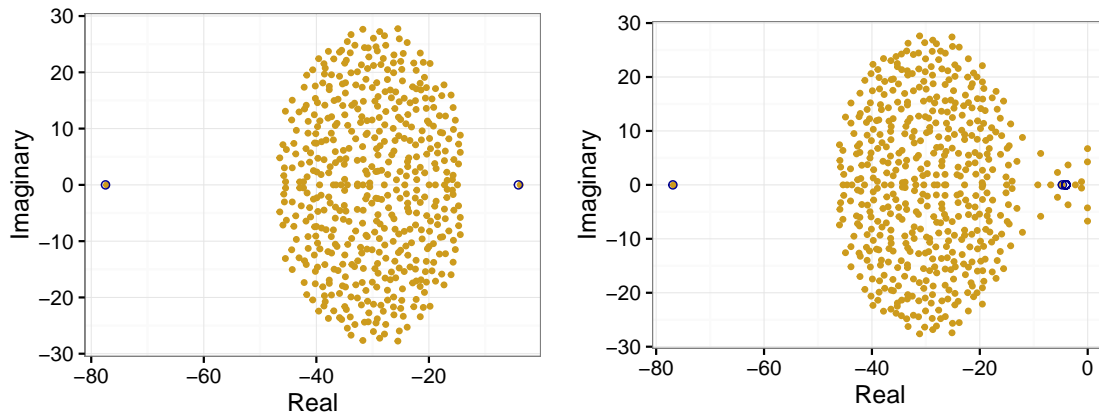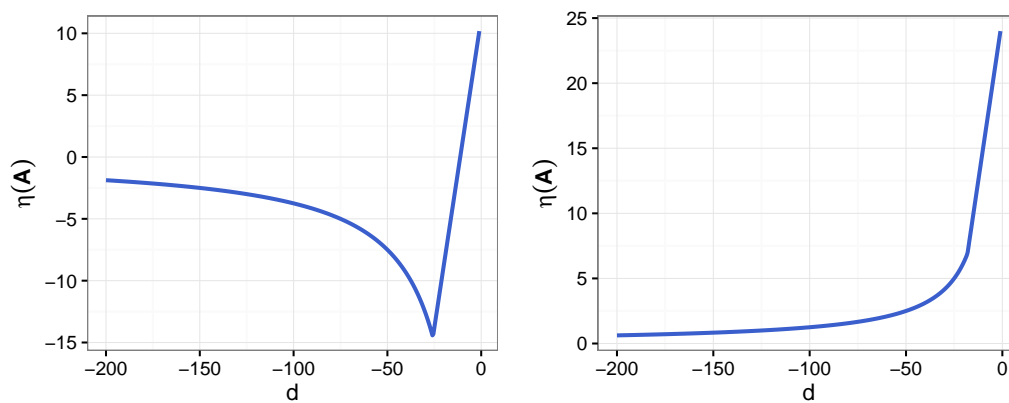

Supplementary Figure 6: Spectrum of elliptic matrices with $S = 500$, $\mu = -0.1$, $V = 1$, $\rho = -0.25$, and with all species self-regulating (with $d = -30$), except for one (left) and fifteen (right) species. The results are the same as in Supplementary Figure 5; the only difference is the extra negative outlier eigenvalue due to the matrix having a negative mean.

one species are strongly self-regulated; the interaction matrix $\mathbf{A}$ is then given by Eq. 2.10 with $\mathbf{D}$ all zeros except for $D_{11} = -d$. If self-regulation is strong, then, to a first-order approximation, $\mathbf{D}$ determines the eigenvalues and eigenvectors of $\mathbf{A}$, to which $\mathbf{M}$ contributes a perturbation that can be evaluated using regular eigenvalue perturbation theory (e.g., Caswell 2001, chapter 9). The $d\mathbf{I}$ term then shifts the eigenvalues by d but leaves the eigenvectors unaffected. The eigenvector of $\mathbf{D}$ belonging to the nonzero eigenvalue $-d$ is $(1, 0, 0, \ldots, 0)$. The perturbing effect of $\mathbf{M}$ contributes a relatively small change to this vector; that is, it will still be true that the eigenvector is localized on species 1. Then, if the eigenvalue belonging to this highly localized eigenvector, given by Eq. 2.11, is positive, this means that the one species will experience unrestricted growth, driving *all* other species towards extinction. Naturally, since the dynamics described by $\mathbf{A}$ is only valid in the vicinity of an equilibrium point (Section 1.1), this instability will generally result in the system settling on some alternative stable state, one where species 1 is at high abundance and the other species are either extinct or at low abundance. Biologically, lifting the burden of strong self regulation from one

single species gives it such a huge competitive advantage that it may become the single dominant species. Therefore, even a single eigenvalue crossing over to the right half plane has a catastrophic effect on the system as a whole.

2.4 For negative correlation, increasing the strength of self-regulation can be destabilizing

The scenario above, when only a handful of species are free of self-regulation, leads to an interesting and counterintuitive result for $\rho < 0$. In that case the spectral abscissa $\eta(\mathbf{A})$, defined by Eq. 1.9, changes nonmonotonically as the strength of self-regulation d increases. Supplementary Figure 7 (left panel) shows an example where $\rho = -3/4$ and only one species lacks self-regulation: as $|d|$ gets larger, $\eta(\mathbf{A})$ first decreases; then, after a critical point, it starts to increase again.

Supplementary Figure 7: The spectral abscissa $\eta(\mathbf{A})$ of $\mathbf{A} = \mathbf{M} + d\mathbf{I} + \mathbf{D}$ as a function of $d < 0$, where $\mathbf{I}$ is the identity matrix, $\mathbf{D}$ is a matrix of all zeros except for $D_{11} = -d$, and $\mathbf{M}$ is an elliptic matrix with $S = 500$, $V = 1$, and $\rho = -3/4$ (left) or $\rho = 1/4$ (right). For negative values of ρ (left), increasing the strength of self-regulation by making d more negative eventually has a destabilizing effect on the system. The same does not hold for $\rho \geq 0$ (right).

The mathematical reason for this is clear. For $|d| < \sqrt{SV}$ (weak self-regulation), the nonzero eigenvalue $-d$ of the perturbing matrix is too small to have an effect on the spectrum of the original elliptic matrix by Eq. 2.2. Then, $\eta(\mathbf{A}) = \sqrt{SV}(1+\rho) + d$ is simply the rightmost point of the ellipse. However, when $|d|$ exceeds $\sqrt{SV}$, the outlier will be given by Eq. 2.11. For $\rho < 0$, this expression is an increasing function of $|d|$, leading to the seemingly paradoxical result that imposing more self-regulation works in the direction of destabilizing the system.

It is possible to give an intuitive, though not very rigorous, interpretation to this phenomenon. For $d \approx 0$ (very weak self-regulation), the system as a whole cannot be stabilized to begin with, as even in the case when all species are self-regulated, d would need to be at least $-\sqrt{SV}(1+\rho)$ for stability. For d very large on the other hand, lifting the burden of self-regulation from just a single species will give that species such a big advantage that it effectively destabilizes the system (Section 2.3). Therefore, under parameterizations which favor stability at least under some circumstances, the most stabilized configuration must be achieved for intermediate values of d. Such a parameterization is provided by $\rho < 0$ but not $\rho \geq 0$, which instead leads to a monotonic decrease of $\eta(\mathbf{A})$ as $-d$ increases (Supplementary Figure 7, right panel).

One could call this phenomenon, somewhat provocatively, the "intermediate self-regulation hypothesis": the most stabilized communities occur at intermediate values of self-interaction strengths. This is a recurring theme not particular to the case examined here: it is a general phenomenon that holds as long as $\rho < 0$ and there is even a single species whose self-regulation is sufficiently weak (see subsequent sections).

2.5 Generating cascade structures via low-rank perturbations of elliptic matrices

Empirical food webs differ from elliptic matrices in important structural ways: they have broader degree distributions, are almost interval, and have an approximate cascade structure (Cohen et al. 1990)—i.e., species can be ordered such that species lower in the hierarchy have zero probability of eating those higher, while higher species have some nonzero probability of consuming lower ones. This latter property can be taken into account by constructing the community matrix $\mathbf{A}$ as a sum of two parts, a deterministic part $\mathbf{H}$ and a random part $\mathbf{Q}$ (Allesina et al. 2015):

$$\mathbf{A} = \mathbf{H} + \mathbf{Q}. \tag{2.12}$$

The deterministic part contains the effect of mean interaction strengths, which differ between the upper and lower triangular parts of the matrix:

$$\mathbf{H} = \begin{pmatrix} 0 & \mu_{\mathrm{U}} & \mu_{\mathrm{U}} & \cdots \\ \mu_{\mathrm{L}} & 0 & \mu_{\mathrm{U}} & \cdots \\ \mu_{\mathrm{L}} & \mu_{\mathrm{L}} & 0 & \cdots \\ \vdots & \vdots & \vdots & \ddots \end{pmatrix}, \tag{2.13}$$

where $\mu_{\mathrm{U}} < 0$ is the average effect of predators on prey, and $\mu_{\mathrm{L}} > 0$ is the average effect of prey on predators. The eigenvalues of this matrix are

$$\lambda_k = -\mu_{\mathrm{U}} + \frac{\mu_{\mathrm{L}} - \mu_{\mathrm{U}}}{(\mu_{\mathrm{L}}/\mu_{\mathrm{U}})^{\frac{1}{S}} e^{i\theta_k} - 1}, \tag{2.14}$$

which lie on the circumference of a circle in the complex plane with center $c_{\mathbf{H}}$ and radius $r_{\mathbf{H}}$

$$c_{\mathbf{H}} = \frac{\mu_{\mathrm{L}} - (-\mu_{\mathrm{L}}/\mu_{\mathrm{U}})^{2/S}\mu_{\mathrm{U}}}{(-\mu_{\mathrm{L}}/\mu_{\mathrm{U}})^{2/S} - 1} + 0i, \qquad r_{\mathbf{H}} = \left| \frac{(\mu_{\mathrm{U}} - \mu_{\mathrm{L}})(-\mu_{\mathrm{L}}/\mu_{\mathrm{U}})^{1/S}}{(-\mu_{\mathrm{L}}/\mu_{\mathrm{U}})^{2/S} - 1} \right|. \tag{2.15}$$

(Allesina et al. 2015). Most of the eigenvalues are very close to zero, with only a few being appreciably different (Supplementary Figure 8). The matrix $\mathbf{H}$ may therefore be thought of as a low-rank matrix plus a small perturbation, one that is negligible for the purposes of applications here.

The matrix $\mathbf{Q}$ has zero diagonal, zero mean, variance σ_{U}^2 for the upper triangular entries, and σ_{L}^2 for the lower triangular ones. The correlation between the (i, j)th and (j, i)th entries is given by ρ_{UL}. Its eigenvalues are uniformly distributed in an ellipse with horizontal/vertical semiaxes $\sqrt{SV_{\mathrm{eff}}}(1 \pm \rho_{\mathrm{eff}})$, where V_{eff} and ρ_{eff} are the variance and average pairwise correlation of an elliptic matrix whose spectrum would be exactly identical to that of $\mathbf{Q}$. Using the results in Allesina et al. (2015), these quantities can be expressed as the solution to

$$SV_{\mathrm{eff}}(1 \pm \rho_{\mathrm{eff}})^2 = a \pm b\rho_{\mathrm{UL}} + c\rho_{\mathrm{UL}}^2, \tag{2.16}$$
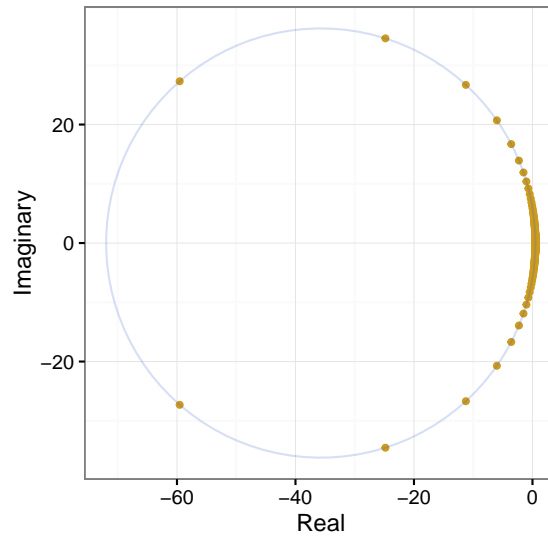
Supplementary Figure 8: Eigenvalues (yellow points) of the matrix $\mathbf{H}$ given by Eq. 2.13, with $S = 500$, $\mu_L = 1/1000$, and $\mu_U = -1$. The eigenvalues fall on the circumference of the blue circle with center and radius given by Eq. 2.15. All but a handful of eigenvalues are very close to zero, making this matrix effectively low-rank.

where

$$a = S\frac{\sigma_L^2 - \sigma_U^2}{\log(\sigma_L^2/\sigma_U^2)}, \qquad b = 2(S-1)\sigma_L\sigma_U, \qquad c = \frac{(S-1)^2\sigma_L^2\sigma_U^2\log(\sigma_L^2/\sigma_U^2)}{S(\sigma_L^2 - \sigma_U^2)}. \qquad (2.17)$$

From this, V_{eff} and ρ_{eff} can be obtained:

$$V_{\text{eff}} = \frac{a + c\rho_{\text{UL}}^2 + \sqrt{\left(a + c\rho_{\text{UL}}^2\right)^2 - b^2\rho_{\text{UL}}^2}}{2S}, \qquad (2.18)$$

$$\rho_{\text{eff}} = \frac{a + c\rho_{\text{UL}}^2 - \sqrt{\left(a + c\rho_{\text{UL}}^2\right)^2 - b^2\rho_{\text{UL}}^2}}{b\rho_{\text{UL}}}. \qquad (2.19)$$

(There is another root to Eq. 2.16, but it always gives a $|\rho_{\text{eff}}|$ greater than one.) This means that $\mathbf{Q}$ has the same spectral distribution as another, much simpler matrix $\mathbf{M_Q}$, which is an elliptic matrix with $\mathbb{E}(M_{ij}) = 0$, $\mathbb{E}(M_{ij}^2) = V_{\text{eff}}$, and $\mathbb{E}(M_{ij}M_{ji}) = \rho_{\text{eff}}V_{\text{eff}}$. The subscript emphasizes that $\mathbf{M_Q}$ is the elliptic matrix associated to $\mathbf{Q}$. For $\mu_L = \mu_U = 0$ and $\sigma_L = \mu_U$, the effective parameters V_{eff} and ρ_{eff} reduce to the original V and ρ in the large S limit.

The spectrum of $\mathbf{A}$ is thus identical to the spectrum of $\mathbf{H} + \mathbf{M_Q}$. Since $\mathbf{M_Q}$ is elliptic and $\mathbf{H}$ is low-rank, the low-rank perturbation formula Eq. 2.2 can be used to predict the eigenvalues of $\mathbf{A}$. Supplementary Figure 9 shows how the full spectrum of a matrix with cascade structure is constructed from the spectrum of the effective elliptic matrix $\mathbf{M_Q}$, plus the low-rank perturbation $\mathbf{H}$.

The matrix thus generated has zero along the diagonal. It would be tempting to consider $\mathbf{A} = \mathbf{M_Q} + \mathbf{H} + \mathbf{D}$ and apply yet another low-rank perturbation via $\mathbf{D}$ to the low-rank perturbed elliptic matrix $\mathbf{M_Q} + \mathbf{H}$. This cannot be done in general: the low-rank theorem applies strictly to elliptic matrices, not low-rank perturbed ones. Instead, the sum $\mathbf{H} + \mathbf{D}$ has to be regarded as the
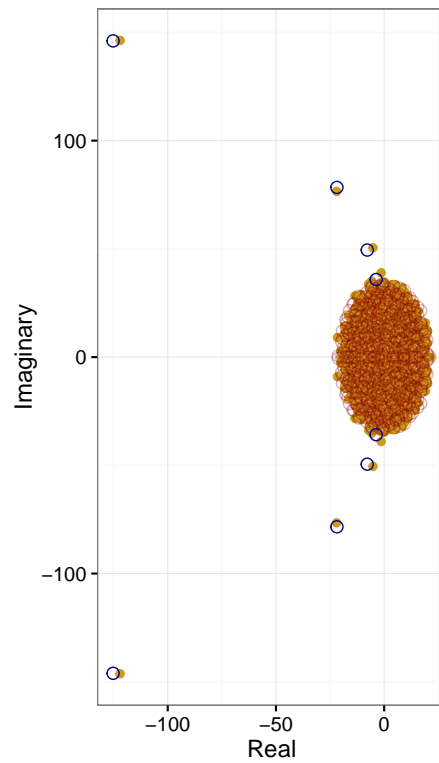
Supplementary Figure 9: Spectrum of community matrix $\mathbf{A} = \mathbf{M_Q} + \mathbf{H}$ with cascade structure, with $S = 500$, $\mu_L = -3/2$, $\mu_U = 1/10$, $\sigma_L = 3/2$, $\sigma_U = 1$, and $\rho_{UL} = -1/4$. Yellow dots are the eigenvalues of $\mathbf{A}$. Red circles are eigenvalues of the effective elliptic matrix $\mathbf{M_Q}$, and blue circles predict the positions of eigenvalues following the low-rank perturbation imposed by $\mathbf{H}$, given by Eq. 2.13. This demonstrates that the spectrum of a matrix possessing the cascade structure can be thought of as an (effective) elliptic matrix plus a low-rank perturbation.

(total) perturbation, to which the low-rank theorem is applicable provided that the sum is indeed low rank. Since the sum of two low-rank matrices may be of any rank, there is no guarantee that the theorem can be applied. Fortunately however, the matrix

$$\mathbf{H} + \mathbf{D} = \begin{pmatrix} d_1 & \mu_U & \mu_U & \cdots \\ \mu_L & d_2 & \mu_U & \cdots \\ \mu_L & \mu_L & 0 & \cdots \\ \vdots & \vdots & \vdots & \ddots \end{pmatrix} \tag{2.20}$$

is still effectively low rank as long as only a minority of the diagonal entries are nonzero (Supplementary Figure 10). Then $\mathbf{M_Q}$ can be low-rank perturbed using this matrix sum. The same arguments therefore apply as before: having just a few species self-regulating cannot stabilize a food web following a cascade structure, and a handful of non-self-regulating species are sufficient to destabilize it.
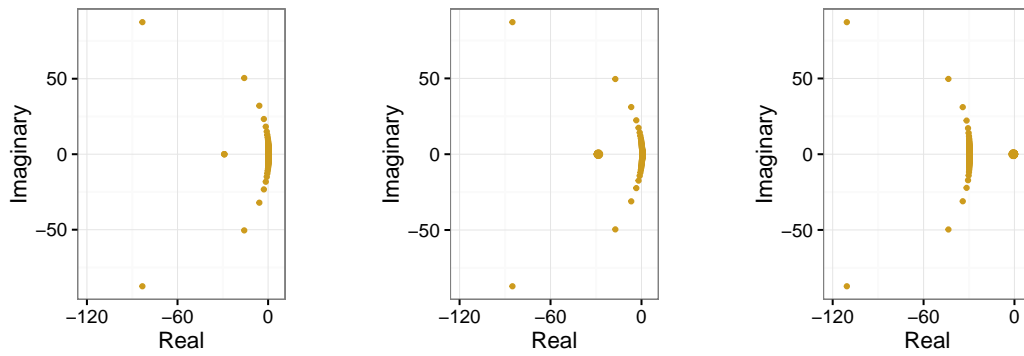
Supplementary Figure 10: Behavior of the spectrum (yellow points) of the matrix $\mathbf{H}+\mathbf{D}$, given by Eq. 2.20. Parameters are $S = 500$, $\mu_{\mathrm{L}} = 0.05$, $\mu_{\mathrm{U}} = -1$, and diagonal entries are randomly sampled to be either -30 with probability P or 0 with probability $1-P$. The probability of self-regulation is $P = 0.01$ (left), $P = 0.1$ (center), and $P = 0.9$ (right). In all cases the effect of the diagonal entries is mostly decoupled from those of the offdiagonal ones. Due to this special property of $\mathbf{H}+\mathbf{D}$, one may indeed think of a cascade matrix with self-regulation as a low-rank perturbed elliptic matrix, plus another low-rank perturbation pertaining to self-regulation.

3   Quaternions

Let $a, b \in \mathbb{R}$. By introducing the imaginary unit i with the property $\mathrm{i}^2 = -1$, a complex number $z \in \mathbb{C}$ can be written as $z = a + b\mathrm{i}$. In analogy with this construction, one may define two further symbols j and k, with the following multiplication properties:

$$\mathrm{i}^2 = \mathrm{j}^2 = \mathrm{k}^2 = \mathrm{ijk} = -1, \quad \mathrm{ij} = \mathrm{k}, \quad \mathrm{ji} = -\mathrm{k}, \quad \mathrm{jk} = \mathrm{i}, \quad \mathrm{kj} = -\mathrm{i}, \quad \mathrm{ki} = \mathrm{j}, \quad \mathrm{ik} = -\mathrm{j}. \quad (3.1)$$

If now $a, b, c, d \in \mathbb{R}$, we can form the following quadruplet, called a *quaternion*:

$$q = a + b\mathrm{i} + c\mathrm{j} + d\mathrm{k}. \quad (3.2)$$

The set of quaternions is denoted $\mathbb{H}$, in honor of Sir William Rowan Hamilton, who first introduced them and studied their properties in the mid-19th century.

A more convenient way of writing quaternions is provided by using $\mathrm{ij} = \mathrm{k}$ in Eq. 3.1. Then any quaternion $q \in \mathbb{H}$ can be written

$$q = a + b\mathrm{i} + c\mathrm{j} + d\mathrm{k} = a + b\mathrm{i} + c\mathrm{j} + d\mathrm{ij} = (a + b\mathrm{i}) + (c + d\mathrm{i})\mathrm{j} = z + u\mathrm{j}, \quad (3.3)$$

where we have introduced the two complex numbers $z = a + b\mathrm{i}$ and $u = c + d\mathrm{i}$. Using this equivalent form of quaternions, we can introduce the two basic algebraic operations of addition and multiplication.

Addition of two quaternions $q_1 = z_1 + u_1\mathrm{j}$ and $q_2 = z_2 + u_2\mathrm{j}$ simply follows

$$q_1 + q_2 = (z_1 + u_1\mathrm{j}) + (z_2 + u_2\mathrm{j}) = (z_1 + z_2) + (u_1 + u_2)\mathrm{j}, \quad (3.4)$$

the sum also being a quaternion. Multiplication is a little more subtle. Unlike for real or complex numbers, quaternion multiplication is not commutative: $q_1 q_2$ is in general not equal to $q_2 q_1$. For example, let $z = a + b\mathrm{i}$ with $a, b \in \mathbb{R}$. Then,

$$z\mathrm{j} = (a + b\mathrm{i})\mathrm{j} = a\mathrm{j} + b\mathrm{k}, \quad (3.5)$$

but

$$jz = j(a + bi) = aj - bk, \tag{3.6}$$

where $ij = k$ and $ji = -k$ were used from Eq. 3.1. Therefore, $zj = j\bar{z}$, where the overbar denotes complex conjugation. We can now write the general multiplication rule:

$$(z_1 + u_1 j)(z_2 + u_2 j) = z_1 z_2 + z_1 u_2 j + u_1 j z_2 + u_1 j u_2 j = z_1 z_2 + z_1 u_2 j + u_1 \bar{z}_2 j + u_1 \bar{u}_2 j^2, \tag{3.7}$$

which, using $j^2 = -1$ from Eq. 3.1, reads

$$(z_1 + u_1 j)(z_2 + u_2 j) = (z_1 z_2 - u_1 \bar{w}_2) + (z_1 u_2 + u_1 \bar{z}_2)j. \tag{3.8}$$

The product is itself a quaternion. Both addition and multiplication are therefore closed operations which do not lead out of the original quaternionic set.

In analogy with complex conjugation, one can introduce the conjugate $\bar{q}$ of a quaternion q. Writing q as $q = a + bi + cj + dk = z + uj$, we have

$$\bar{q} = a - bi - cj - dk = \bar{z} - uj. \tag{3.9}$$

The product $q\bar{q}$ is the squared norm $|q|^2$ of the quaternion, which is real, nonnegative, and zero if and only if $q = 0$:

$$\begin{aligned} |q|^2 = q\bar{q} = (z + uj)(\bar{z} - uj) &= z\bar{z} - zuj + uj\bar{z} - uj uj = z\bar{z} - zuj + uzj - u\bar{u}j^2 \\ &= z\bar{z} + u\bar{u} = |z|^2 + |u|^2. \end{aligned} \tag{3.10}$$

It is easy to show that $q\bar{q} = \bar{q}q$, therefore the order of multiplication, in this case, does not matter. Indeed,

$$|q|^2 = \bar{q}q = (\bar{z} - uj)(z + uj) = \bar{z}z + \bar{z}uj - ujz - u\bar{u}j^2 = \bar{z}z + u\bar{u} = |z|^2 + |u|^2, \tag{3.11}$$

which is the same as before.

Let $q \in \mathbb{H}$ be nonzero. The inverse q^{-1} of q is, by definition, the quaternion such that $q^{-1}q = 1$. Note that, although multiplication is noncommutative, the inverse is always unique: $qq^{-1} = q^{-1}q = 1$. Indeed, were we to introduce a "right-inverse" q_R^{-1} such that $qq_R^{-1} = 1$, and a "left-inverse" q_L^{-1} such that $q_L^{-1}q = 1$, we would have $qq_R^{-1} = q_L^{-1}q$, and after multiplying by q_R^{-1} from the right, we have $(qq_R^{-1})q_R^{-1} = q_L^{-1}(qq_R^{-1})$, showing that $q_R^{-1} = q_L^{-1}$. To calculate the inverse, one can rely on the conjugate, just as in the case of complex numbers:

$$q^{-1} = \frac{\bar{q}}{|q|^2} = \frac{\bar{q}}{q\bar{q}} = \frac{\bar{z} - uj}{|z|^2 + |u|^2}. \tag{3.12}$$

Multiplying this with q, we get 1, therefore the above expression is indeed the inverse of q. The inverse is itself a quaternion: for any nonzero $q \in \mathbb{H}$, we have $q^{-1} \in \mathbb{H}$, as seen from the above formula.

Finally, we introduce the following notation for future convenience. Let $q_1 = z_1 + u_1 j$ and $q_2 = z_2 + u_2 j$ be two quaternions. Their *entrywise product* $q_1 \circ q_2$ is, by definition,

$$q_1 \circ q_2 = (z_1 + u_1 j) \circ (z_2 + u_2 j) = z_1 z_2 + u_1 u_2 j. \tag{3.13}$$

4   The method of quaternionic resolvents

4.1   Spectral density and the resolvent for symmetric matrices

Let $\mathbf{M}$ be a symmetric $S \times S$ matrix with spectral density $w(x)$; due to symmetry, $x \in \mathbb{R}$. One disadvantage of the function $w(x)$ is that it is difficult to use for direct calculations. A much more wieldy object, the *resolvent*, can be defined via

$$G(z) = \int_{\mathbb{R}} \frac{w(x')}{x' - z} \, dx'. \tag{4.1}$$

The above integral has pole singularities at the eigenvalues, where the denominator becomes zero. This problem is circumvented by allowing z to be complex, and considering the resolvent as a function of $z \in \mathbb{C}$. Knowing the resolvent, the spectral distribution can be recovered with the formula

$$w(x) = -\frac{1}{\pi} \lim_{\varepsilon \to 0^+} \mathrm{Im}(G(x + \varepsilon i)), \tag{4.2}$$

where ε approaches zero from positive values and $\mathrm{Im}(\cdot)$ denotes the imaginary part.

It is easy to show that this equation holds. By Eq. 1.7 the spectral distribution of any given matrix is a sum of Dirac deltas. One way of defining the Dirac delta function is

$$\delta(x) = \frac{1}{\pi} \lim_{\varepsilon \to 0^+} \frac{\varepsilon}{x^2 + \varepsilon^2}. \tag{4.3}$$

But the fraction above can also be written as $\mathrm{Im}(1/(x - \varepsilon i))$. Indeed,

$$\mathrm{Im}\left(\frac{1}{x - \varepsilon i}\right) = \mathrm{Im}\left(\frac{x + \varepsilon i}{(x - \varepsilon i)(x + \varepsilon i)}\right) = \mathrm{Im}\left(\frac{x + \varepsilon i}{x^2 + \varepsilon^2}\right) = \frac{\varepsilon}{x^2 + \varepsilon^2}. \tag{4.4}$$

Therefore,

$$\delta(x) = \frac{1}{\pi} \lim_{\varepsilon \to 0^+} \frac{\varepsilon}{x^2 + \varepsilon^2} = \frac{1}{\pi} \lim_{\varepsilon \to 0^+} \mathrm{Im}\left(\frac{1}{x - \varepsilon i}\right). \tag{4.5}$$

We now write $w(x)$ using Eqs. 4.1 and 4.2:

$$w(x) = -\frac{1}{\pi} \lim_{\varepsilon \to 0^+} \mathrm{Im}\left(\int_{\mathbb{R}} \frac{w(x')}{x' - x + \varepsilon i} \, dx'\right) = \frac{1}{\pi} \lim_{\varepsilon \to 0^+} \int_{\mathbb{R}} \frac{w(x')\varepsilon}{(x' - x)^2 + \varepsilon^2} \, dx', \tag{4.6}$$

where we used Eq. 4.4 in the last step. Substituting $w(x')$ from Eq. 1.7, we continue to write

$$
\begin{aligned}
w(x) &= \frac{1}{\pi} \lim_{\varepsilon \to 0^+} \int_{\mathbb{R}} \frac{1}{S} \sum_{i=1}^{S} \delta(\lambda_i - x') \frac{\varepsilon}{(x' - x)^2 + \varepsilon^2} \, dx' = \frac{1}{\pi} \lim_{\varepsilon \to 0^+} \frac{1}{S} \sum_{i=1}^{S} \frac{\varepsilon}{(\lambda_i - x)^2 + \varepsilon^2} \\
&= \frac{1}{S} \sum_{i=1}^{S} \underbrace{\left(\frac{1}{\pi} \lim_{\varepsilon \to 0^+} \frac{\varepsilon}{(\lambda_i - x)^2 + \varepsilon^2}\right)}_{\delta(\lambda_i - x)} = \frac{1}{S} \sum_{i=1}^{S} \delta(\lambda_i - x),
\end{aligned}
\tag{4.7}
$$

which is equal to $w(x)$ by Eq. 1.7. This shows that Eq. 4.2 indeed recovers the spectral distribution.

The resolvent can be used to calculate the spectral distribution of the sum of a symmetric random matrix $\mathbf{M}$ and another "deterministic" symmetric matrix $\mathbf{D}$ with known spectral distribution $p(x)$. Let $\mathbf{M}$ be a standard elliptic matrix with $\rho = 1$ (Section 1.3); the correlation of unity ensures

symmetry. The spectral distribution of $\mathbf{M}$ then reduces to the Wigner semicircle law (Wigner 1958). The resolvent $G(z)$ of $\mathbf{M} + \mathbf{D}$ is given by the formula of Pastur (1972):

$$G(z) = G_{\mathbf{D}}(z + G(z)), \tag{4.8}$$

where $G_{\mathbf{D}}(z)$ is the resolvent of $\mathbf{D}$. This can be written, using Eq. 4.1 and the fact that $\mathbf{D}$'s spectral distribution is given by $p(x)$, as

$$G_{\mathbf{D}}(z) = \int_{\mathbb{R}} \frac{p(x')}{x' - z} \, dx'. \tag{4.9}$$

Therefore, Eq. 4.8 reads

$$G(z) = \int_{\mathbb{R}} \frac{p(x')}{x' - z - G(z)} \, dx'. \tag{4.10}$$

Solving this equation for $G(z)$ yields the resolvent.

Below, we extend this method to the nonsymmetric case.

4.2   Spectral density and the resolvent for nonsymmetric matrices

Let $\mathbf{M}$ be a standard elliptic matrix with spectral density $w(z)$, $z \in \mathbb{C}$ (Section 1.3). Just as in the symmetric case, direct calculations with $w(z)$ are cumbersome: it is more convenient to do calculations with the resolvent

$$G(z) = \int_{\mathbb{C}} \frac{w(z')}{z' - z} \, dz'. \tag{4.11}$$

The integration goes across the whole complex plane, since the eigenvalues are themselves complex. However, this means that the resolvent has pole singularities whenever z is equal to one of the eigenvalues. To regularize the resolvent, one must consider the quaternionic resolvent $G(q) \in \mathbb{H}$, as a function of the quaternionic argument $q \in \mathbb{H}$ (Rogers 2010). The quaternionic resolvent reads

$$G(q) = \int_{\mathbb{C}} w(z')(z' - q)^{-1} \, dz', \tag{4.12}$$

which is well-defined as long as $q = z + u\mathrm{j}$ with $u \neq 0$. Note that, since quaternionic multiplication is not commutative, we use the inverse notation q^{-1} for quaternions.

As in the symmetric case, the spectral density function can be recovered from the resolvent—this time via the formula

$$w(z) = -\frac{1}{\pi} \lim_{\varepsilon \to 0^+} \mathrm{Re}\left(\frac{\partial}{\partial \bar{z}} G(z + \varepsilon \mathrm{j}) \right) \tag{4.13}$$

(Rogers 2010), where $\mathrm{Re}(\cdot)$ denotes the real part, ε approaches zero from positive values, and $\partial/\partial \bar{z}$ is the antiholomorphic derivative, which can also be written in terms of components: if $z = x + y\mathrm{i}$ with $x, y \in \mathbb{R}$, we have

$$\frac{\partial}{\partial \bar{z}} = \frac{1}{2}\left(\frac{\partial}{\partial x} + \mathrm{i} \frac{\partial}{\partial y} \right). \tag{4.14}$$

Using this, the spectral density reads

$$w(z) = -\frac{1}{2\pi} \lim_{\varepsilon \to 0^+} \mathrm{Re}\left(\left(\frac{\partial}{\partial x} + \mathrm{i} \frac{\partial}{\partial y} \right) G(x + y\mathrm{i} + \varepsilon \mathrm{j}) \right). \tag{4.15}$$

In principle, the limit must be taken after the real part of the derivative is evaluated. In practice, this only makes a difference if the derivative behaves singularly at $\varepsilon = 0$. As long as this is not the case, we can take the limit right away and write

$$w(z) = -\frac{1}{2\pi}\operatorname{Re}\left(\left(\frac{\partial}{\partial x} + i\frac{\partial}{\partial y}\right)G(x+yi)\right). \tag{4.16}$$

In our applications, there is never any singular behavior at $\varepsilon = 0$, so Eq. 4.16 can be used.

The generalization of Pastur's (1972) formula Eq. 4.8 to the nonsymmetric case was derived by Rogers (2010):

$$G(q) = G_{\mathbf{D}}(q + (\rho + j) \circ G(q)). \tag{4.17}$$

Let the spectral density of $\mathbf{D}$ be given by $p(h)$; the resolvent $G_{\mathbf{D}}(h)$ then reads

$$G_{\mathbf{D}}(h) = \int_{\mathbb{C}} p(h)(h-q)^{-1}\,\mathrm{d}h. \tag{4.18}$$

Substituting into Eq. 4.17, we get

$$G(q) = \int_{\mathbb{C}} p(h)(h-q-(\rho+j)\circ G(q))^{-1}\,\mathrm{d}h. \tag{4.19}$$

4.3   Calculation of the quaternionic resolvent

Let $\mathbf{M}$ be a standard elliptic matrix (Section 1.3), and let $\mathbf{D}$ be a matrix of known spectral density $p(h)$, with resolvent $G_{\mathbf{D}}(h)$. Let $G(q)$ be the resolvent of $\mathbf{M} + \mathbf{D}$. Our task is to find this resolvent, and use it to obtain the spectral distribution of $\mathbf{M} + \mathbf{D}$ via Eq. 4.13.

We start from Eq. 4.19. Writing $q = z + \varepsilon j$ and taking the $\varepsilon \to 0^+$ limit now (as stated before, this can be done unless the resolvent is singular at $\varepsilon = 0$), this simplifies to

$$G(z) = \int_{\mathbb{C}} p(h)(h-z-(\rho+j)\circ G(z))^{-1}\,\mathrm{d}h. \tag{4.20}$$

Since G is quaternionic, we can write it as $G = \alpha + \beta j$ (we suppressed the arguments for better readability). We now have

$$\alpha + \beta j = \int_{\mathbb{C}} p(h)(h-z-\rho\alpha-\beta j)^{-1}\,\mathrm{d}h, \tag{4.21}$$

where we used the entrywise product rule of Eq. 3.13. Using the conjugate to express the inverse as in Eq. 3.12, this is equivalently written as

$$\alpha + \beta j = \int_{\mathbb{C}} p(h)\frac{\bar{h}-\bar{z}-\rho\bar{\alpha}+\beta j}{|h-z-\rho\alpha|^2+|\beta|^2}\,\mathrm{d}h, \tag{4.22}$$

where the denominator is now a nonnegative real number.

Both sides of this equation are quaternionic. Two quaternions $q_1 = z_1 + u_1 j$ and $q_2 = z_2 + u_2 j$ are equal if and only if $z_1 = z_2$ and $u_1 = u_2$ simultaneously. We can therefore write

$$\beta = \int_{\mathbb{C}} p(h)\frac{\beta}{|h-z-\rho\alpha|^2+|\beta|^2}\,\mathrm{d}h, \tag{4.23}$$

$$\alpha = \int_{\mathbb{C}} p(h)\frac{\bar{h}-\bar{z}-\rho\bar{\alpha}}{|h-z-\rho\alpha|^2+|\beta|^2}\,\mathrm{d}h. \tag{4.24}$$

From the first of these equations, we can see that $\beta = 0$ is always a solution. Whether it leads to a positive spectral density has to be ascertained by solving for α via Eq. 4.24 (setting $|\beta|^2 = 0$), and evaluating $w(z)$ using Eq. 4.13. Otherwise, assuming $\beta \neq 0$, Eqs. 4.23 and 4.24 read

$$1 = \int_{\mathbb{C}} p(h) \frac{1}{|h - z - \rho\alpha|^2 + |\beta|^2} \, dh, \tag{4.25}$$

$$\alpha = \int_{\mathbb{C}} p(h) \frac{\bar{h} - \bar{z} - \rho\bar{\alpha}}{|h - z - \rho\alpha|^2 + |\beta|^2} \, dh. \tag{4.26}$$

Writing $\alpha \in \mathbb{C}$ as $\alpha = \alpha_{re} + \alpha_{im}i$ with $\alpha_{re}, \alpha_{im} \in \mathbb{R}$, we have

$$1 = \int_{\mathbb{C}} p(h) \frac{1}{|h - z - \rho(\alpha_{re} + \alpha_{im}i)|^2 + |\beta|^2} \, dh, \tag{4.27}$$

$$\alpha_{re} + \alpha_{im}i = \int_{\mathbb{C}} p(h) \frac{\bar{h} - \bar{z} - \rho(\alpha_{re} - \alpha_{im}i)}{|h - z - \rho(\alpha_{re} + \alpha_{im}i)|^2 + |\beta|^2} \, dh. \tag{4.28}$$

We can do the same with $z = x + yi$:

$$1 = \int_{\mathbb{C}} p(h) \frac{1}{|h - x - yi - \rho(\alpha_{re} + \alpha_{im}i)|^2 + |\beta|^2} \, dh, \tag{4.29}$$

$$\alpha_{re} + \alpha_{im}i = \int_{\mathbb{C}} p(h) \frac{\bar{h} - x + yi - \rho(\alpha_{re} - \alpha_{im}i)}{|h - x - yi - \rho(\alpha_{re} + \alpha_{im}i)|^2 + |\beta|^2} \, dh. \tag{4.30}$$

Expanding in the denominators:

$$1 = \int_{\mathbb{C}} p(h) \frac{1}{(h - x - \rho\alpha_{re})^2 + (y + \rho\alpha_{im})^2 + |\beta|^2} \, dh, \tag{4.31}$$

$$\alpha_{re} + \alpha_{im}i = \int_{\mathbb{C}} p(h) \frac{\bar{h} - x + yi - \rho(\alpha_{re} - \alpha_{im}i)}{(h - x - \rho\alpha_{re})^2 + (y + \rho\alpha_{im})^2 + |\beta|^2} \, dh. \tag{4.32}$$

In the second equation, the real and imaginary parts must separately be equal. We therefore have the following three equations:

$$1 = \int_{\mathbb{C}} p(h) \frac{1}{(h - x - \rho\alpha_{re})^2 + (y + \rho\alpha_{im})^2 + |\beta|^2} \, dh, \tag{4.33}$$

$$\alpha_{re} = \int_{\mathbb{C}} p(h) \frac{\operatorname{Re}(h) - x - \rho\alpha_{re}}{(h - x - \rho\alpha_{re})^2 + (y + \rho\alpha_{im})^2 + |\beta|^2} \, dh, \tag{4.34}$$

$$\alpha_{im} = \int_{\mathbb{C}} p(h) \frac{-\operatorname{Im}(h) + y + \rho\alpha_{im}}{(h - x - \rho\alpha_{re})^2 + (y + \rho\alpha_{im})^2 + |\beta|^2} \, dh. \tag{4.35}$$

This is a set of three equations for the real variables $|\beta|$, α_{re}, and α_{im}, and is as far as one can go without specifying $p(h)$. The solution gives the quaternionic resolvent $G = \alpha + \beta j$, from which the spectral density can be obtained via Eq. 4.16. One can also use these equations to study properties other than the spectral distribution, such as its support or the spectral abscissa. Below we give examples of using the equations in this way.

4.4 Calculation of the quaternionic resolvent in case the deterministic matrix has purely real eigenvalues

Further simplification is possible if the eigenvalues of $\mathbf{D}$ are purely real. Then $\text{Re}(h) = h$, $\text{Im}(h) = 0$, and the integrals sweep through the real axis only:

$$1 = \int_{\mathbb{R}} p(h) \frac{1}{(h - x - \rho\alpha_{\text{re}})^2 + (y + \rho\alpha_{\text{im}})^2 + |\beta|^2} \, dh, \tag{4.36}$$

$$\alpha_{\text{re}} = \int_{\mathbb{R}} p(h) \frac{h - x - \rho\alpha_{\text{re}}}{(h - x - \rho\alpha_{\text{re}})^2 + (y + \rho\alpha_{\text{im}})^2 + |\beta|^2} \, dh, \tag{4.37}$$

$$\alpha_{\text{im}} = \int_{\mathbb{R}} p(h) \frac{y + \rho\alpha_{\text{im}}}{(h - x - \rho\alpha_{\text{re}})^2 + (y + \rho\alpha_{\text{im}})^2 + |\beta|^2} \, dh. \tag{4.38}$$

The numerator in the last equation does not depend on h. It can therefore be brought out in front of the integral:

$$\alpha_{\text{im}} = (y + \rho\alpha_{\text{im}}) \int_{\mathbb{R}} p(h) \frac{1}{(h - x - \rho\alpha_{\text{re}})^2 + (y + \rho\alpha_{\text{im}})^2 + |\beta|^2} \, dh. \tag{4.39}$$

But the integral is equal to 1 according to Eq. 4.36. We therefore have

$$\alpha_{\text{im}} = y + \rho\alpha_{\text{im}}, \tag{4.40}$$

whose solution is

$$\alpha_{\text{im}} = \frac{y}{1 - \rho}. \tag{4.41}$$

Substituting this back into Eqs. 4.36 and 4.37, we eliminate α_{im}:

$$1 = \int_{\mathbb{R}} p(h) \frac{1}{(h - x - \rho\alpha_{\text{re}})^2 + y^2/(1 - \rho)^2 + |\beta|^2} \, dh, \tag{4.42}$$

$$\alpha_{\text{re}} = \int_{\mathbb{R}} p(h) \frac{h - x - \rho\alpha_{\text{re}}}{(h - x - \rho\alpha_{\text{re}})^2 + y^2/(1 - \rho)^2 + |\beta|^2} \, dh. \tag{4.43}$$

We are therefore left having to solve only these two equations.

5 The effect of diagonal entries on the spectrum of elliptic matrices

In this section we use the quaternionic resolvent method to obtain stability criteria for random ecological networks with varying patterns of self-regulation. The interaction matrix $\mathbf{A}$ is constructed $\mathbf{A} = \mathbf{M} + \mathbf{D}$, where $\mathbf{M}$ is a standard elliptic matrix (Section 1.3), and $\mathbf{D}$ is a diagonal matrix with a known distribution $p(h)$ of its diagonal entries ($h \in \mathbb{R}$). Since for a diagonal matrix the diagonal entries are the eigenvalues themselves, $p(h)$ is also equal to $\mathbf{D}$'s spectral distribution. Then, one can use the method of quaternionic resolvents to calculate the spectral distribution of $\mathbf{A} = \mathbf{M} + \mathbf{D}$. For evaluating network stability, we ultimately would like to know the spectral abscissa $\eta(\mathbf{A})$, defined in Eq. 1.9: $\eta(\mathbf{A}) < 0$ implies local stability.

5.1 Uniformly distributed diagonal entries

Let the diagonal entries of $\mathbf{D}$ be sampled from the uniform distribution

$$p(h) = \frac{\Theta(h - d_1) - \Theta(h - d_2)}{d_2 - d_1}, \tag{5.1}$$

where $d_1 < d_2$, and $\Theta(\cdot)$ is the Heaviside step function, equal to 0 for negative arguments and to 1 otherwise. To obtain the spectral distribution of $\mathbf{A} = \mathbf{M} + \mathbf{D}$, we write the equations for the resolvent via Eqs. 4.42 and 4.43. The integrals evaluate to

$$1 = \frac{\tan^{-1}\left(\dfrac{x + \rho\alpha_{\mathrm{re}} - d_2}{\sqrt{y^2/(1 - \rho)^2 + |\beta|^2}}\right) - \tan^{-1}\left(\dfrac{x + \rho\alpha_{\mathrm{re}} - d_1}{\sqrt{y^2/(1 - \rho)^2 + |\beta|^2}}\right)}{(d_1 - d_2)\sqrt{y^2/(1 - \rho)^2 + |\beta|^2}}, \tag{5.2}$$

$$\alpha_{\mathrm{re}} = \frac{1}{2(d_2 - d_1)} \log\left(\frac{(x + \rho\alpha_{\mathrm{re}} - d_2)^2 + y^2/(1 - \rho)^2 + |\beta|^2}{(x + \rho\alpha_{\mathrm{re}} - d_1)^2 + y^2/(1 - \rho)^2 + |\beta|^2}\right). \tag{5.3}$$

In principle, one should solve this system of equations for α_{re} and β, obtaining an explicit formula for the quaternionic resolvent $G = \alpha_{\mathrm{re}} + \alpha_{\mathrm{im}}\mathrm{i} + \beta\mathrm{j}$, where $\alpha_{\mathrm{im}} = y/(1 - \rho)$ from Eq. 4.41. In practice, the solution cannot be obtained in explicit form. However, what we are really interested in is not the full spectral distribution, but the spectral abscissa $\eta(\mathbf{A})$, determining the stability properties of the system. Since $|\beta| \geq 0$, any point $x + y\mathrm{i}$ in the complex plane can only be part of the support of $w(z)$ if the corresponding $|\beta|$ is nonnegative. The values of $x + y\mathrm{i}$ at which $|\beta|$ becomes exactly zero therefore signal the outer edge of the spectral distribution. We can simplify our search by restricting it along the real axis, i.e., setting $y = 0$. By this we assume that the rightmost point of the spectral distribution along the real axis is also the rightmost point overall (this assumption has been confirmed in every scenario we looked at). We then solve the equations for x in the limit of $|\beta| \to 0$, the largest real root of which yields the spectral abscissa $\eta(\mathbf{A})$.

First we write Eqs. 5.2 and 5.3 for $y = 0$:

$$1 = \frac{\tan^{-1}\left(\dfrac{x + \rho\alpha_{\mathrm{re}} - d_2}{|\beta|}\right) - \tan^{-1}\left(\dfrac{x + \rho\alpha_{\mathrm{re}} - d_1}{|\beta|}\right)}{(d_1 - d_2)|\beta|}, \tag{5.4}$$

$$\alpha_{\mathrm{re}} = \frac{1}{2(d_2 - d_1)} \log\left(\frac{(x + \rho\alpha_{\mathrm{re}} - d_2)^2 + |\beta|^2}{(x + \rho\alpha_{\mathrm{re}} - d_1)^2 + |\beta|^2}\right). \tag{5.5}$$

We can now take the $|\beta| \to 0$ limit. In doing so, notice that the right hand side of the first equation behaves singularly at $|\beta| = 0$. To evaluate the limit, one can use L'Hôpital's rule: take the derivative of the numerator and the denominator separately, and evaluate their ratio at $|\beta| = 0$. Then the two equations read, in the $|\beta| \to 0$ limit, as

$$1 = \frac{1}{(x + \rho\alpha_{\mathrm{re}} - d_2)(x + \rho\alpha_{\mathrm{re}} - d_1)}, \tag{5.6}$$

$$\alpha_{\mathrm{re}} = \frac{1}{d_2 - d_1} \log\left(\left|\frac{x + \rho\alpha_{\mathrm{re}} - d_2}{x + \rho\alpha_{\mathrm{re}} - d_1}\right|\right). \tag{5.7}$$

We now need to solve this system of equations for x. We do this by introducing the new variable $X = x + \rho\alpha_{re}$. We then have

$$1 = \frac{1}{(X - d_2)(X - d_1)}, \tag{5.8}$$

$$\alpha_{re} = \frac{1}{d_2 - d_1}\log\left(\left|\frac{X - d_2}{X - d_1}\right|\right), \tag{5.9}$$

decoupling the two equations. The first is quadratic in X, so the solution can be written immediately:

$$X_\pm = \frac{d_2 + d_1}{2} \pm \sqrt{\left(\frac{d_2 - d_1}{2}\right)^2 + 1}. \tag{5.10}$$

Substituting this back into Eq. 5.9 and simplifying, we get, for α_{re},

$$\alpha_{re,\pm} = \mp\frac{2}{d_2 - d_1}\tanh^{-1}\left(\frac{d_2 - d_1}{\sqrt{(d_2 - d_1)^2 + 4}}\right). \tag{5.11}$$

Since $X = x + \rho\alpha_{re}$, the solution for x reads $x = X_\pm - \rho\alpha_{re,\pm}$. The spectral abscissa $\eta(\mathbf{A})$ is the maximum possible value of x, which we obtain by taking the larger of the two roots. We therefore have $\eta(\mathbf{A}) = X_+ - \rho\alpha_{re,+}$:

$$\eta(\mathbf{A}) = \frac{d_2 + d_1}{2} + \sqrt{\left(\frac{d_2 - d_1}{2}\right)^2 + 1} + \frac{2\rho}{d_2 - d_1}\tanh^{-1}\left(\frac{d_2 - d_1}{\sqrt{(d_2 - d_1)^2 + 4}}\right). \tag{5.12}$$

This expression has some properties that are immediately apparent. First, it is linear in ρ. The dependence on the correlation is therefore especially simple. Second, note that $d_2 + d_1$ is proportional to the mean, and $d_2 - d_1 > 0$ to the standard deviation of the uniform distribution $p(h)$. For fixed mean and correlation, $\eta(\mathbf{A})$ is a monotonically increasing function of the standard deviation. This means that, for a given mean, increasing the variance will always increase $\eta(\mathbf{A})$, and will therefore work towards destabilizing the system, as would be expected in general (Section 1.2). Third, assume momentarily that $\rho = 0$, and that $d_2 = 0$. This means that the species' self-regulation values are uniformly drawn from $[d_1, 0]$, where d_1 is some fixed negative value. We then have

$$\eta(\mathbf{A}) = \frac{d_1}{2} + \sqrt{\left(\frac{d_1}{2}\right)^2 + 1}, \tag{5.13}$$

which is always positive, and approaches zero for $d_1 \to -\infty$. A system with zero correlation and uniformly sampled diagonal entries with an upper bound of $d_2 = 0$ can therefore never be stabilized. Relaxing the requirement of $\rho = 0$, we can see from Eq. 5.12 that any $\rho > 0$ will contribute another positive term to the already positive $\eta(\mathbf{A})$, further destabilizing the system. In conclusion, for $d_2 = 0$, stability can only be achieved by negative correlation.

Take now the $\rho < 0$ case with $d_2 = 0$. Then $\eta(\mathbf{A})$ attains a minimum at some $d_1 < 0$, as is clear by taking derivatives in Eq. 5.12. Beyond this point, increasing the strength of self-regulation by increasing d_1 has a destabilizing effect (Supplementary Figure 11). This is in fact the same phenomenon as in the left panel of Supplementary Figure 7, further supporting the idea that, for negative correlation, the most stabilized communities occur at intermediate self-regulation strengths.
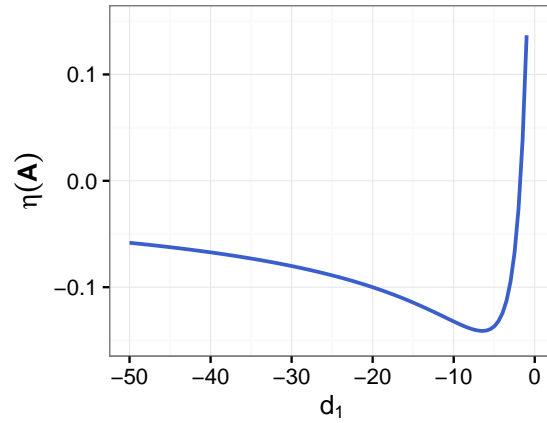
Supplementary Figure 11: Spectral abscissa $\eta(\mathbf{A})$ as a function of d_1, with $\rho = -1/2$ and $d_2 = 0$. The curve has a minimum at some intermediate value of d_1. Just as before in Supplementary Figure 7, increasing the average strength of self-regulation by increasing d_1 becomes destabilizing beyond this point as long as $\rho < 0$.

5.2 Diagonal entries sampled from two discrete values

We now sample the diagonal entries of $\mathbf{D}$ from the distribution

$$p(h) = P\delta(h - d_1) + (1 - P)\delta(h - d_2), \tag{5.14}$$

where $\delta(\cdot)$ is the Dirac delta function. In words, any one diagonal entry will be set equal to d_1 with probability P and to d_2 with probability $1 - P$. Since $\mathbf{D}$ is diagonal, its diagonal entries are also equal to its eigenvalues. We assume $d_1 < d_2$ without loss of generality.

We wish to know the spectral distribution of $\mathbf{A} = \mathbf{M} + \mathbf{D}$, where $\mathbf{M}$ is a standard elliptic matrix. The integrals in Eqs. 4.42 and 4.43 can be evaluated using the Dirac deltas:

$$1 = \frac{P}{(x + \rho\alpha_{\mathrm{re}} - d_1)^2 + y^2/(1 - \rho)^2 + |\beta|^2} + \frac{1 - P}{(x + \rho\alpha_{\mathrm{re}} - d_2)^2 + y^2/(1 - \rho)^2 + |\beta|^2}, \tag{5.15}$$

$$\alpha_{\mathrm{re}} = -\frac{P(x + \rho\alpha_{\mathrm{re}} - d_1)}{(x + \rho\alpha_{\mathrm{re}} - d_1)^2 + y^2/(1 - \rho)^2 + |\beta|^2} - \frac{(1 - P)(x + \rho\alpha_{\mathrm{re}} - d_2)}{(x + \rho\alpha_{\mathrm{re}} - d_2)^2 + y^2/(1 - \rho)^2 + |\beta|^2}. \tag{5.16}$$

Assuming, as before, that the spectral abscissa lies along the real axis, we can set $y = 0$ and write

$$1 = \frac{P}{(x + \rho\alpha_{\mathrm{re}} - d_1)^2 + |\beta|^2} + \frac{1 - P}{(x + \rho\alpha_{\mathrm{re}} - d_2)^2 + |\beta|^2}, \tag{5.17}$$

$$\alpha_{\mathrm{re}} = -\frac{P(x + \rho\alpha_{\mathrm{re}} - d_1)}{(x + \rho\alpha_{\mathrm{re}} - d_1)^2 + |\beta|^2} - \frac{(1 - P)(x + \rho\alpha_{\mathrm{re}} - d_2)}{(x + \rho\alpha_{\mathrm{re}} - d_2)^2 + |\beta|^2}. \tag{5.18}$$

In the $|\beta| \to 0$ limit, we have

$$1 = \frac{P}{(x + \rho\alpha_{\mathrm{re}} - d_1)^2} + \frac{1 - P}{(x + \rho\alpha_{\mathrm{re}} - d_2)^2}, \tag{5.19}$$

$$\alpha_{\mathrm{re}} = -\frac{P}{x + \rho\alpha_{\mathrm{re}} - d_1} - \frac{1 - P}{x + \rho\alpha_{\mathrm{re}} - d_2}. \tag{5.20}$$

To solve these equations, let us introduce the new variable $X = x - d_2 + \rho\alpha_{re}$ and the new parameter $\Delta = d_2 - d_1 > 0$:

$$1 = \frac{P}{(X+\Delta)^2} + \frac{1-P}{X^2}, \tag{5.21}$$

$$\alpha_{re} = -\frac{P}{X+\Delta} - \frac{1-P}{X}. \tag{5.22}$$

The first equation is a fourth-order polynomial in X. One root is always real and larger than the real part of the other three roots:

$$X = -\frac{\Delta}{2} + \frac{\sqrt{3}}{6}\sqrt{2\Delta^2 + \frac{6\sqrt{3}\Delta(1-2P)\sqrt{Q}}{\sqrt{\Delta^4 + \Delta^2(Q-2) + (Q+1)^2}} - \frac{(\Delta^2-1)^2}{Q} - Q + 4}$$
$$+ \frac{\sqrt{3}}{6}\sqrt{\frac{\Delta^4 + \Delta^2(Q-2) + (Q+1)^2}{Q}}, \tag{5.23}$$

where

$$Q = \Big[\Delta^6 - 3\Delta^4 + \Delta^2\big(54P^2 - 54P + 3\big) - 1$$
$$+ 6\sqrt{3}\Delta\sqrt{(P-1)P(\Delta^6 - 3\Delta^4 + 3\Delta^2(9P^2 - 9P + 1) - 1)}\Big]^{1/3}. \tag{5.24}$$

Substituting Eq. 5.23 into Eq. 5.22 yields α_{re}. The spectral abscissa $\eta(\mathbf{A})$ is then obtained via $\eta(\mathbf{A}) = X + d_2 - \rho\alpha_{re}$:

$$\eta(\mathbf{A}) = X + d_2 + \rho\left(\frac{P}{X+\Delta} + \frac{1-P}{X}\right). \tag{5.25}$$

Like in the uniform case before, the solution is linear in ρ. We can also easily obtain the solution in two limiting cases: $d_1 \to d_2$ and $d_1 \to -\infty$. In the former case, Eqs. 5.21 and 5.22 simplify to

$$1 = \frac{1}{X^2}, \tag{5.26}$$

$$\alpha_{re} = -\frac{1}{X}, \tag{5.27}$$

yielding $X_\pm = \pm 1$, $\alpha_{re,\pm} = \mp 1$. The spectral abscissa $\eta(\mathbf{A}) = X + d_2 - \rho\alpha_{re}$ is given by the larger root:

$$\eta(\mathbf{A}) = 1 + \rho + d_2. \tag{5.28}$$

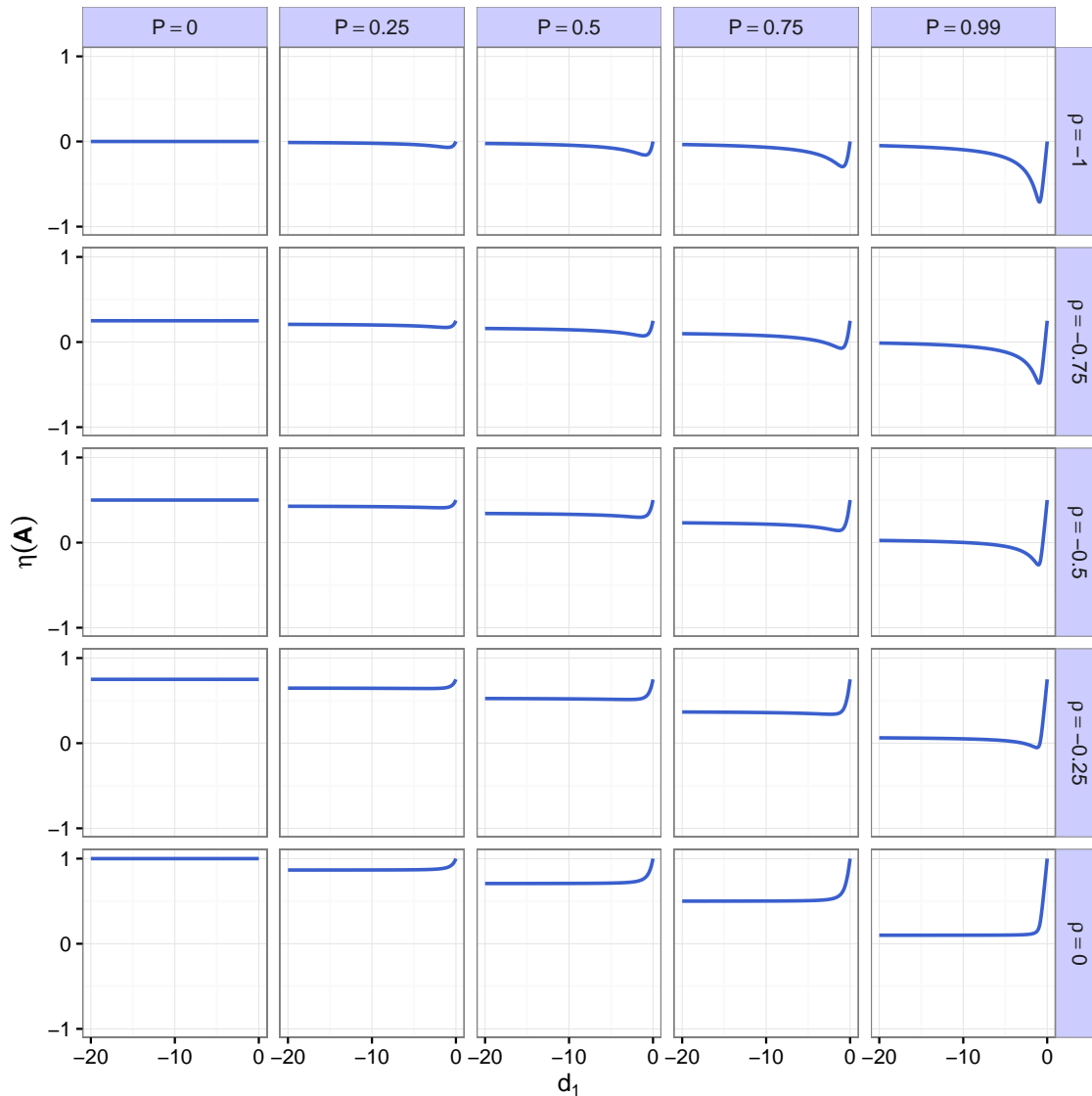In the latter limiting case of $d_1 \to -\infty$, we have

$$1 = \frac{1-P}{X^2}, \tag{5.29}$$

$$\alpha_{re} = -\frac{1-P}{X}, \tag{5.30}$$

yielding $X_\pm = \pm\sqrt{1-P}$, $\alpha_{re,\pm} = \mp\sqrt{1-P}$. The spectral abscissa $\eta(\mathbf{A}) = X + d_2 - \rho\alpha_{re}$ is

$$\eta(\mathbf{A}) = \sqrt{1-P}(1+\rho) + d_2. \tag{5.31}$$

Supplementary Figure 12: Spectral abscissa $\eta(\mathbf{A})$ plotted against $d_1 < 0$ when each diagonal entry of $\mathbf{D}$ is either d_1 or d_2. Here we assume $d_2 = 0$. Insets are for various combinations of ρ (correlation) and P (probability of nonzero self-regulation). The $\rho > 0$ case is not plotted, as stability cannot ever be achieved in that case. Note that the $P = 1$ case is not plotted, as that simply corresponds to the matrix having a constant diagonal, leading to a simple linear relationship between $\eta(\mathbf{A})$ and d_1. However, as long as P is not precisely 1, a very different behavior is observed (rightmost column, corresponding to $P = 0.99$), with intermediate values of d_1 leading to the most stabilized communities.

In between these two extremes, it is easy to map out the behavior of the full solution $\eta(\mathbf{A})$, given by Eq. 5.25. Supplementary Figure 12 shows this, exploring the effect of the three parameters d_1, P, and ρ (setting $d_2 = 0$). The $\rho > 0$ regime is not shown, because this always result in $\eta(\mathbf{A}) > 0$ and therefore an unstable system.

Assume $d_2 = 0$. Biologically, this means that there are two groups of species: those that possess self-regulation (with d_1 in the corresponding diagonal entry of $\mathbf{A} = \mathbf{M} + \mathbf{D}$), and those that do not. In this case, the spectral abscissas for the limiting cases of Eqs. 5.28 and 5.31 are nonnegative. Therefore, the system cannot be stabilized in either of these limits. As before, for $\rho < 0$, stability may be achieved for intermediate values of d_1 (Supplementary Figure 12). This holds as long as there is even just one single species that is not self-regulated.

5.3   The zero-inflated uniform distribution

Let the diagonal entries of $\mathbf{D}$ be sampled from the distribution

$$p(h) = P\frac{\Theta(h - d_1) - \Theta(h - d_2)}{d_2 - d_1} + (1 - P)\delta(h). \tag{5.32}$$

Here $d_1 < d_2$, $\Theta(\cdot)$ is the Heaviside step function (equal to 0 for negative arguments and to 1 otherwise), and $\delta(\cdot)$ is the Dirac delta function. The distribution $p(h)$ is a zero-inflated uniform distribution: each entry is sampled uniformly from $[d_1, d_2]$ with probability P, or else set to zero with probability $1 - P$.

To get the spectral distribution of $\mathbf{A} = \mathbf{M} + \mathbf{D}$, we write the equations for the resolvent via Eqs. 4.42 and 4.43. The integrals evaluate to

$$1 = P\frac{\tan^{-1}\left(\dfrac{x + \rho\alpha_{\mathrm{re}} - d_2}{\sqrt{y^2/(1-\rho)^2 + |\beta|^2}}\right) - \tan^{-1}\left(\dfrac{x + \rho\alpha_{\mathrm{re}} - d_1}{\sqrt{y^2/(1-\rho)^2 + |\beta|^2}}\right)}{(d_1 - d_2)\sqrt{y^2/(1-\rho)^2 + |\beta|^2}} \\ + \frac{1 - P}{(x + \rho\alpha_{\mathrm{re}})^2 + y^2/(1-\rho)^2 + |\beta|^2} \tag{5.33}$$

and

$$\alpha_{\mathrm{re}} = \frac{P}{2(d_2 - d_1)}\log\left(\frac{(x + \rho\alpha_{\mathrm{re}} - d_2)^2 + y^2/(1-\rho)^2 + |\beta|^2}{(x + \rho\alpha_{\mathrm{re}} - d_1)^2 + y^2/(1-\rho)^2 + |\beta|^2}\right) \\ - \frac{(1 - P)(x + \rho\alpha_{\mathrm{re}})}{(x + \rho\alpha_{\mathrm{re}})^2 + y^2/(1-\rho)^2 + |\beta|^2}. \tag{5.34}$$

We look for the spectral abscissa along the real axis, setting $y = 0$:

$$1 = P\frac{\tan^{-1}\left(\dfrac{x + \rho\alpha_{\mathrm{re}} - d_2}{|\beta|}\right) - \tan^{-1}\left(\dfrac{x + \rho\alpha_{\mathrm{re}} - d_1}{|\beta|}\right)}{(d_1 - d_2)|\beta|} + \frac{1 - P}{(x + \rho\alpha_{\mathrm{re}})^2 + |\beta|^2}, \tag{5.35}$$

$$\alpha_{\mathrm{re}} = \frac{P}{2(d_2 - d_1)}\log\left(\frac{(x + \rho\alpha_{\mathrm{re}} - d_2)^2 + |\beta|^2}{(x + \rho\alpha_{\mathrm{re}} - d_1)^2 + |\beta|^2}\right) - \frac{(1 - P)(x + \rho\alpha_{\mathrm{re}})}{(x + \rho\alpha_{\mathrm{re}})^2 + |\beta|^2}, \tag{5.36}$$

and now take the $|\beta| \to 0$ limit, using L'Hôpital's rule in the first term of the right hand side of Eq. 5.35:

$$1 = \frac{P}{(x+\rho\alpha_{re}-d_2)(x+\rho\alpha_{re}-d_1)} + \frac{1-P}{(x+\rho\alpha_{re})^2}, \tag{5.37}$$

$$\alpha_{re} = \frac{P}{d_2-d_1}\log\left(\left|\frac{x+\rho\alpha_{re}-d_2}{x+\rho\alpha_{re}-d_1}\right|\right) - \frac{1-P}{x+\rho\alpha_{re}}. \tag{5.38}$$

Let us introduce the new variable $X = x + \rho\alpha_{re}$:

$$1 = \frac{P}{(X-d_2)(X-d_1)} + \frac{1-P}{X^2}, \tag{5.39}$$

$$\alpha_{re} = \frac{P}{d_2-d_1}\log\left(\left|\frac{X-d_2}{X-d_1}\right|\right) - \frac{1-P}{X}. \tag{5.40}$$

The first of these equations is a fourth-order polynomial in X. Its largest (real) root is

$$\begin{aligned}
X = &\frac{d_1+d_2}{4} + \frac{\sqrt{3}}{12}\sqrt{3d_1^2 - 2d_2d_1 + 3d_2^2 + 4Q/R + 2^{5/3}R + 8} \\
&+ \frac{\sqrt{6}}{12}\left[\frac{3\sqrt{3}(d_1+d_2)\left(d_1^2 - 2d_2d_1 + d_2^2 + 8P - 4\right)}{\sqrt{3d_1^2 - 2d_2d_1 + 3d_2^2 + 4Q/R + 2^{5/3}R + 8}}\right. \\
&\left. + 3d_1^2 - 2d_1d_2 + 3d_2^2 - 2Q/R - 2^{2/3}R + 8\right]^{1/2},
\end{aligned} \tag{5.41}$$

where

$$Q = \sqrt[3]{2}\left[d_1^2\left(d_2^2 - 3P + 3\right) + 2d_2d_1(3P-4) - 3d_2^2(P-1) + 1\right] \tag{5.42}$$

and

$$\begin{aligned}
R = &\left[-9(d_1+d_2)^2(d_1d_2-1)(P-1) - 72d_1d_2(d_1d_2-1)(P-1) + 27(d_1+d_2)^2(P-1)^2\right. \\
&+ 27d_1d_2(d_1+d_2)^2(P-1) + \left[\left\{-9(d_1+d_2)^2(d_1d_2-1)(P-1) - 72d_1d_2\right.\right. \\
&(d_1d_2-1)(P-1) + 27(d_1+d_2)^2(P-1)^2 + 27d_1d_2(d_1+d_2)^2(P-1) \\
&\left.+ 2(d_1d_2-1)^3\right\}^2 - 4\left\{-3(d_1+d_2)^2(P-1) + 12d_1d_2(P-1) + (d_1d_2-1)^2\right\}^3\right]^{1/2} \\
&\left.+ 2(d_1d_2-1)^3\right]^{1/3}.
\end{aligned} \tag{5.43}$$

Next, α_{re} is obtained by substituting the above expression for X into Eq. 5.40. The spectral abscissa $\eta(\mathbf{A}) = X - \rho\alpha_{re}$ is then given by

$$\eta(\mathbf{A}) = X + \rho\left[\frac{1-P}{X} - \frac{P}{d_2-d_1}\log\left(\left|\frac{X-d_2}{X-d_1}\right|\right)\right]. \tag{5.44}$$

The behavior of this solution is qualitatively the same as that of Eq. 5.25, as shown in Supplementary Figure 13 (compare with Supplementary Figure 12). The difference between the two is due to a
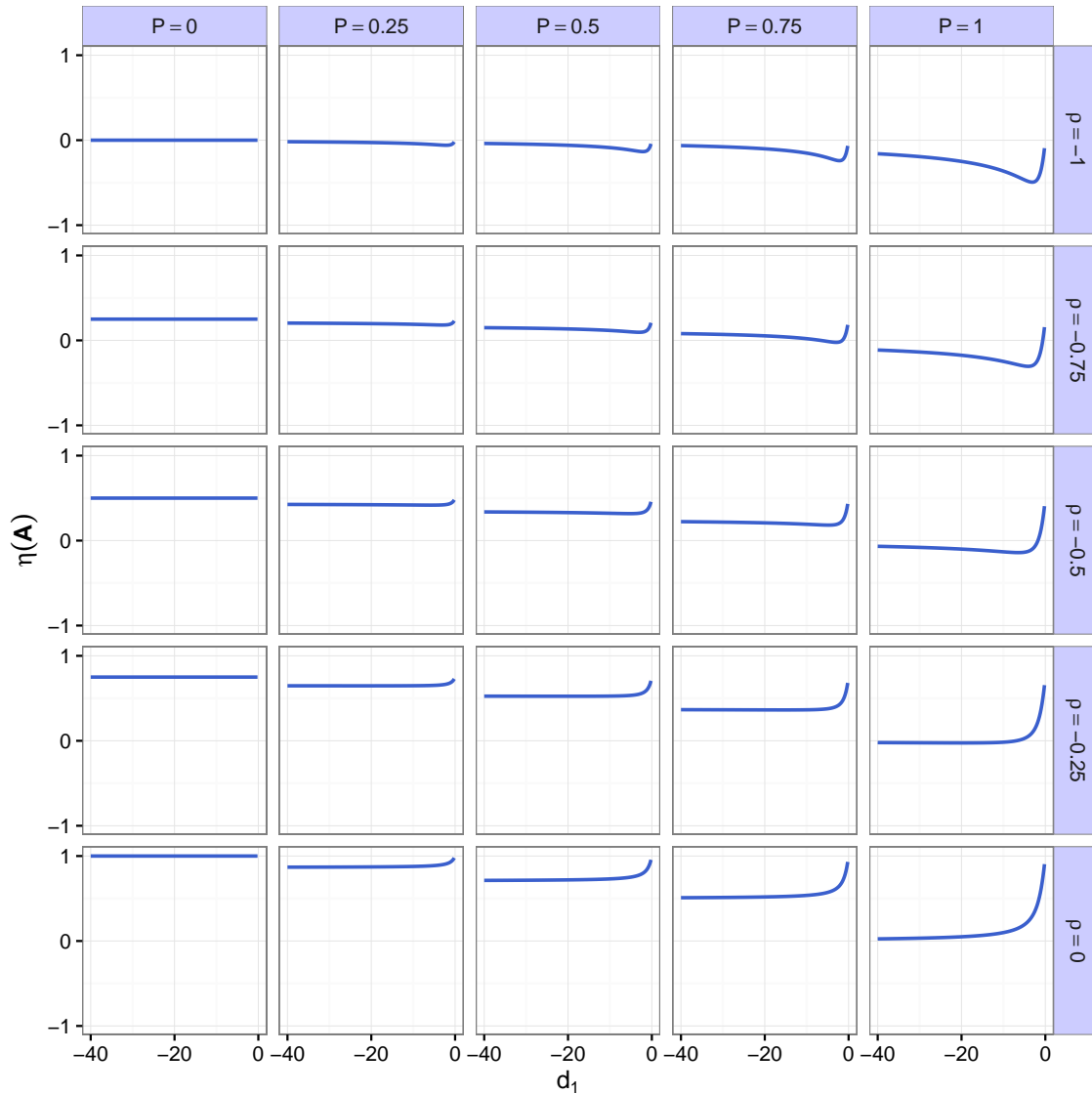
Supplementary Figure 13: The spectral abscissa $\eta(\mathbf{A})$ plotted against $d_1 < 0$ when the diagonal entries are drawn from the zero-inflated uniform distribution Eq. 5.32. Here we assume $d_2 = 0$. Insets are for various combinations of ρ (correlation) and P (probability of nonzero self-regulation). Results are qualitatively the same as in Supplementary Figure 12. Note that here it makes sense to plot results for $P = 1$, which leads to the diagonal being uniformly distributed without zero-inflation—so we recover the results of Section 5.1. The subplot with $P = 1$ and $\rho = -1/2$ is in fact simply a rescaled version of Supplementary Figure 11.

difference in the variance of the diagonal entries, because the eigenvalues acquire more spread along the real axis by having greater diagonal variance (Section 1.2). Assuming $d_2 = 0$, the variance of the distribution given by Eq. 5.14 is $d_1^2 P(1 - P)$, and of the zero-inflated uniform distribution given by Eq. 5.32, $d_1^2 P(1/3 - P/4)$. The first of these has the larger variance for the same values of P and d_1 as long as $P < 8/9$, and will therefore possess a larger $\eta(\mathbf{A})$, leading to diminished chances for stability. For $8/9 < P < 1$, the zero-inflated uniform distribution has the higher variance and therefore $\eta(\mathbf{A})$. These can all be seen by comparing Supplementary Figures 12 and 13.

The results of Section 5.1, 5.2, and 5.3 are exact in the $S \to \infty$ limit. To assess how well they perform for finite S, we can compare their predictions with simulated results—see Supplementary Figures 14 and 15, where this comparison is performed for the case when the diagonal entries are sampled from Eq. 5.14. The approximation works exceptionally well even for $S = 500$. Note that, since the actual matrices are elliptic but not standard elliptic (Section 1.3), the formulae for $\eta(\mathbf{A})$ need to be appropriately rescaled by $\sqrt{SV}$ before they can be applied.

## 5.4 The likelihood of stability in random networks

The most important consequence of the equations that were derived for $\eta(\mathbf{A})$ is that stability can only be reasonably achieved if the fraction of self-regulating species P is very high. Supplementary Figure 16 shows the minimum fraction of self-regulating species P as a function of the correlation ρ and the scaled self-regulation strength $d_1/\sqrt{SV}$, for the cases when the diagonal entries are either sampled from Eq. 5.14 or Eq. 5.32 (we do not consider Eq. 5.1 here, since that is equivalent to Eq. 5.32 with $P = 1$, so all species self-regulate to some extent). Regions where stability is possible without $P \approx 1$ are confined to a small corner of parameter space. Importantly, stability is easy to achieve for either $\rho \approx -1$ or $P \approx 1$ (except in the gray shaded regions, where stability is impossible).

The first of these, $\rho \approx -1$, implies that the effect of predators on prey is exactly the same, just with opposite sign, as the effect of prey on predators. This is a very unlikely scenario, both because it is fine-tuned and because prey generally have a smaller effect on predators than vice versa due to physical limits on the efficiency of energy conversion.

One is therefore left with the other option, $P \approx 1$. The conclusion is the same as in Section 2. The results obtained via the method of quaternionic resolvents can be thought of as a generalization and extension to those obtained via the low-rank perturbation theorem. To stabilize a random network, the vast majority of species must exhibit substantial self-regulation.
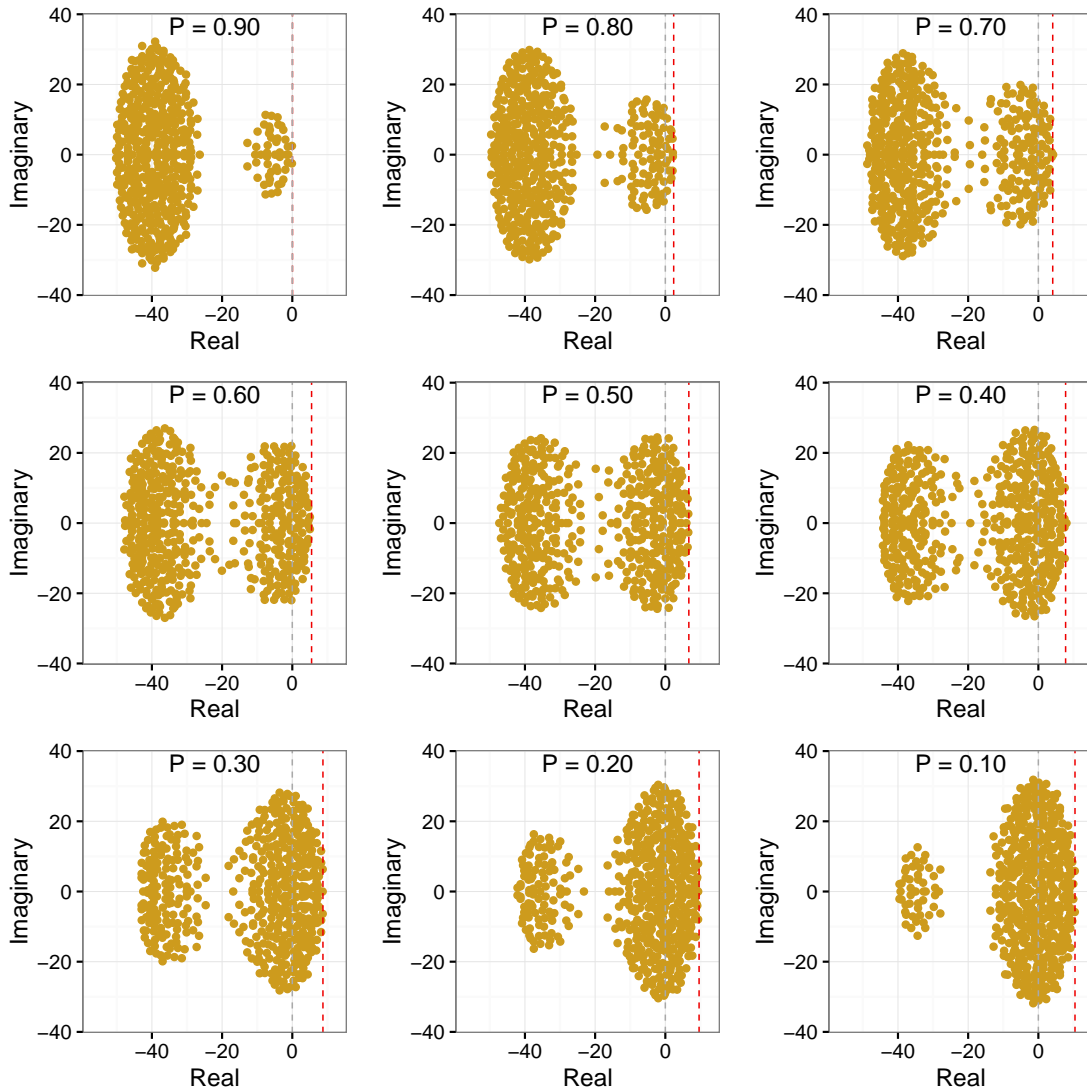
Supplementary Figure 14: Spectra (yellow points) of matrices $\mathbf{A} = \mathbf{M} + \mathbf{D}$. Here $\mathbf{M}$ is a fixed elliptic matrix with $S = 500$, $V = 1$, and $\rho = -1/2$, while $\mathbf{D}$ is sampled from Eq. 5.14 with $d_1 = -40$, $d_2 = 0$, and different values for P (panels). The grey dashed line separates the left and right halves of the complex plane. The red dashed line shows the analytical prediction for $\eta(\mathbf{A})$, calculated from Eq. 5.25 with appropriate rescaling by $\sqrt{SV}$ due to the fact that the matrix, though elliptic, is not standardized. The analytical prediction captures the actual value of $\eta(\mathbf{A})$ very well in all cases.
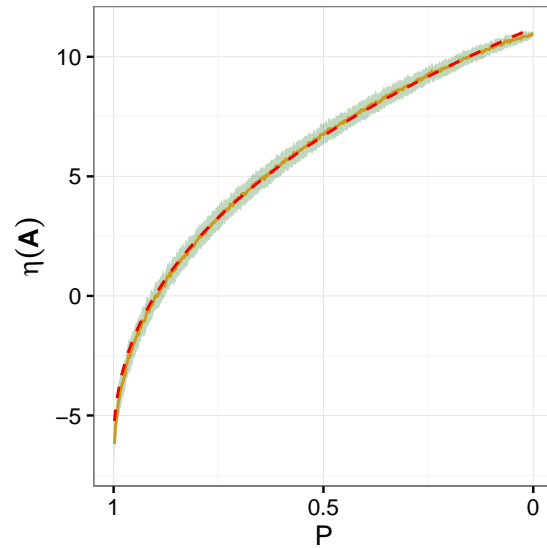
Supplementary Figure 15: As Supplementary Figure 14, but showing only $\eta(\mathbf{A})$ as a function of P, the fraction of self-regulating species. Green band: the standard deviation of $\eta(\mathbf{A})$ out of 100 independent simulated realizations of $\mathbf{D}$. Yellow line: the mean $\eta(\mathbf{A})$ over the 100 realizations. Red dashed line: the theoretical expectation from Eq. 5.25 (notice that it is right on top of the yellow line).
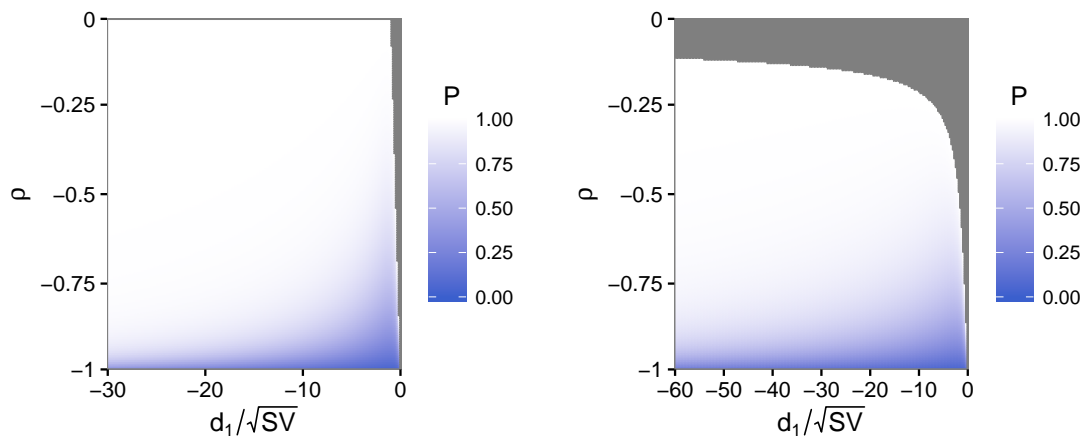
Supplementary Figure 16: The minimum fraction of self-regulating species P needed to stabilize an elliptic matrix, given as a function of ρ and the scaled self-regulation strength $d_1/\sqrt{SV}$. To obtain the minimum P, we use Eqs. 5.25 (left) and 5.44 (right) by finding the smallest $0 \le P \le 1$ for which $\eta(\mathbf{A}) = 0$, for given values of ρ and $d_1/\sqrt{SV}$. Diagonal entries are sampled from Eq. 5.14 (left) and Eq. 5.32 (right); in both cases $d_2 = 0$. Offdiagonal entries form an elliptic matrix, not necessarily standardized—hence the scaling of the diagonal entries by $\sqrt{SV}$. In the gray shaded regions stability cannot be achieved for any value of P. Broadly speaking, stability is only possible for $P \approx 1$ and/or $\rho \approx -1$.

6   The effect of diagonal entries on matrices with cascade structure

As discussed in Section 2.5, a community matrix with cascade structure is written as $\mathbf{A} = \mathbf{H} + \mathbf{Q}$, where the low-rank perturbation $\mathbf{H}$ is given by Eq. 2.13, and $\mathbf{Q}$ is a random matrix with zero mean but different variances in its upper and lower triangular entries. The spectrum of $\mathbf{Q}$ is equivalent to that of an elliptic matrix $\mathbf{M_Q}$, with effective variance and correlation V_{eff} and ρ_{eff} calculated from the raw parameters of the actual ecological network via Eqs. 2.17, 2.18, and 2.19. To evaluate the spectral abscissa of $\mathbf{A} = \mathbf{H} + \mathbf{Q}$, it is therefore sufficient to determine the spectrum of $\mathbf{M_Q} + \mathbf{H}$, which is a low-rank perturbed elliptic matrix.

We add self-regulation to species, using the diagonal matrix $\mathbf{D}$:

$$\mathbf{A} = \mathbf{M_Q} + \mathbf{H} + \mathbf{D}. \tag{6.1}$$

Since the spectrum of $\mathbf{H} + \mathbf{D}$ is known (Supplementary Figure 10), we could apply the method of quaternionic resolvents, via Eqs. 4.33, 4.34, and 4.35. To do so, we need the spectral distribution $p(h)$ of $\mathbf{H} + \mathbf{D}$. Now, in general the joint distribution $p(h)$ *cannot* be written as the simple sum of the spectral distributions. However, in our particular case, this is a reasonable approximation, as evidenced by Supplementary Figure 10. This fortunate coincidence allows one to approximate $p(h)$ as

$$p(h) = \frac{S-k}{S} p_{\mathbf{D}}(h) + \frac{k}{S} \sum_{i=1}^{k} \delta(h - \lambda_i), \tag{6.2}$$

where $p_{\mathbf{D}}(h)$ is the distribution of diagonal entries (given, for instance, by Eq. 5.14), k is the (effective) rank of $\mathbf{H}$ with corresponding nonzero eigenvalues λ_i (given by Eq. 2.14 and shown on Supplementary Figure 9 by the blue circles), and $\delta(\cdot)$ is the Dirac delta function.

Since $k \ll S$, the second term in Eq. 6.2 goes to zero in the limit of large S. As such, it is not expected to influence the spectral distribution except right at the points λ_i, where the term cannot be neglected due to the presence of the Dirac delta peaks. However, the λ_i always lie to the left of the spectral abscissa as long as $|\mu_{\mathrm{L}}| > |\mu_{\mathrm{U}}|$ (Section 2.5, Supplementary Figures 8 & 9; Allesina et al. 2015), and therefore do not have an appreciable impact on $\eta(\mathbf{A})$. Our strategy for calculating $\eta(\mathbf{A})$ is therefore especially simple: take the effective elliptic matrix $\mathbf{M_Q}$ and obtain the spectrum of $\mathbf{M_Q} + \mathbf{D}$ via the method of quaternionic resolvents. This means that all the results of Section 5 carry over; the only difference is that, instead of the actual variance V and correlation ρ, the effective parameters V_{eff} and ρ_{eff} must be used. These in turn can be calculated using Eqs. 2.17, 2.18, and 2.19.

Since to arrive at this simple result we employed two important approximations (the spectrum of the sum of $\mathbf{H}$ and $\mathbf{D}$ decomposes into the sum of the spectra, and the influence of $\mathbf{H}$ on the spectral abscissa is negligible; neither statement can be strictly true), we must check how well the method works in practice. As shown in Supplementary Figures 17 and 18 for a cascade network with $S = 500$, $\eta(\mathbf{A})$ is captured very accurately, showing that the method works in practice.

7   Self-regulation and stability in empirical networks

7.1   Food web parameterization

For investigating how self-regulation affects stability in real-world systems, we looked at two types of data. First, we used published Jacobian matrices that were obtained using an Ecopath modeling
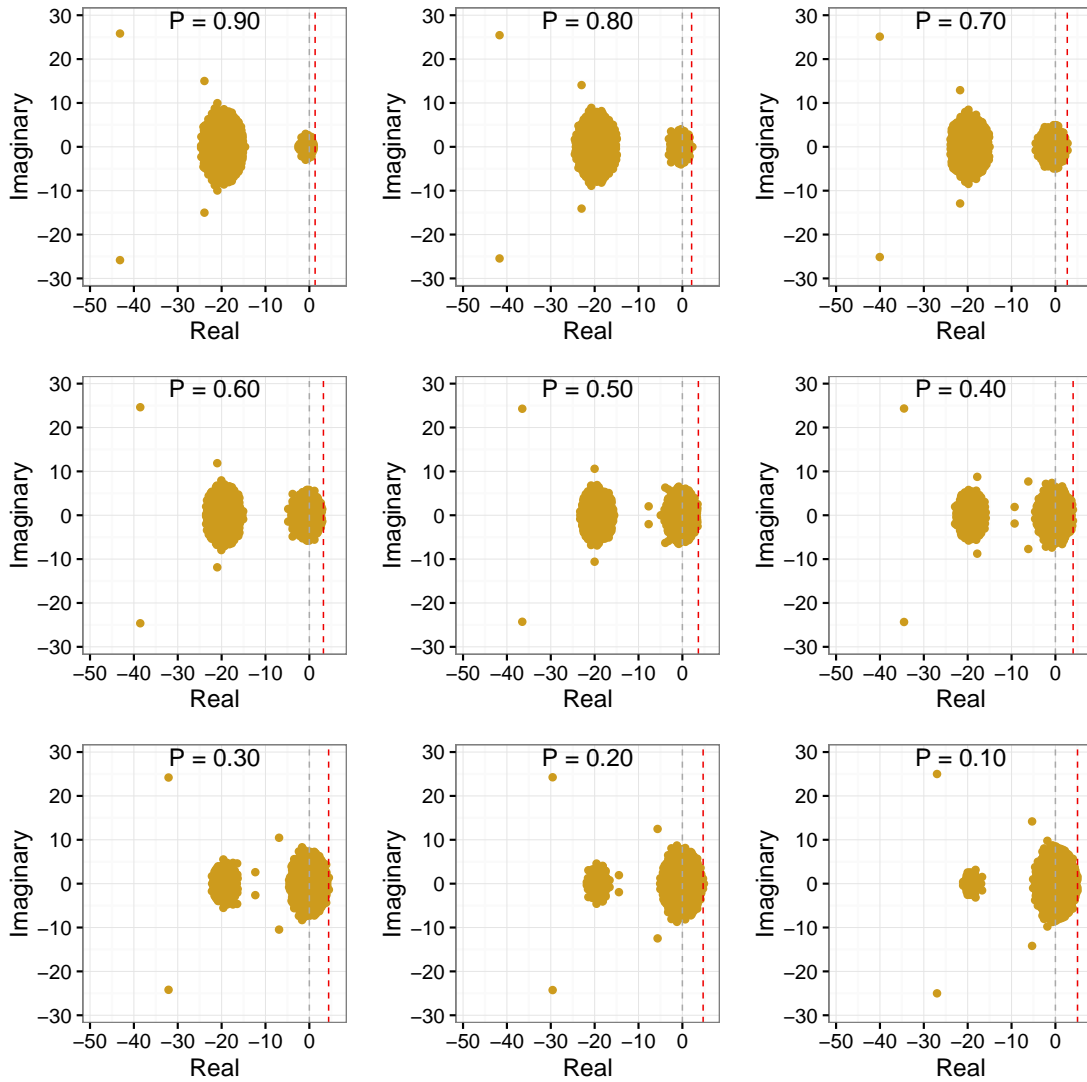
Supplementary Figure 17: Spectra (yellow points) of matrices $\mathbf{A} = \mathbf{Q} + \mathbf{H} + \mathbf{D}$, where $\mathbf{Q} + \mathbf{H}$ yield the cascade structure, and the entries of the diagonal matrix $\mathbf{D}$ are sampled from Eq. 5.14 with $d_1 = -20$, $d_2 = 0$, and different values for P (panels). $\mathbf{H}$ is given by Eq. 2.13, and $\mathbf{Q}$ has zero diagonal, zero mean, variance σ_U^2 for the upper triangular entries, σ_L^2 for the lower triangular ones, and correlation ρ_{UL} between the (i,j)th and (j,i)th entries. The grey dashed line separates the left and right halves of the complex plane. The red dashed line shows the analytical prediction for $\eta(\mathbf{A})$, based on applying Eq. 5.25 to the effective elliptic matrix $\mathbf{M_Q}$ rescaled by $\sqrt{SV_{\text{eff}}}$ because the matrices were not standardized. The analytical prediction captures the actual value of $\eta(\mathbf{A})$ very well in all cases. Parameters: $S = 500$, $\mu_U = -1$, $\mu_L = 0.05$, $\sigma_U = 0.55$, $\sigma_L = 0.055$, $\rho_{UL} = -0.5$.
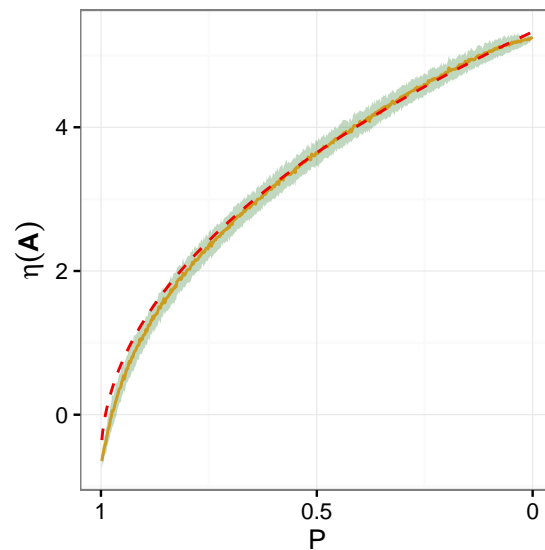
Supplementary Figure 18: As Supplementary Figure 17, but showing only $\eta(\mathbf{A})$ as a function of P, the fraction of self-regulating species. Green band: standard deviation of $\eta(\mathbf{A})$ out of 100 independent simulated realizations of $\mathbf{D}$. Yellow line: the mean $\eta(\mathbf{A})$ over the 100 realizations. Red dashed line: the theoretical expectation from Eq. 5.25, but applied to the low-rank perturbed effective elliptic matrix $\mathbf{M_Q} + \mathbf{H}$.

framework (Jacquet et al. 2016). These were already fully parameterized and therefore ready for direct analysis. Their downside is that even the largest seven Ecopath matrices had only between 39 and 51 species. The webs used in this study are listed in Table 1. Second, we parameterized 12 well-resolved empirical food webs (Table 2), which had between 170 and 484 species. Before parameterizing these matrices, we removed cannibalistic self-loops, and in the few cases two species mutually predated on each other, we dropped one of the two feeding links at random.

To parameterize the adjacency matrices of the well-resolved webs, we followed the methodology in Tang et al. (2014) and Allesina et al. (2015). In brief, we assumed that all nonzero pairs (A_{ij}, A_{ji}) of the interaction matrix $\mathbf{A}$ are determined via body mass scaling allometries and a type I functional response:

$$A_{ij} = -a_{ij}N_i^*, \quad A_{ji} = e_{ij}a_{ij}N_j^*, \tag{7.1}$$

Name	Species	Links	Reference
Chesapeake (present)	41	167	Christensen et al. (2009)
Mid Atlantic Bight	51	515	Okey and Pugliese (2001)
Moorea Barrier Reef	39	267	Arias-Gonzalez et al. (1997)
Newfoundland Grand Banks (1900)	48	519	Heymans and Pitcher (2002)
Newfoundland Grand Banks (mid-1980s)	48	519	Heymans and Pitcher (2002)
Newfoundland Grand Banks (mid-1990s)	48	525	Heymans and Pitcher (2002)
Tampa Bay	48	340	Walters et al. (2005)

Supplementary Table 1: Information on the seven largest Ecopath networks parameterized by Jacquet et al. (2016), with each row corresponding to a different web. Columns indicate, respectively, the name of the web, its number of species S, and number of links L.

where N_i^* are species' equilibrium biomasses, a_{ij} are the attack rates, and e_{ij} the conversion efficiencies. The N_i^* were parameterized using the known linear relationship between numerical abundance N_i^*/m_i and body mass m_i on the log scale (Tang et al. 2014):

$$N_i^* = 10^{n_0+g+\varepsilon_i} m_i^{g+1}, \tag{7.2}$$

where $n_0 = -1.16$, ε_i are drawn from a normal distribution with mean 0 and standard deviation 0.2, and g (controlling the scaling between body mass and equilibrium abundance) was set to either -0.55, -0.75, or -0.95. The body masses m_i were obtained from the database of Brose et al. (2005) on consumer-resource interactions; see Allesina et al. (2015) for details. The attack rates a_{ij} were modeled via

$$a_{ij} = 10^{-3.5} m_j \frac{(m_i/m_j)^{0.46}}{1+(m_i/m_j)^2}, \tag{7.3}$$

where m_j is the consumer and m_i the resource mass. The factor $10^{3.5}$ simply converts units of mass into grams, while the fractional term quantifies the well-documented unimodal relationship between search and consumption rates and size ratios (this choice, as well as the motivations for the numerical values of the exponents, are found in Pawar et al. 2012). Finally, the efficiencies e_{ij} were sampled uniformly from the interval $[0.1, 0.25]$.

Having obtained all the effects of prey on predators and predators on prey (call their distributions X and Y, respectively), they were combined into the bivariate distribution $Z(X,Y)$. The nonzero pairs of entries (A_{ij}, A_{ji}) were then sampled from this bivariate distribution to complete the parameterization of the food webs. Each parameterization was performed three times: with $g = -0.55$, $g = -0.75$, and $g = -0.95$, after Allesina et al. (2015).

Name	Species	Links	Structural rank	Reference
Carpinteria Salt Marsh	272	3878	197	Hechinger et al. (2011)
Flensburg Fjord	180	1567	128	Zander et al. (2011)
Kongs Fjorden	268	1632	164	Jacob et al. (2011)
Little Rock Lake	181	2316	150	Martinez (1991)
Lough Hyne	349	5088	287	Riede et al. (2011)
Otago Harbour	180	1856	158	Mouritsen et al. (2011)
Punta Banda	355	5291	234	Hechinger et al. (2011)
Caribbean Reef	249	3293	204	Opitz (1996)
San Quintin	289	3934	179	Hechinger et al. (2011)
Serengeti	170	585	54	Baskerville et al. (2011)
Sylt Tidal Basin	230	3298	215	Thieltges et al. (2011)
Weddell Sea	484	15435	448	Jacob (2005)

Supplementary Table 2: Well-resolved empirical food web data used in this paper. Each row corresponds to a different food web. Columns indicate, respectively, the name of the web, its number of species S, number of links L, structural rank R_S (which is the maximum possible rank the matrix of the web can attain assuming its nonzero entries are arbitrary; Reinschke 1988), and a reference for the source of the original data.

7.2   Introducing self-regulation

The diagonal entries of the parameterized matrices **A** were set to d with probability P, or to zero with probability $1-P$. This leads to the distribution Eq. 5.14 for the diagonal entries with $d_1 = d$

and $d_2 = 0$. The strength of self-regulation d was chosen as follows. First, the spectral abscissa $\eta(\mathbf{A})$ of each food web was calculated without self-effects. Then, d could take on the values $d = -2^q \, \eta(\mathbf{A})$, where $q = 0.5, 1.5, 2.5, \ldots, 7.5$. That is, eight different strengths of self-regulation were implemented for each web, measured in units of the leading eigenvalue $\eta(\mathbf{A})$. Note that, since the trace of the matrices without the diagonal entries is zero, and the trace is also the sum of all eigenvalues, $\eta(\mathbf{A})$ is necessarily positive; hence the negative sign above in the definition of d.

The protocol for examining food web stability was as follows. We run through each of the 12 webs in Table 2, and each web is parameterized using the three different values of g as described in Section 7.1, leading to 36 combinations. For each of these, the number of self-regulating species was increased one by one from the structural rank (Reinschke 1988; see also below) of the matrix (fewer species self-regulating than this cannot lead to stability) to the total number of species in the given network. The number of self-regulating species divided by their total number yields P. For each value of P, d was varied via the parameter q as described above. For each combination of P and d, the sampling of the diagonal entries was repeated 1000 times. We recorded the fraction of stable matrices out of these 1000 and interpreted the result as the probability of achieving stability with the given P and d. The results are in Supplementary Figures 19-30 (first column).

7.3 Handling rank-deficiency

The empirical webs of Table 2 have the striking (and possibly unrealistic) feature that they are often heavily rank-deficient, containing several rows of entries that are linearly dependent irrespective of parameterization. This has been pointed out before by Haerter et al. (2016) but otherwise has not received much attention. To characterize the algebraic degeneracy of the matrices, we employed the concept of *structural rank*, which is the maximum possible rank a matrix may attain with its nonzero entries being completely arbitrary (Reinschke 1988). The structural rank values are reported in Table 2. The lower this number is compared to the number of species, the more linearly dependent rows the matrix has. Clearly, some of the webs are not much affected by degeneracy (e.g., Weddell Sea), while others, such as Kongs Fjorden or Serengeti, are highly degenerate.

Biologically, linearly dependent rows mean that the species corresponding to those rows are not segregated in their diet. As such, one would expect competitive exclusion to favor the most fit species, driving all the others extinct. Mathematically, this phenomenon manifests itself via the simple fact that an $S \times S$ matrix of rank k necessarily has $S - k$ eigenvalues equal to zero; the system is therefore unstable and will remain so until at least $S - k$ species are removed.

Introducing separate diagonal entries to each such linearly dependent species resolves their algebraic degeneracy. However, as long as even just two species remain linearly dependent, the matrix cannot be stabilized, regardless of the strength of self-regulation. The difference of the number of species S and the structural rank R_S therefore imposes a theoretical minimum on the number of species that must be self-regulating for the system to be stable. In some cases, this theoretical minimum is already very high: for Kongs Fjorden, $S - R_S = 104$, which is 39% of the species, and for Serengeti, $S - R_S = 116$, or 68% of species.

To see if this potentially artifactual limit plays a role in shaping the fraction of species P that must self-regulate to ensure stability, we also considered alternative, extended parameterizations of the food webs such that predators preying on shared resources experience interference competition, and two prey species sharing predators experience indirect positive effects due to the fact that the predator must divide its time eating its multiple resources. Such interference terms arise naturally e.g. in the presence of saturating (type II) functional responses coupling predators and prey.
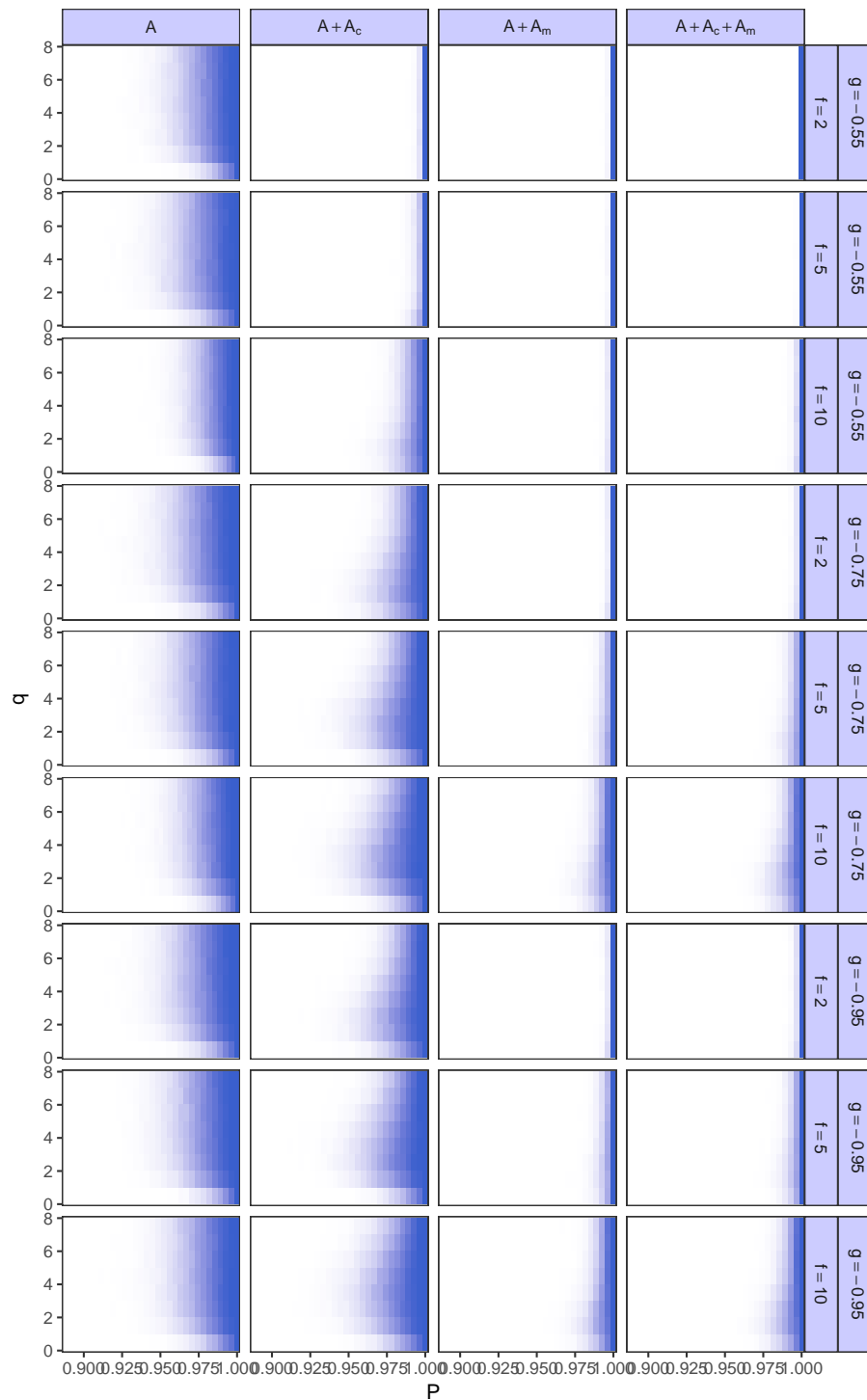
Supplementary Figure 19: Probability of stability (white: 0%; blue: 100%) in the Carpinteria Salt Marsh web (Table 2), as a function of the fraction of self-regulating species P and self-regulation strength q. Rows represent different parameter value combinations of g (Section 7.1) and f (Section 7.3). Columns: 1) no indirect effects; 2) indirect negative effects; 3) indirect positive effects; 4) indirect negative and positive effects (Section 7.3).
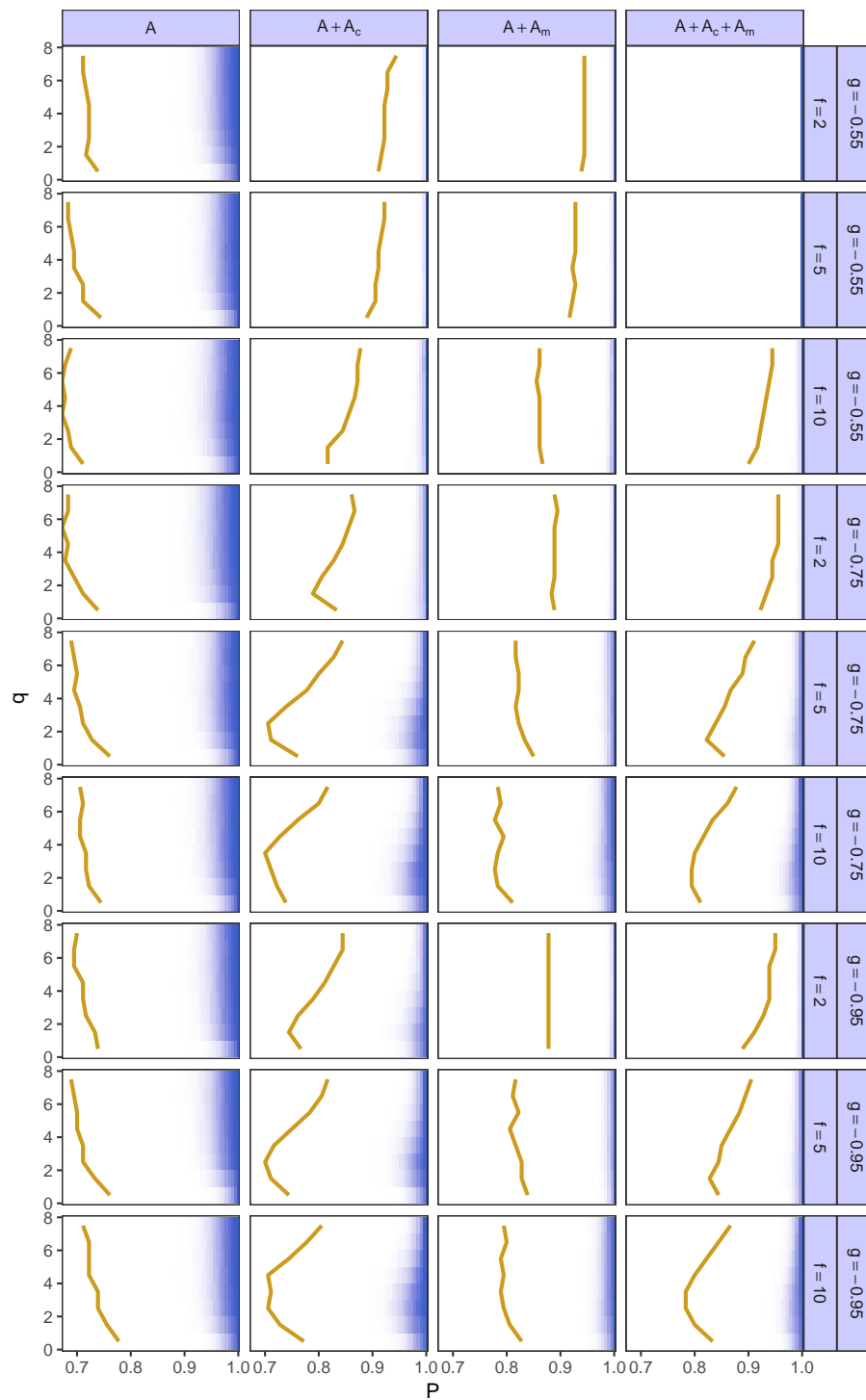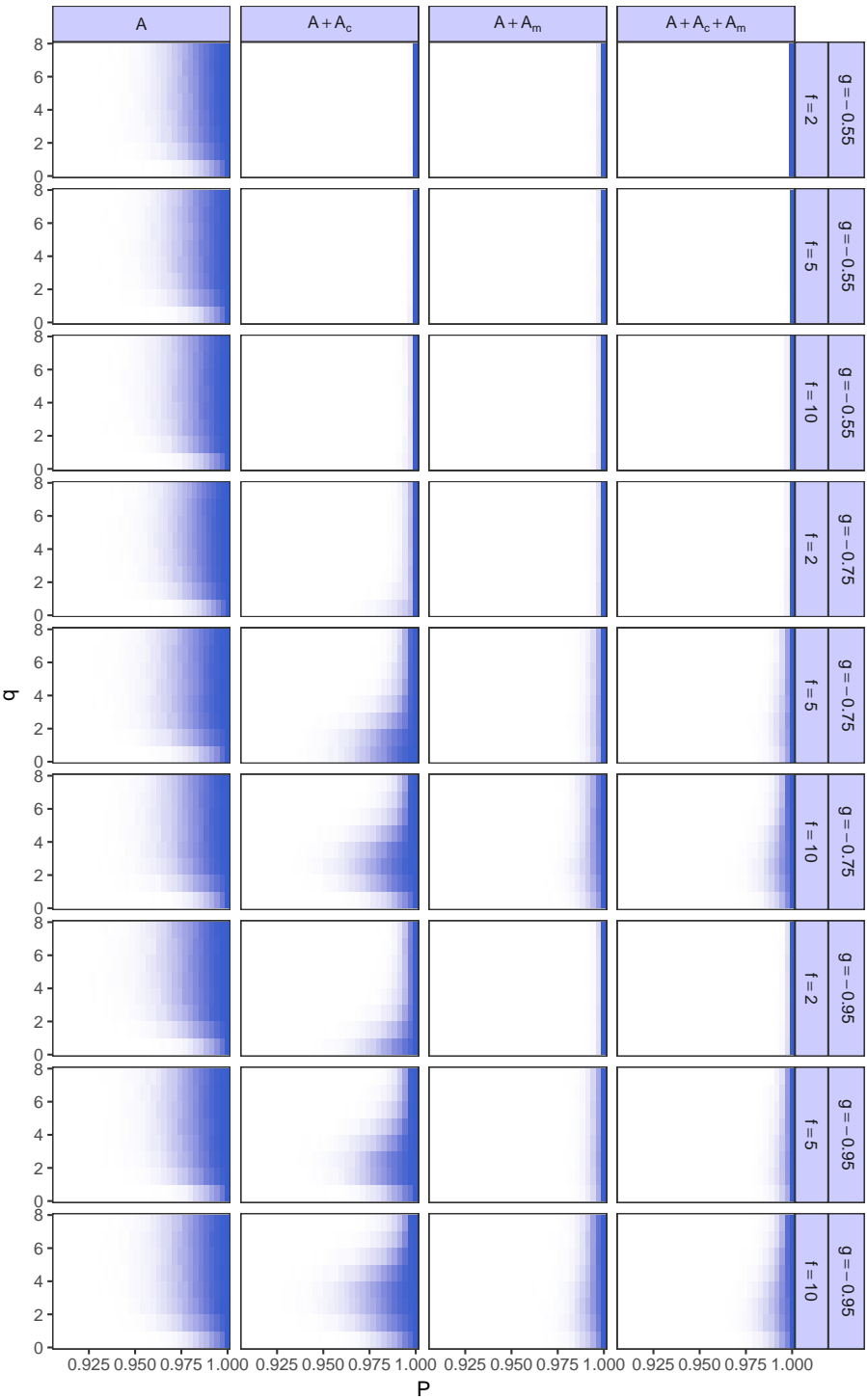
Supplementary Figure 20: As Supplementary Figure 19, but for the Flensburg Fjord web (Table 2). Yellow lines show the minimum fraction of species P that must self-regulate if the network is to be stable at all (Section 7.4). The yellow line is absent if no stable webs were found with $P < 1$.
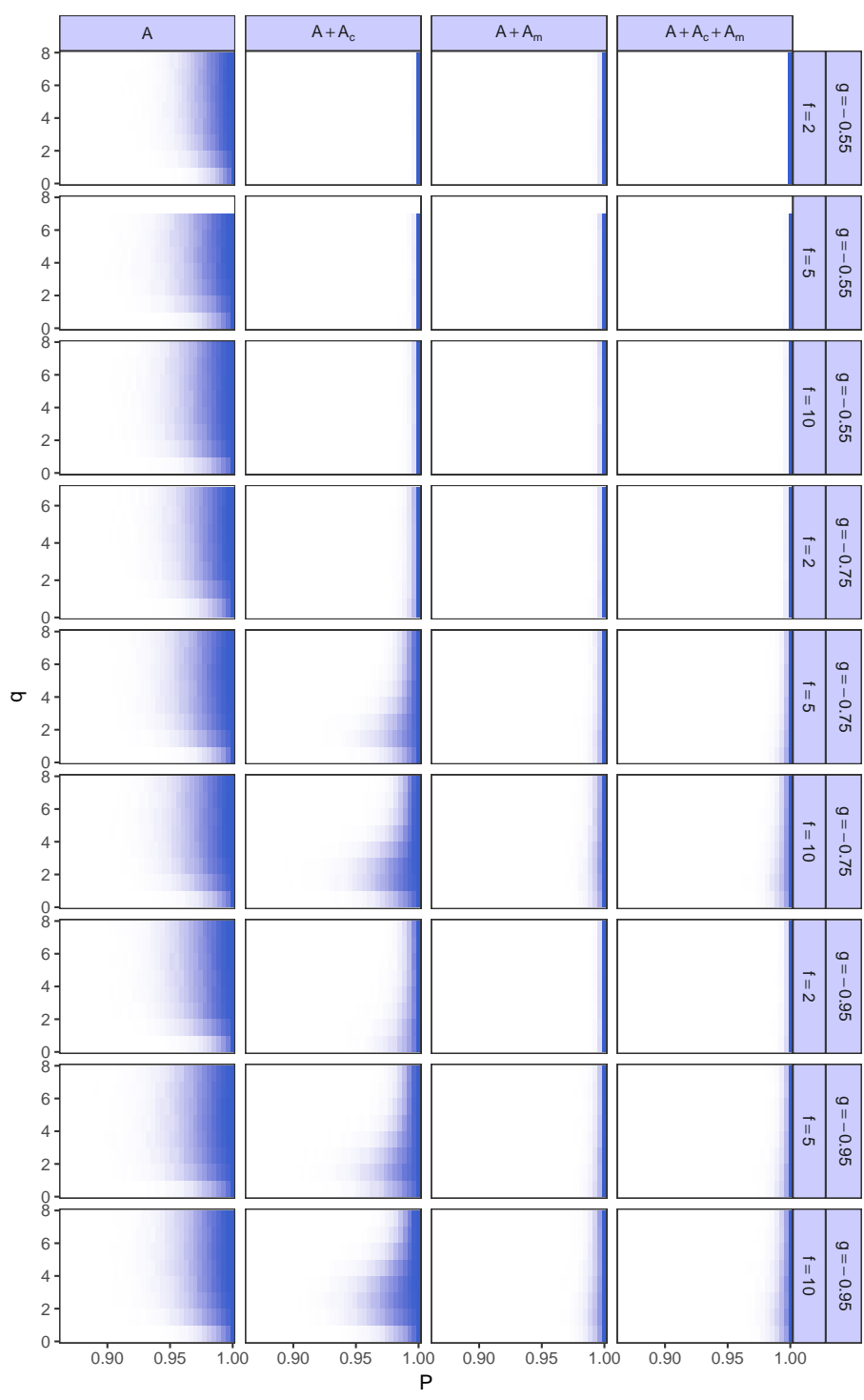
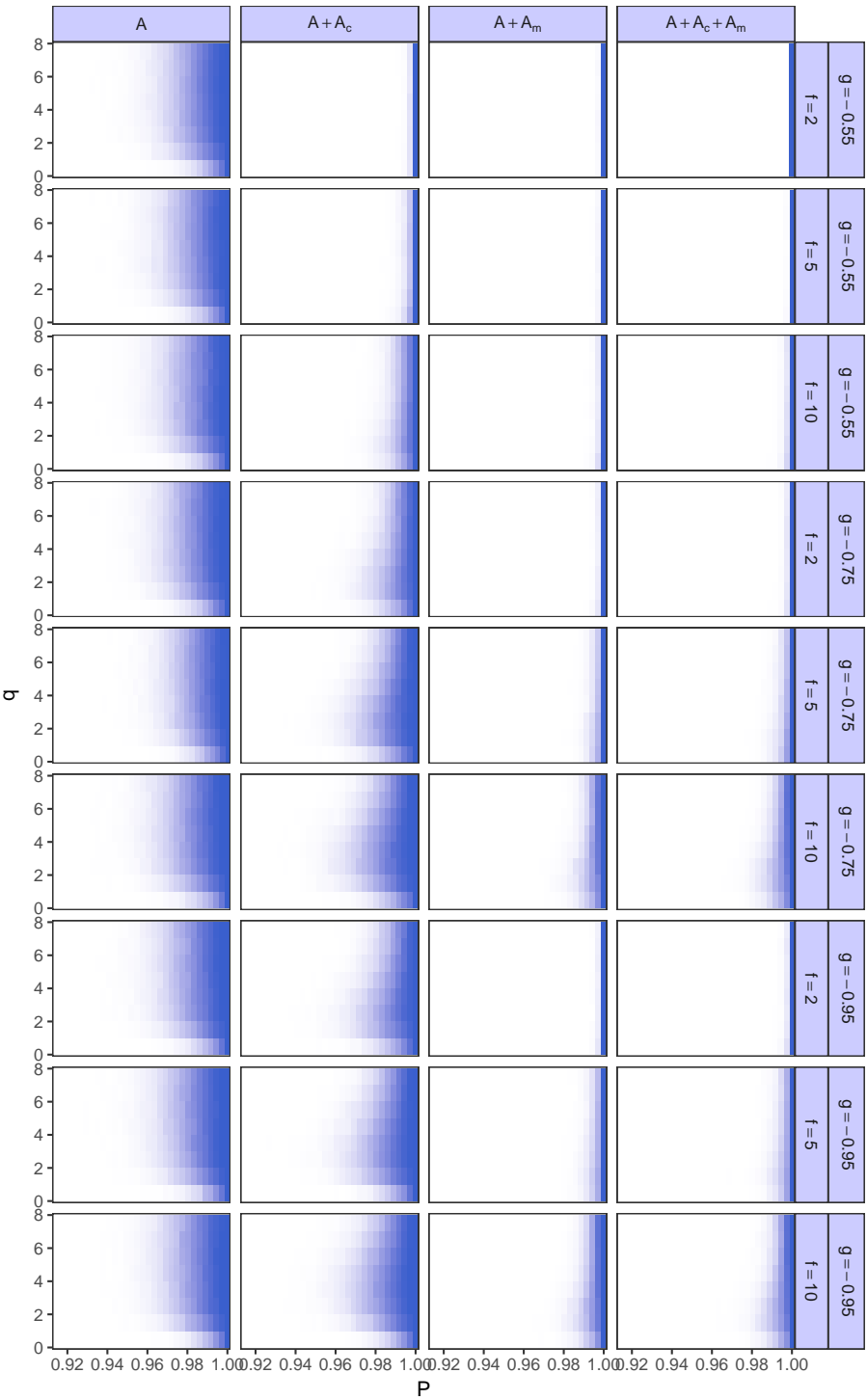**Supplementary Figure 21:** As Supplementary Figure 19, but for the Kongs Fjorden web (Table 2).
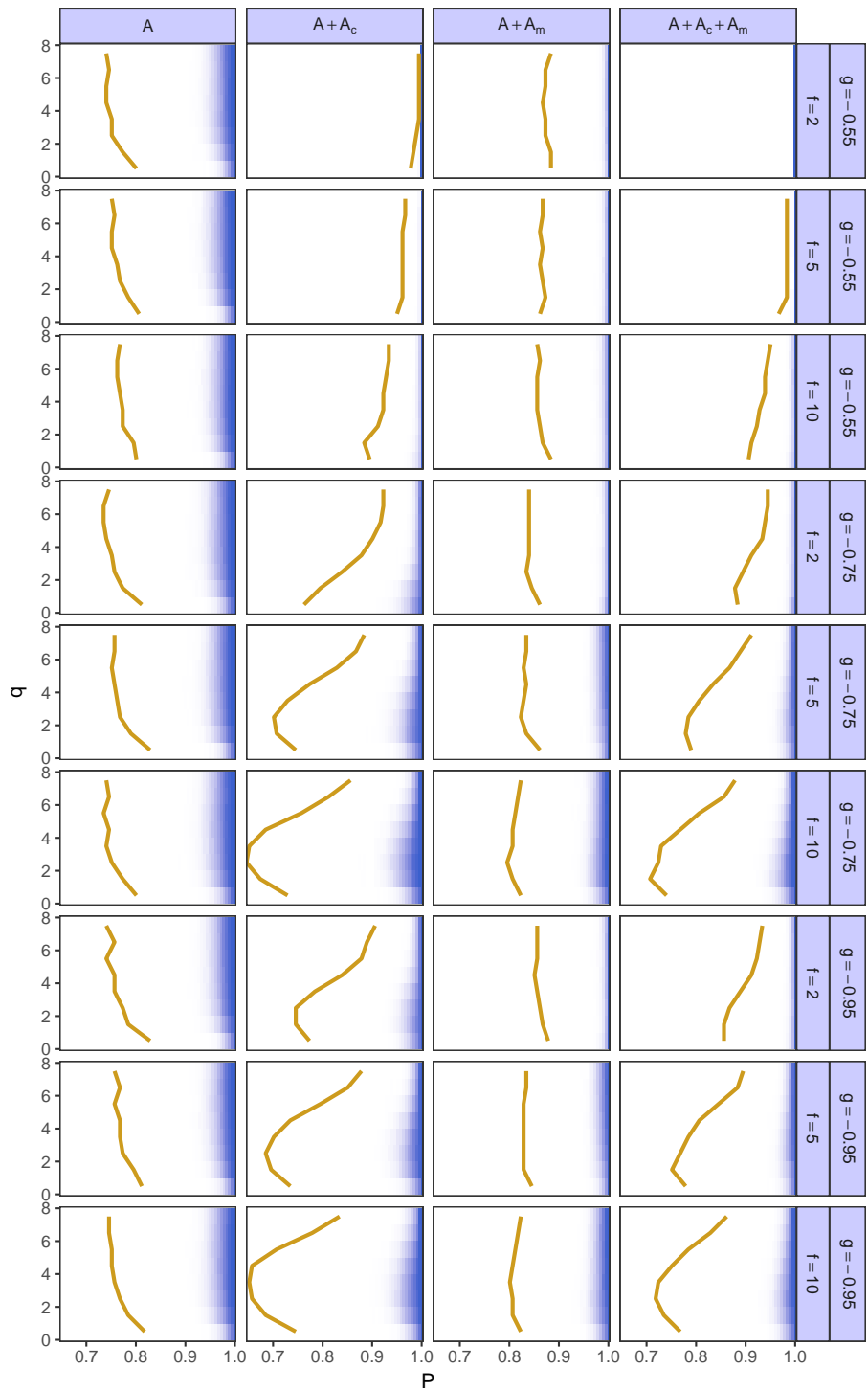
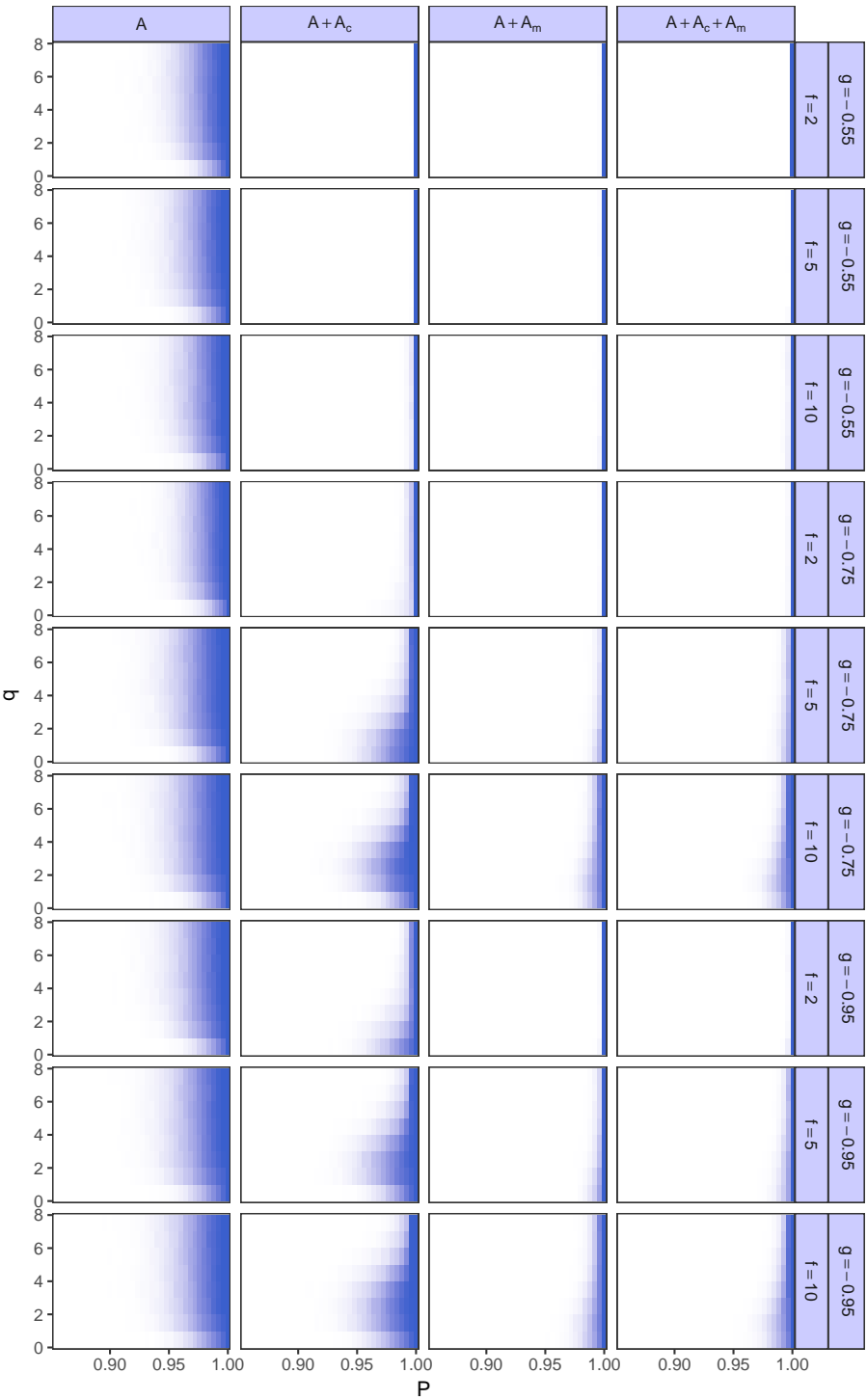**Supplementary Figure 22:** As Supplementary Figure 20, but for the Little Rock Lake web (Table 2).

Supplementary Figure 23: As Supplementary Figure 19, but for the Lough Hyne web (Table 2).
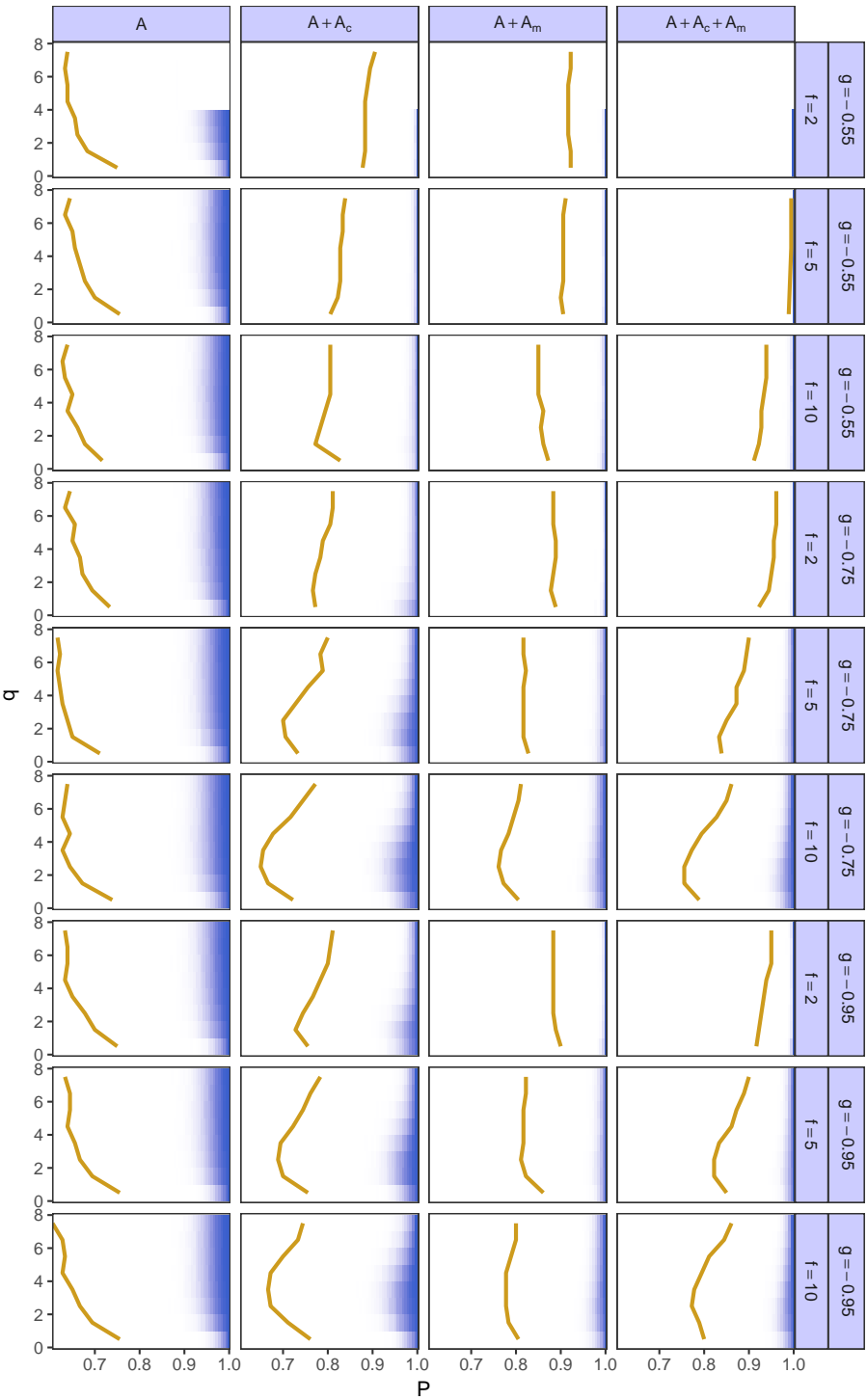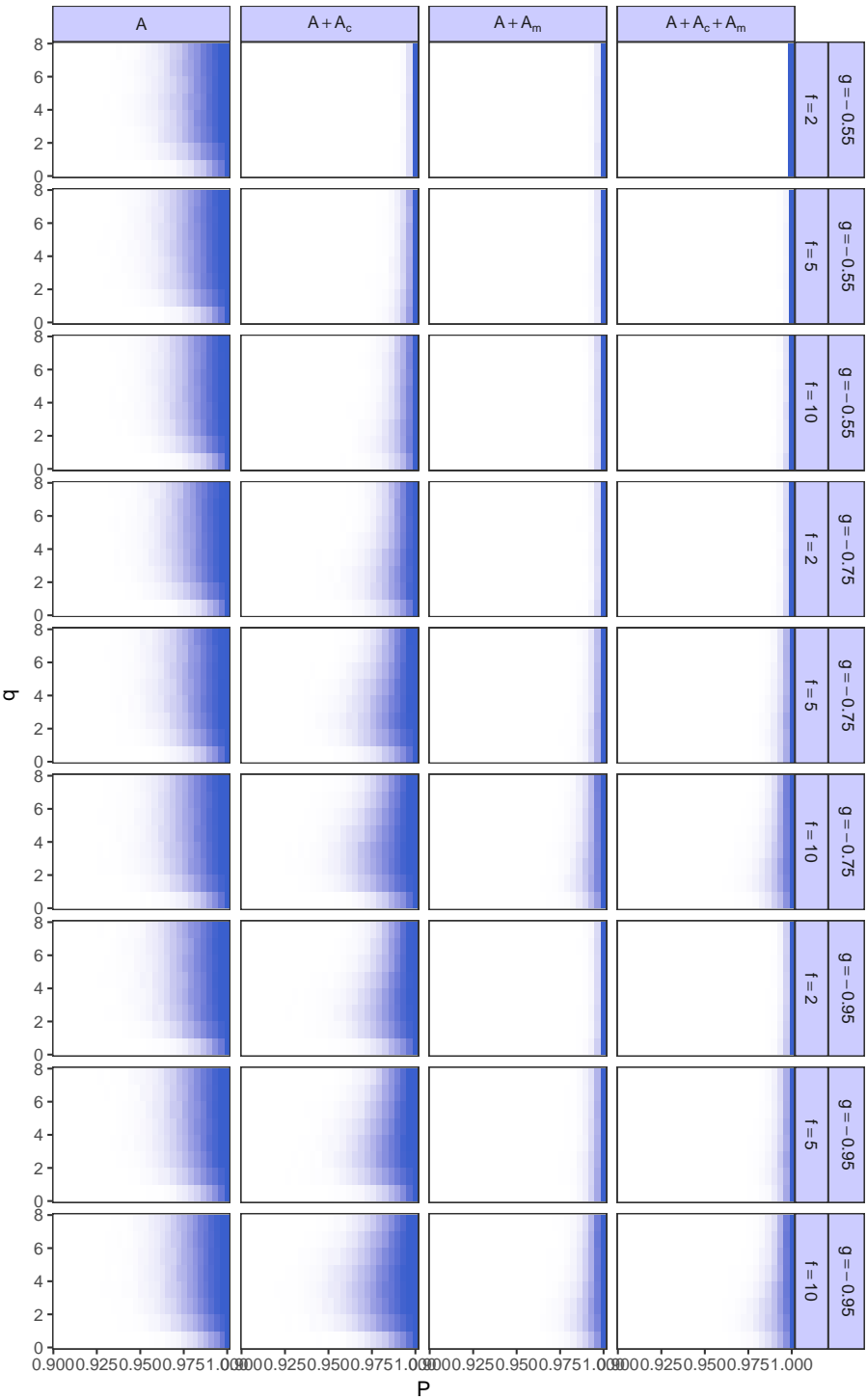
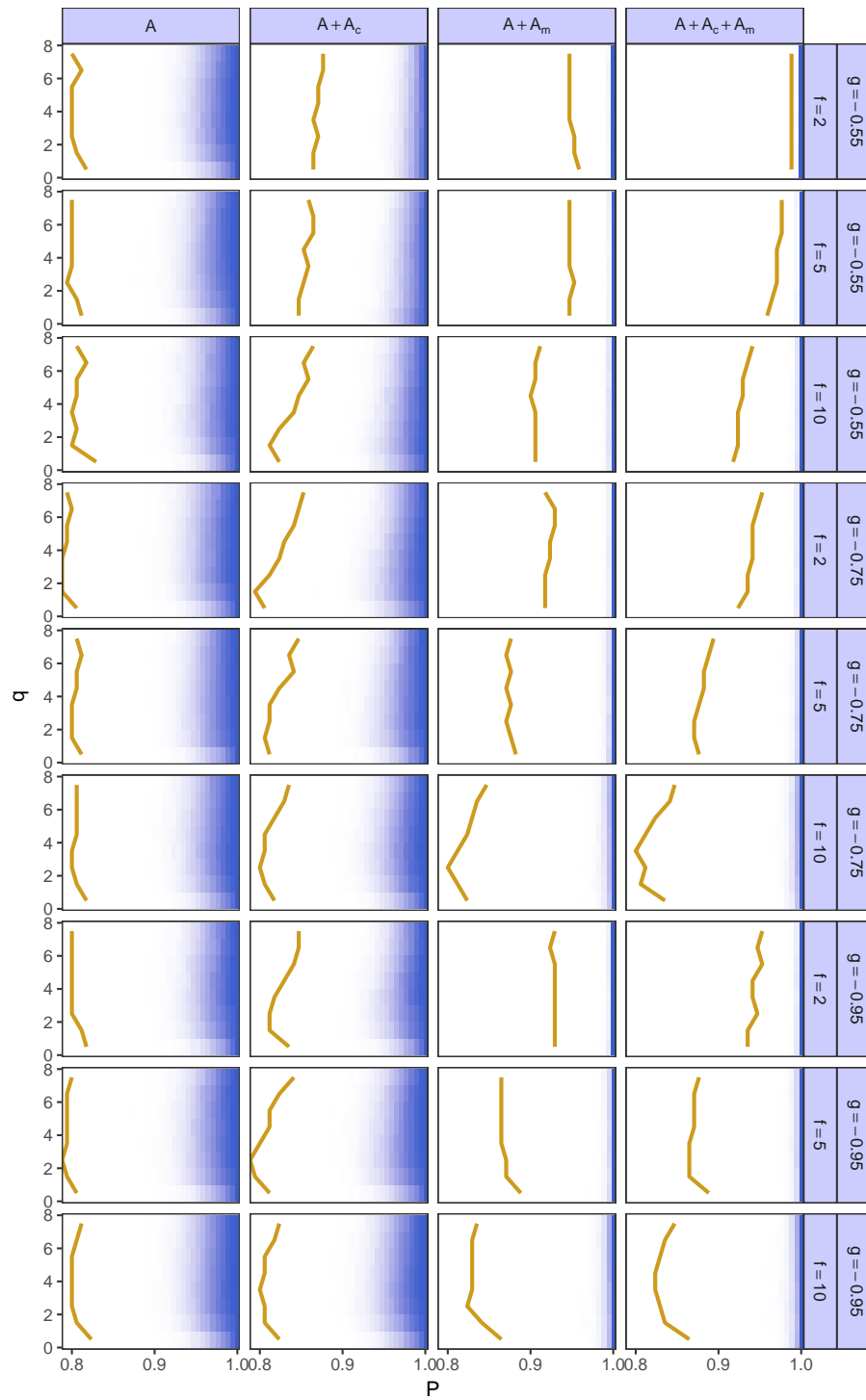**Supplementary Figure 24:** As Supplementary Figure 20, but for the Otago Harbour web (Table 2).

Supplementary Figure 25: As Supplementary Figure 19, but for the Punta Banda web (Table 2).
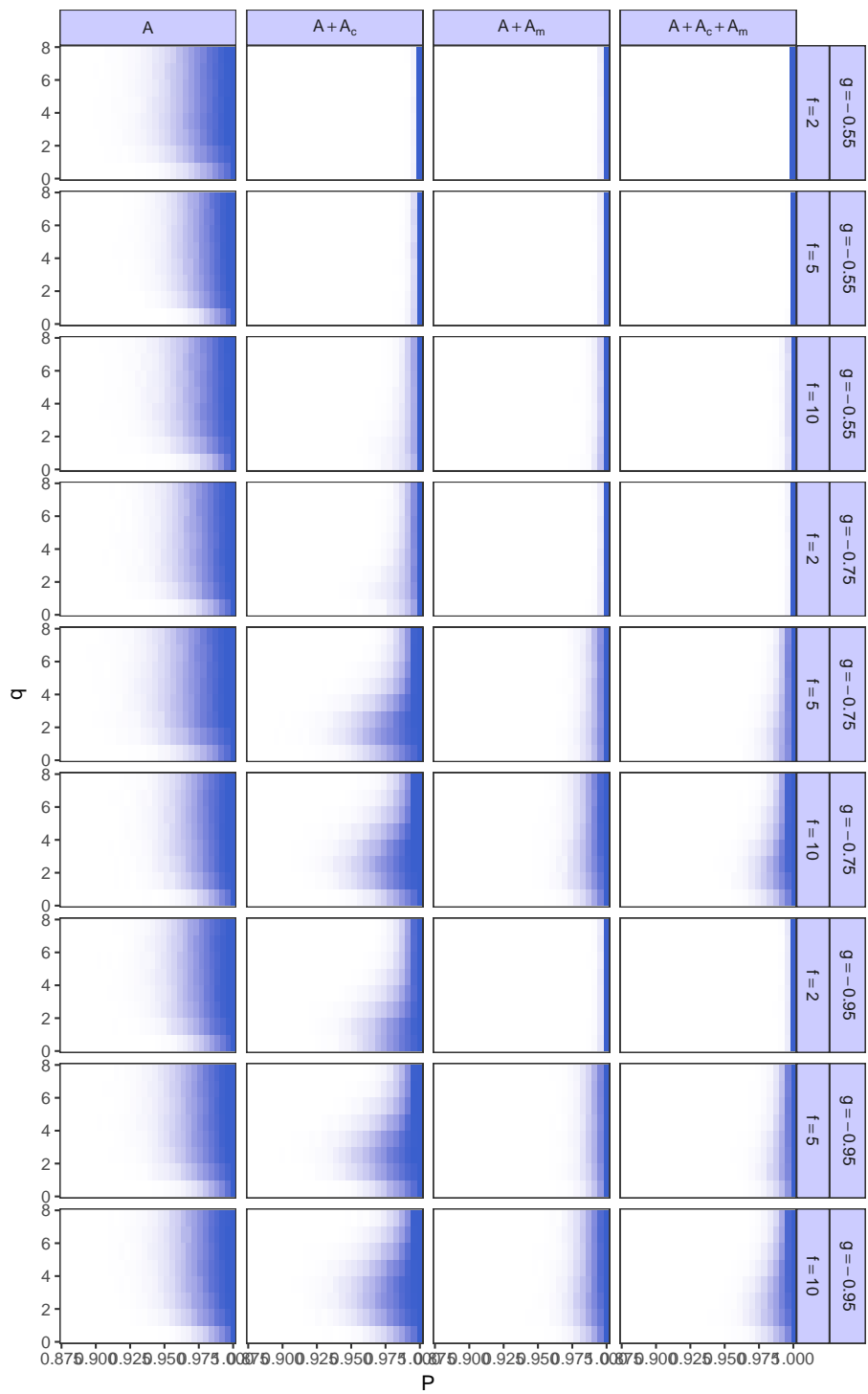
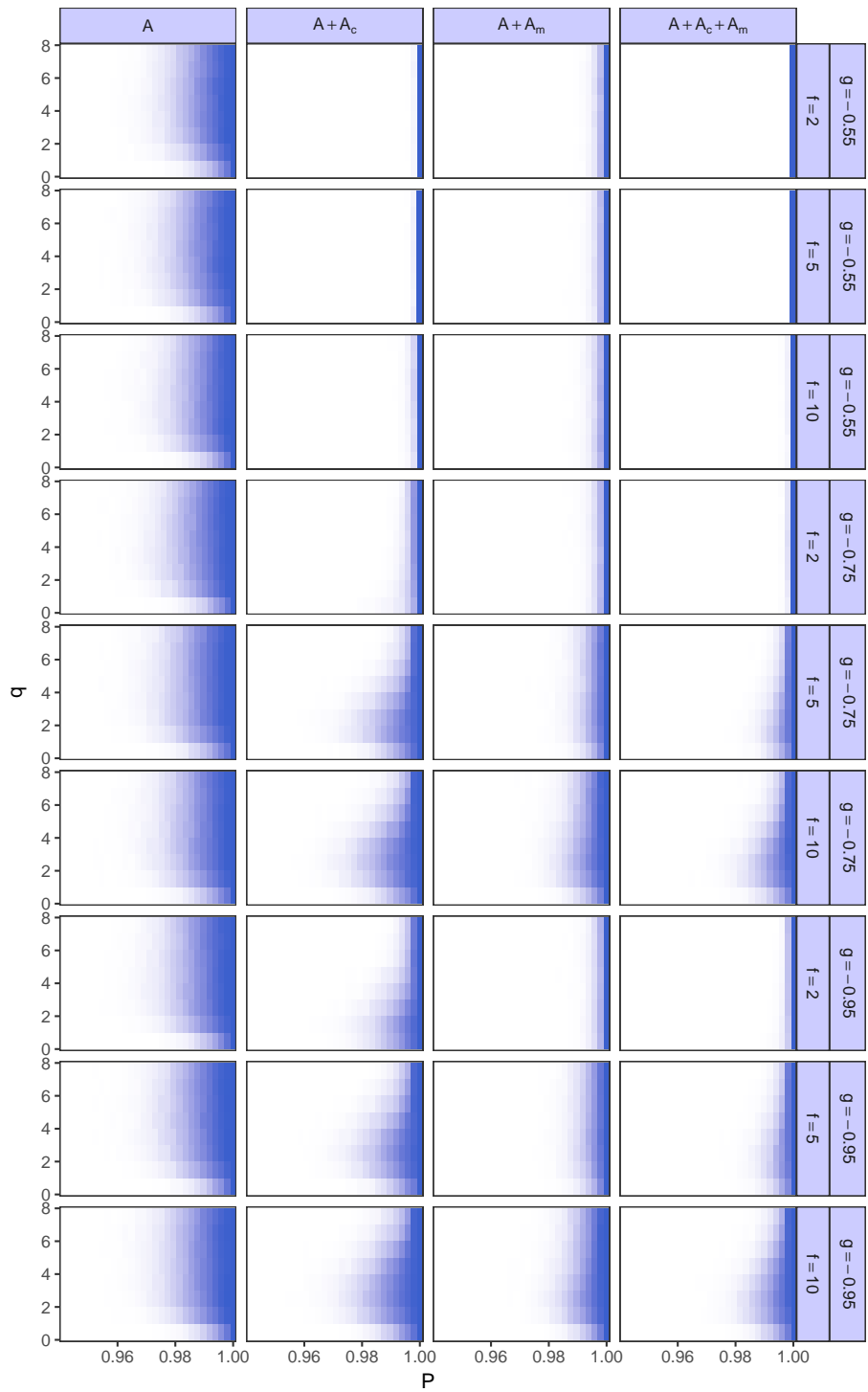**Supplementary Figure 26:** As Supplementary Figure 19, but for the Caribbean Reef web (Table 2).

Supplementary Figure 27: As Supplementary Figure 19, but for the San Quintin web (Table 2).

Supplementary Figure 28: As Supplementary Figure 20, but for the Serengeti web (Table 2).

Supplementary Figure 29: As Supplementary Figure 19, but for the Sylt Tidal Basin web (Table 2).

Supplementary Figure 30: As Supplementary Figure 19, but for the Weddell Sea web (Table 2).

To parameterize interference competition, we assigned negative pairs of entries to species sharing a common resource. The matrix $\mathbf{A}_c$ contains these indirect competition coefficients, with all other entries being zero. Since we have no way of knowing *a priori* what the values of these coefficients would be (they are model- and parameterization-dependent), we sampled them independently and uniformly from the interval $[\mathbb{E}(\mathbf{A}_-)/f, 0]$, where $\mathbf{A}_-$ is the set of negative entries in the original parameterized empirical matrix $\mathbf{A}$, $\mathbb{E}(\mathbf{A}_-)$ is their expectation, and f is a factor we set to either 2, 5, or 10, controlling the strength of indirect competition relative to the strength of direct negative effects. The parameter f allows us to explore the sensitivity of the results to the strength of indirect effects. Indirect positive effects between prey sharing a consumer was parameterized and stored in the matrix $\mathbf{A}_m$ analogously, except the positive pairs of entries were drawn from $[0, \mathbb{E}(\mathbf{A}_+)/f]$ where $\mathbf{A}_+$ is the set of positive entries in $\mathbf{A}$.

Apart from the original matrix $\mathbf{A}$ then, we also performed the analysis of self-regulation, as described in Section 7.2, on the matrices $\mathbf{A} + \mathbf{A}_c$, $\mathbf{A} + \mathbf{A}_m$, and $\mathbf{A} + \mathbf{A}_c + \mathbf{A}_m$. Our results are robust to this alteration, however, with no qualitative difference occurring in the results (Supplementary Figure 19-30, columns 2-4). The rank deficiency of the empirical food webs therefore does not appear to influence the tendency that the majority of species must be self-regulated for stability. In fact, there is a slight but visible trend to the contrary, with $\mathbf{A} + \mathbf{A}_c + \mathbf{A}_m$ being more difficult to stabilize than $\mathbf{A}$.

7.4   A lower bound on the number of self-regulating species

So far we have been distributing diagonal entries randomly to estimate the probability of stability. One could ask a different question however: were we to place the self-regulation terms strategically, targeting specific species, what is the minimum number of self-regulating species that is theoretically necessary to achieve stability? Is it possible that in this way many fewer species would need to exhibit self-regulation?

To test this idea, we took all of our parameterized food webs, and starting with $P \approx 1$ tried to find an arrangement of the diagonal entries such that the network was stable. We did this by actually minimizing the leading eigenvalue via a combination of two stochastic search algorithms (code available at https://github.com/dysordys/diagonal). First, a hill-climbing algorithm was used in which, starting out from one diagonal arrangement, we create 1000 mutants by randomly swapping two diagonal entries, calculate their leading eigenvalues, and choose the one with the lowest real part. This matrix then becomes the basis for mutations in the next generation of 1000 variants, and so on. Second, we used a genetic algorithm in which 500 individual matrices form a population, can recombine with one another, and the most "fit" fraction of the population (those with the lowest real part of the leading eigenvalue) is carried into the next generation.

The run of the algorithm was stopped the moment the leading eigenvalue's real part was reduced below zero, i.e., when a stable solution was found. At that point, we reduced P by having one fewer species self-regulate than before, and repeated the above stochastic search. We did this until one hundred generations of the hill climber and five subsequent generations of the genetic algorithm failed to find a stable configuration. The smallest P where a stable configuration was found was then taken to be the minimum fraction of self-regulating species necessary for stability. Results are shown, for four of the well-resolved webs, by the yellow lines on Supplementary Figures 20, 22, 24, and 28. For the Ecopath networks, see Supplementary Figure 32. The theoretical minimum is indeed lower than what we have found by randomly distributing the diagonal entries.

However, this effect is not especially dramatic. We still find that even under the most optimistic estimate, 70-80% of species must exhibit self-regulation for stability in the well-resolved webs. For the Ecopath webs, the original ratio of $P \approx 50\%$ drops to about 25%. Of course, it is not clear why such an extreme fine-tuned scenario would be realized in nature. One may be tempted to invoke non-adaptive selection arguments (Proulx et al. 2005, Borrelli et al. 2015) favoring a self-regulation structure minimizing $\eta(\mathbf{A})$, but one must bear in mind that self-regulation is only partially a property of an organism's physiological traits under evolutionary control. As such, though the idea that the distribution of self-regulation terms is selected to be highly nonrandom may have merit, further evidence is needed to make this claim convincing.

7.5   The quality of the analytical approximation for empirical webs

The results we have obtained here for empirical webs are certainly consistent with the theoretical ones developed in Sections 5 and 6. However, one may still ask how well the analytical approximation performs on empirical networks—that is, whether one could generate the analogue of Supplementary Figure 17 using the observed underlying network structures instead of randomly generated ones.

We have, in fact, generated all such plots in detail and compiled them into animations for each parameterization of all 12 webs, fixing the value of q at 1.5 which leads to self-regulation strengths of $d = -2^{1.5}\eta(\mathbf{A})$ (altering d does not change the quality of approximation). The analytical approximation does a very good job of capturing the actual $\eta(\mathbf{A})$ in every single case. As an example, we show here, in Supplementary Figure 31, snapshots of the San Quintin web (Hechinger et al. 2011) parameterized with $g = -0.75$, $f = 5$, and with all indirect effects included. The animations for all parameterizations of each web may be viewed at https://github.com/dysordys/diagonal.

## 7.6   Analysis of the Ecopath matrices

Applying the same methodology that we used for the 12 well-resolved webs to the seven largest Ecopath webs found in Jacquet et al. (2016) was considerably eased by the fact that these matrices were already parameterized. Therefore, the allometric method for parameterization was not needed; nor were there several alternative parameterizations. The results on the stability of these networks as a function of the fraction of self-regulating species is seen in Supplementary Figure 32.

The general shape of the results is consistent with our other analyses: one can see that the highest likelihood of stability happens at intermediate self-regulation strengths, and that a large fraction of species in the community must self-regulate if the webs are to be stable. However, there is a big quantitative difference: for the well-resolved webs, it was not possible to have stability before more than 90% of species were self-regulating, but here this fraction is between 50% and 60%. Also, when minimizing P via the genetic algorithm (Section 7.4), it turns out that the theoretically required minimum P for stability is between 20% and 25% of all species, which is much lower than the previously obtained 70-80%.

We conclude that, while the qualitative properties of the previous results still hold, these matrices require a considerably lower fraction of self-regulating species for stability. It is not clear yet whether this is due to structural properties of Ecopath matrices, or their smaller species richness (or both).

7.7   No pattern to the trophic identity of self-regulating species

The received ecological view is that basal species and top predators are much more likely to exhibit self-regulation than species at intermediate trophic levels: for basal species nutrient and spatial
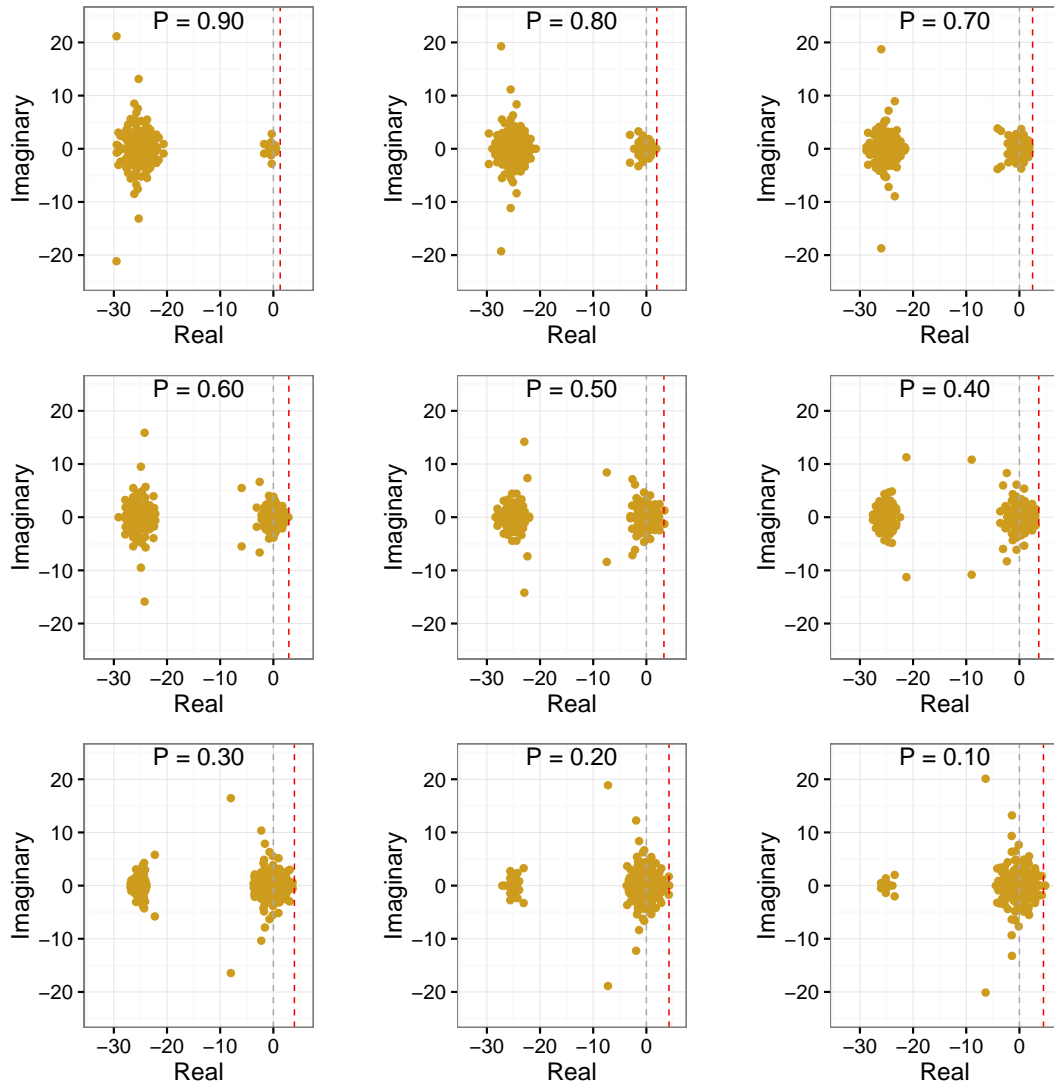
Supplementary Figure 31: Spectra (yellow points) of matrices $\mathbf{A} = \mathbf{M} + \mathbf{D}$. Here $\mathbf{M}$ is the parameterized version of the San Quintin food web (Hechinger et al. 2011; $g = -0.75$, $f = 5$, and with all direct and indirect effects included), while $\mathbf{D}$ is sampled from Eq. 5.14 with $d_1 = -5\eta(\mathbf{M})$, $d_2 = 0$, and different values for P (panels). The value of $\eta(\mathbf{M})$ is the spectral abscissa of $\mathbf{M}$, i.e., the matrix without any self-effects; its numerical value is $\eta(\mathbf{M}) \approx 5.07$. The grey dashed line separates the left and right halves of the complex plane. The red dashed line shows the analytical prediction for $\eta(\mathbf{A})$, calculated from Eq. 5.25 using the effective parameters V_{eff} and ρ_{eff} (calculated using Eqs. 2.17, 2.18, and 2.19), and with appropriate rescaling by $\sqrt{SV_{\text{eff}}}$. The analytical prediction captures the actual value of $\eta(\mathbf{A})$ very well in all cases.
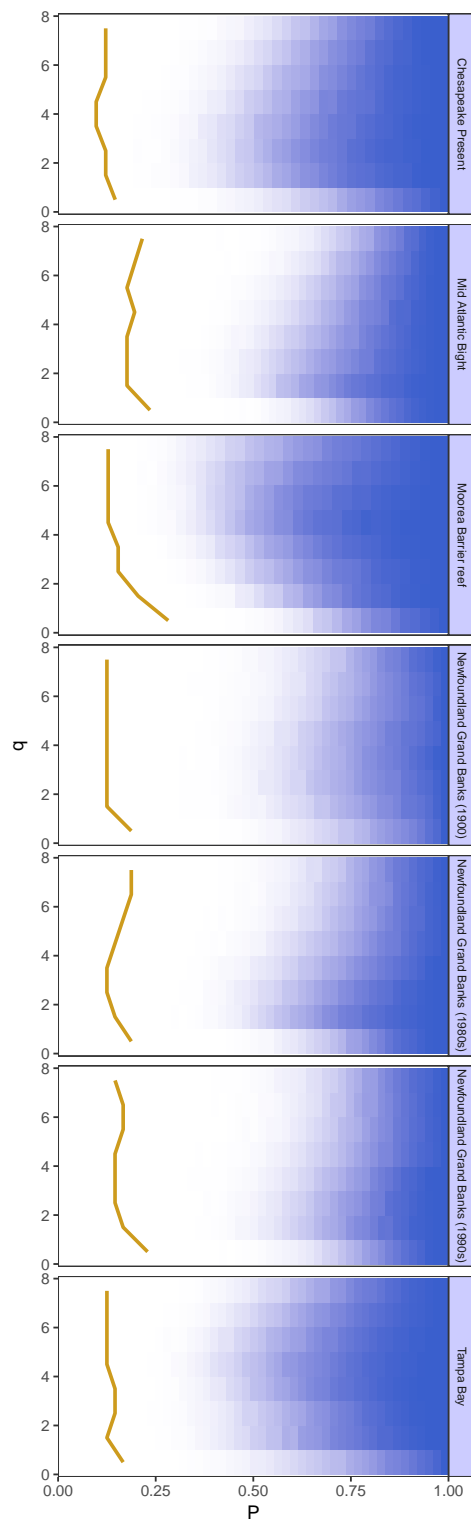
Supplementary Figure 32: As Supplementary Figure 19, but for the seven parameterized Ecopath webs taken from Jacquet et al. (2016). Each row shows a different web.

limitation, for top predators territoriality and intraspecific interference will habitually create negative self-effects. One could ask whether communities can be stabilized by specifically targeting these two species groups with self-regulation. Another question is whether there is any such trophic pattern to the minimum fraction of self-regulating species (Section 7.4) found in our webs earlier (yellow lines in Supplementary Figures 20, 22, 24, 28, and 32). In other words, do the self-regulating species tend to come preferentially from the basal and top level whenever their fraction is the smallest possible?

Let us start with the well-resolved webs in Table 2. We used four webs out of the twelve in Table 2: Flensburg Fjord, Little Rock Lake, Otago Harbour, and Serengeti. Self-regulation was assigned to all basal and top species but no others; otherwise, the same parameterizations were implemented as before. We then checked how often the resulting webs turned out stable (Supplementary Figure 33). The short summary of the results is that *none* of the community matrices were stable. It is therefore impossible to stabilize these communities by assigning self-regulation only to basal species and top predators.

Similarly, we checked the trophic distribution of self-regulating species when their fraction was minimized (Supplementary Figure 34). What we see in every case we looked at is that there is no trophic pattern to self-regulation. For example, it is not true that basal species or top predators are more likely to be self-regulating than the other species. In fact, the distribution of self-regulating species across trophic levels is more or less even.

The Ecopath matrices often did not have unambiguously basal or top species, therefore we did not ask whether they can be stabilized by assigning self-regulation only to those ones. Instead, we only checked the trophic distribution of self-regulating species when their fraction was minimized (Supplementary Figure 35). As in the case of the well-resolved webs, there is no clear trophic pattern to self-regulation: there is no trophic category that would be more important for the purposes of network stability than others.

In summary, *if* empirical ecological networks are to be locally stable, *then* self-regulation seems to be equally important across all trophic levels, not just at the bottom and the top. This, of course, is perfectly compatible with all or most of basal and top species exhibiting self-regulation in nature. It just means that all others must have substantial self-regulation as well.
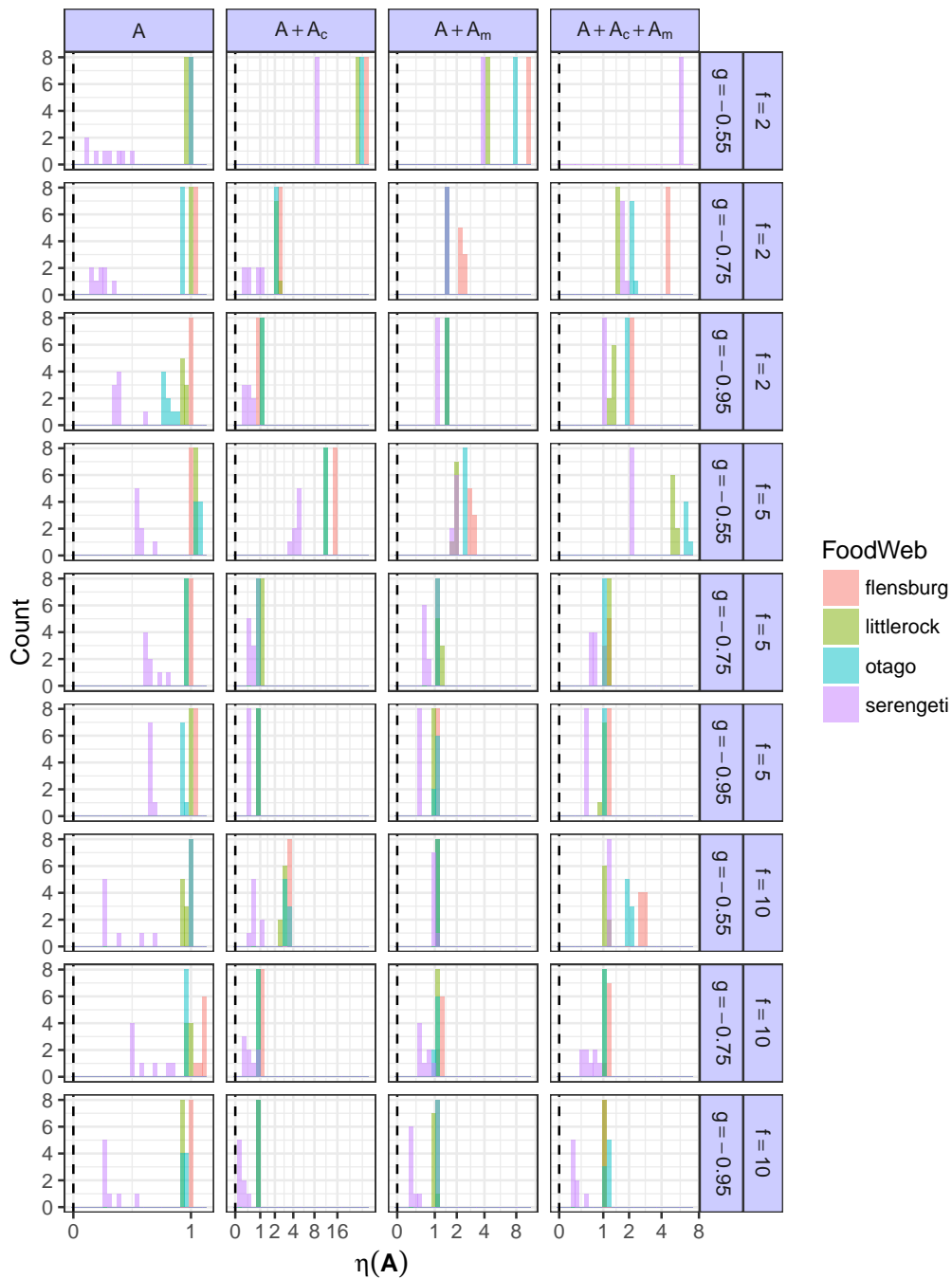
Supplementary Figure 33: Histograms of the spectral abscissas (*x*-axis) of four food webs, when only basal and top species are self-regulating. Black dashed lines show the stability boundary where $\eta(\mathbf{A}) = 0$ in each subpanel. Rows and columns show various parameterizations in the same way as in Supplementary Figure 19. In each subpanel, the color shows the food web identity (legend on the right), and the histograms are obtained from the eight different values of self-regulation strength, measured by q. In no cases are the resulting matrices stable.
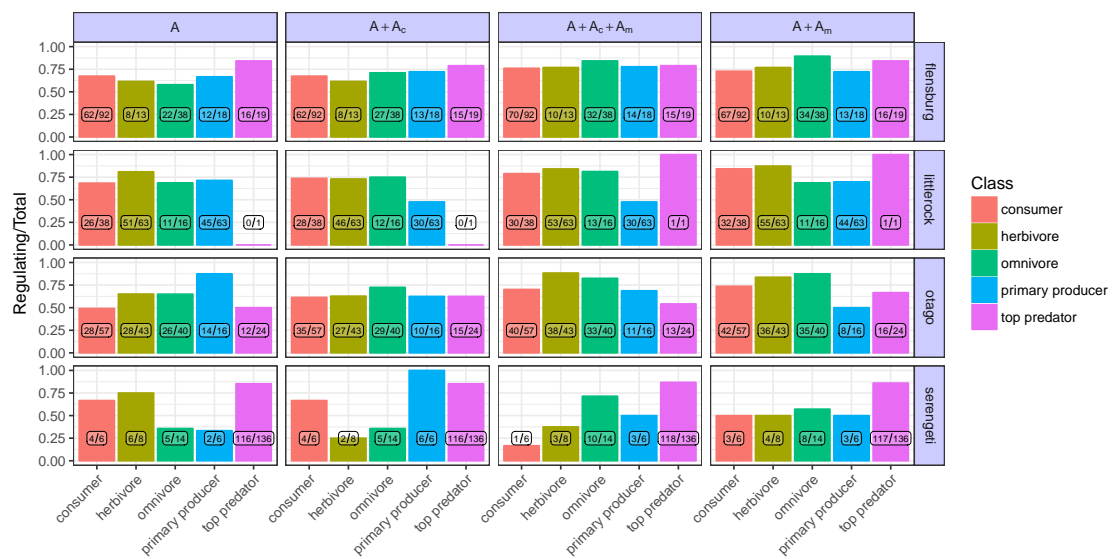
Supplementary Figure 34: Fraction of self-regulating species as a function of trophic level in each of four food webs (rows) and various parameterizations of indirect effects (columns). We used the matrices in which the fraction of self-regulating species was minimized (Section 7.4). The numbers on the bars show the number of self-regulating species and the number of species at that trophic level altogether. The trophic identity of self-regulating species is by and large evenly distributed across trophic levels.
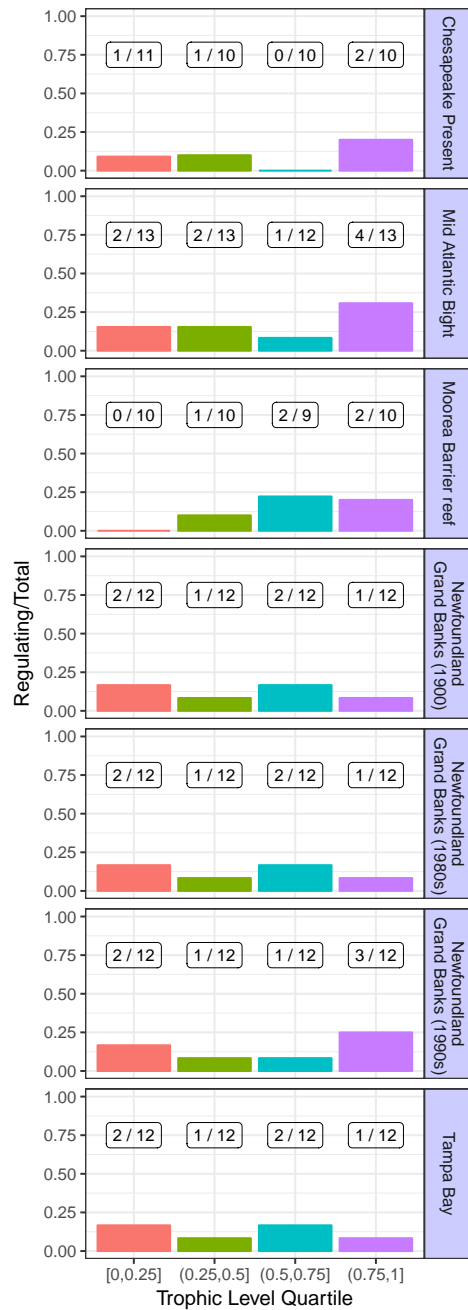
Supplementary Figure 35: As Supplementary Figure 34, but for the seven Ecopath matrices (rows).

8   Diagonal entries generated by nonlinear functional responses typically do not stabilize large ecological networks

Up to this point, all mechanisms generating negative diagonal entries in the community matrix were called self-regulation. However, some such contributions may not satisfy our intuition for being "true" self-regulation. To illustrate this point, consider a very simple population model of the form

$$\frac{\mathrm{d}n}{\mathrm{d}t} = n(b - \alpha n) + I, \tag{8.1}$$

where n is the population's abundance, t is time, b is the intrinsic growth rate, α the intraspecific competition coefficient, and I an immigration rate from outside sources. Based on the definition of Section 1.2, self-regulation is present when the per capita growth rate has direct dependence on n. For this model, an effective per capita growth rate r can be written as

$$r = \frac{1}{n}\frac{\mathrm{d}n}{\mathrm{d}t} = b - \alpha n + \frac{I}{n}. \tag{8.2}$$

The corresponding diagonal entry in the community matrix can be expressed via the derivative of this growth rate with respect to n (Section 1.2):

$$n^* \left.\frac{\partial r}{\partial n}\right|_{n=n^*} = n^*\left[-\alpha - \frac{I}{n^{*2}}\right]. \tag{8.3}$$

The first term corresponds to "true" self-regulation: intraspecific crowding directly reducing the per capita growth rate of the prey. However, the second term stems from immigration and may therefore be considered, in a sense, artifactual. Opinions of ecologists may be divided on whether to classify this term as true self-regulation.

An even more confounding example may be constructed by assuming that the above population is also being consumed by a generalist predator:

$$\frac{\mathrm{d}n}{\mathrm{d}t} = n(b - \alpha n) + I - \frac{an^2 p}{k^2 + n^2}, \tag{8.4}$$

where a and k are parameters of the type III functional response, and p is the predator density. The per capita growth rate r now reads

$$r = \frac{1}{n}\frac{\mathrm{d}n}{\mathrm{d}t} = b - \alpha n + \frac{I}{n} - \frac{anp}{k^2 + n^2}, \tag{8.5}$$

with the corresponding self-effect in the community matrix reading

$$n^* \left.\frac{\partial r}{\partial n}\right|_{n=n^*} = n^*\left[-\alpha - \frac{I}{n^{*2}} - \frac{a(k^2 - n^{*2})p}{(k^2 + n^{*2})^2}\right]. \tag{8.6}$$

As long as $k^2 > n^2$, the final term contributes to self-regulation (as opposed to self-enhancement). However, assuming that the type III response arises from switching behavior on the part of the predator which may have nothing to do with what prey individuals do, one is strongly tempted not to call this an instance of true self-regulation.

These examples illustrate that some contributions to the diagonal entries of the community matrix are unambiguously considered self-regulation (for instance, those due to direct intraspecific

interference or crowding); some, like immigration, are at the very least ambiguous; and some, like those stemming from nonlinear functional responses, may easily be considered artifactual. The problem here is that, to our knowledge, there has never been a definitive catalogue of what should be considered true self-regulation.

Attempting to create such a catalogue here would likely be a pointless exercise in artificial prescription. Instead, we perform a study of self-regulation such that functional response-generated negative diagonal entries will not be considered examples of true self-regulation. Note that this choice is conservative. Indeed, in some cases there is ambiguity in how the self-effects arising from functional responses should be interpreted. A type III functional response may produce negative diagonal entries—but whether it counts as true self-regulation depends on the mechanistic interpretation of the response. If the predator's reduced kill rate at low prey abundance is not the result of some switching behavior on the part of the predator, but the result of a prey refuge available only to a handful of prey items, then there will be competition for those refuges, and so the negative diagonal entry will at least partially stem from true self-regulation. Since the type III functional response is a phenomenological construct, there is no way to tell *a priori* whether the corresponding diagonal entries are due to true self-regulation. Here however, we will consider all such diagonal contributions as artifactual. In this way, our choice is conservative, underestimating the actual extent of true self-regulation in a system.

To be able to disentangle funcional response effects from true self-regulation effects in the diagonal of the community matrix, one needs an underlying dynamical model from which those diagonal entries are derived. Here we explore two different models: a simple dynamical model where equilibrium biomasses follow Damuth's law (Damuth 1981), and the metabolically scaled network model of Schneider et al. (2016).

8.1   Dynamical food web model with Damuth's Law

We used an explicit model of food web dynamics with type II and type III functional responses. In this model the dynamics of species' population densities follow the equation

$$\frac{\mathrm{d}B_i}{\mathrm{d}t} = b_i B_i + B_i \sum_{j=1}^{S} e_{ij} w_{ij} F_{ij} - \sum_{j=1}^{S} B_j w_{ji} F_{ji} - d_i B_i^2, \tag{8.7}$$

where B_i is the density of species i, b_i is its baseline per capita growth rate, w_{ij} is the adjacency matrix of the food web (equal to 1 if species i eats j and to 0 otherwise), e_{ij} is species i's assimilation efficiency when eating species j, F_{ij} is a generalized functional response, and d_i measures the strength of direct intraspecific competition—i.e., the strength of true self-regulation. The function F_{ij} is given as

$$F_{ij} = \frac{\omega_{ij} B_j^h}{B_{0i}^h + \sum_{l=1}^{S} w_{il} \omega_{il} B_l^h}. \tag{8.8}$$

In this functional response, ω_{ij} is the proportion of i's maximum consumption rate targeted at consuming j, B_{0i} is species i's half-saturation density, and h is an exponent determining the Holling type of the functional response.

Introducing the simplifying notation

$$X_i = \frac{1}{B_{0i}^h + \sum_{l=1}^{S} w_{il} \omega_{il} B_l^h}, \tag{8.9}$$

we have

$$F_{ij} = X_i \omega_{ij} B_j^h. \tag{8.10}$$

The model can now be rewritten as

$$\frac{dB_i}{dt} = b_i B_i + B_i \sum_{j=1}^{S} X_i e_{ij} w_{ij} \omega_{ij} B_j^h - B_i^h \sum_{j=1}^{S} w_{ji} \omega_{ji} B_j X_j - d_i B_i^2. \tag{8.11}$$

Only the product $w_{ij}\omega_{ij}$ appears in the equation. Calling this product W_{ij}:

$$\frac{dB_i}{dt} = b_i B_i + B_i \sum_{j=1}^{S} X_i e_{ij} W_{ij} B_j^h - B_i^h \sum_{j=1}^{S} B_j X_j W_{ji} - d_i B_i^2. \tag{8.12}$$

We now calculate the Jacobian J_{ik} of this model. First we determine the derivative of X_i with respect to B_k:

$$\frac{\partial X_i}{\partial B_k} = \frac{\partial}{\partial B_k}\left[\frac{1}{B_{0i}^h + \sum_{l=1}^{S} W_{il} B_l^h}\right] = -h X_i^2 \sum_{l=1}^{S} W_{il} B_l^{h-1} \delta_{kl} = -h X_i^2 W_{ik} B_k^{h-1}, \tag{8.13}$$

where δ_{kl} is the Kronecker symbol (equal to 1 if $k = l$ and to 0 otherwise). The Jacobian then reads

$$J_{ik} = \frac{\partial (dB_i/dt)}{\partial B_k} = b_i \delta_{ik} + \delta_{ik} \sum_{j=1}^{S} X_i e_{ij} W_{ij} B_j^h - h B_i X_i^2 W_{ik} B_k^{h-1} \sum_{j=1}^{S} e_{ij} W_{ij} B_j^h$$

$$+ h B_i X_i \sum_{j=1}^{S} e_{ij} W_{ij} B_j^{h-1} \delta_{jk} - h B_i^{h-1} \delta_{ik} \sum_{j=1}^{S} B_j X_j W_{ji} - B_i^h \sum_{j=1}^{S} \delta_{jk} X_j W_{ji} \tag{8.14}$$

$$+ h B_i^h \sum_{j=1}^{S} B_j X_j^2 W_{jk} B_k^{h-1} W_{ji} - 2 d_i B_i \delta_{ik}.$$

Rearranging and performing summations using the Kronecker symbols:

$$J_{ik} = \delta_{ik}\left(b_i + X_i \sum_{j=1}^{S} e_{ij} W_{ij} B_j^h - h B_i^{h-1} \sum_{j=1}^{S} B_j X_j W_{ji} - 2 d_i B_i\right) + h B_i X_i e_{ik} W_{ik} B_k^{h-1}$$

$$\tag{8.15}$$

$$- X_k W_{ki} B_i^h - h B_i X_i^2\left(\sum_{j=1}^{S} e_{ij} W_{ij} B_j^h\right) W_{ik} B_k^{h-1} + h B_i^h B_k^{h-1} \sum_{j=1}^{S} B_j X_j^2 W_{jk} W_{ji}.$$

For parameterizing the model, we have used those empirical networks in Table 2 for which body mass data was available: Carpinteria, Kongs Fjorden, Lough Hyne, Punta Banda, Caribbean Reef, San Quintin, and Weddell Sea[1]. Species for which body mass information was missing were discarded from the webs. The adjacency matrix w_{ij} was given empirically; e_{ij} was set to 0.1 for strict herbivores and to 0.2 for carnivores (i.e., trophic level higher than 2); ω_{ij} was set equal to the inverse of the total number of prey items for each prey species a predator consumed (equal hunting effort on each prey species); and h either took the value 1 (type II functional response) or 2 (type III response).

---

[1]Body masses in Weddell Sea greater than 1000kg were double-checked against the cited source (Trites and Pauly 1998) for such values in Jacob (2005) and corrected when necessary.

Name	Species	$h = 1$	$h = 2$
Carpinteria Salt Marsh	201	0.0033	0.0001
San Quintin	218	0.0022	0.0001
Punta Banda	268	0.0023	0.0006
Kongs Fjorden	252	14.7811	11.6753
Lough Hyne	326	41.7021	0.7892
Caribbean Reef	213	128.5347	0.0143
Weddell Sea	358	617.9564	0.0347

Supplementary Table 3: Empirical webs with body mass data. This is a subset of the webs in Table 2. The number of species is lower than earlier, because only those species are retained in the network for which body mass data was available. The column $h = 1$ shows the minimum strength of direct self-regulation such that, were all d_i equal to this value (all species self-regulate to the same extent), the web would be stable, given that the Holling parameter h is equal to 1 (type II functional response). The column $h = 2$ is the same except for h equal to 2 (type III functional response).

In choosing the intrinsic growth rates b_i, assigning them either randomly or based on allometric considerations lead to nonfeasible communities almost invariably (i.e., zero or negative densities B_i), even when all species were simultaneously self-regulating by having positive d_i values. We therefore approached the problem from the other end. First, we pre-determined the equilibrium densities B_i. They were chosen to be proportional to the $-3/4$th power of individual body masses to satisfy Damuth's Law (Damuth 1981). We then solved for the b_i such that the equilibrium solution to Eq. 8.12 would yield those equilibrium densities: setting $dB_i/dt = 0$, we have, from Eq. 8.12,

$$b_i = d_i B_i - \sum_{j=1}^{S} X_i e_{ij} W_{ij} B_j^h + B_i^{h-1} \sum_{j=1}^{S} B_j X_j W_{ji}. \tag{8.16}$$

In order for the right hand side to be fully specified, the B_{0i} still have to be determined. They were drawn, for each species, independently and uniformly from the interval $[B_i/2, B_i]$, ensuring that the half-saturation constants are at least half as large as the equilibrium densities themselves.

We initially set all $d_i = 0$. We then determined, for each web and for both values of $h = 1$ and $h = 2$, the minimum amount of self-regulation required for stability provided that all species simultaneously self-regulate (this was simply done by numerical trial-and-error; see Table 3 for these values). Calling this baseline strength d_{base}, we did the exact same study as before: setting the strength of self-regulation to $d = d_{\text{base}} \times 2^q$ and the fraction of self-regulating species P, we swept through the values $q = 0.5, 1.5, \ldots, 7.5$ for each value of P (i.e., each d_i was set to d with probability P and to 0 with probability $1 - P$), reassigned the diagonal entries' arrangement 1000 times, and tallied the number of times the community ended up being stable. The code performing this simulation can be downloaded from https://github.com/dysordys/diagonal; results are shown below.

What we see is that substantial self-regulation is *still* required for community stability, both for $h = 1$ and $h = 2$. While far from being perfect, this study does demonstrate that negative diagonal entries generated by functional responses cannot necessarily stabilize communities. Community stability requires that the vast majority of species experience self-regulation whose source is not simply in the trophic coupling of the system.
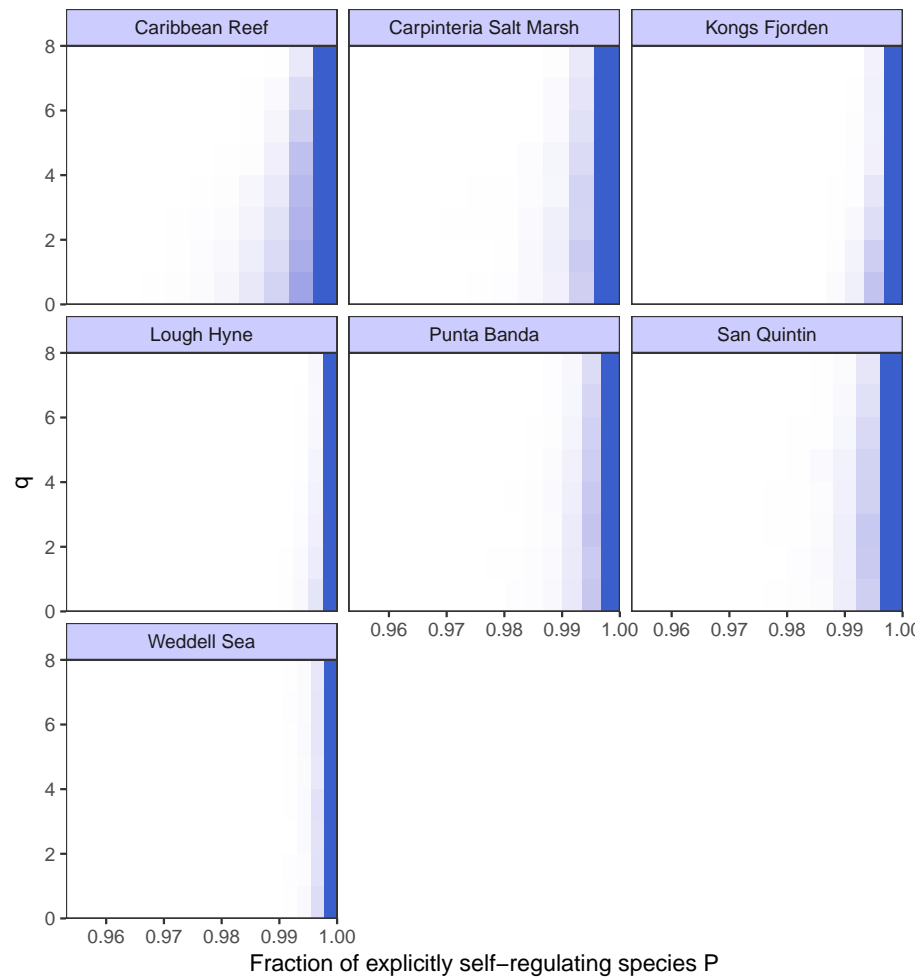
Supplementary Figure 36: As Supplementary Figure 19, except the panels refer to various webs that have been parameterized using Eq. 8.12. All functional responses are type II ($h = 1$). We see that almost all species must *explicitly* self-regulate if the communities are to be stable.
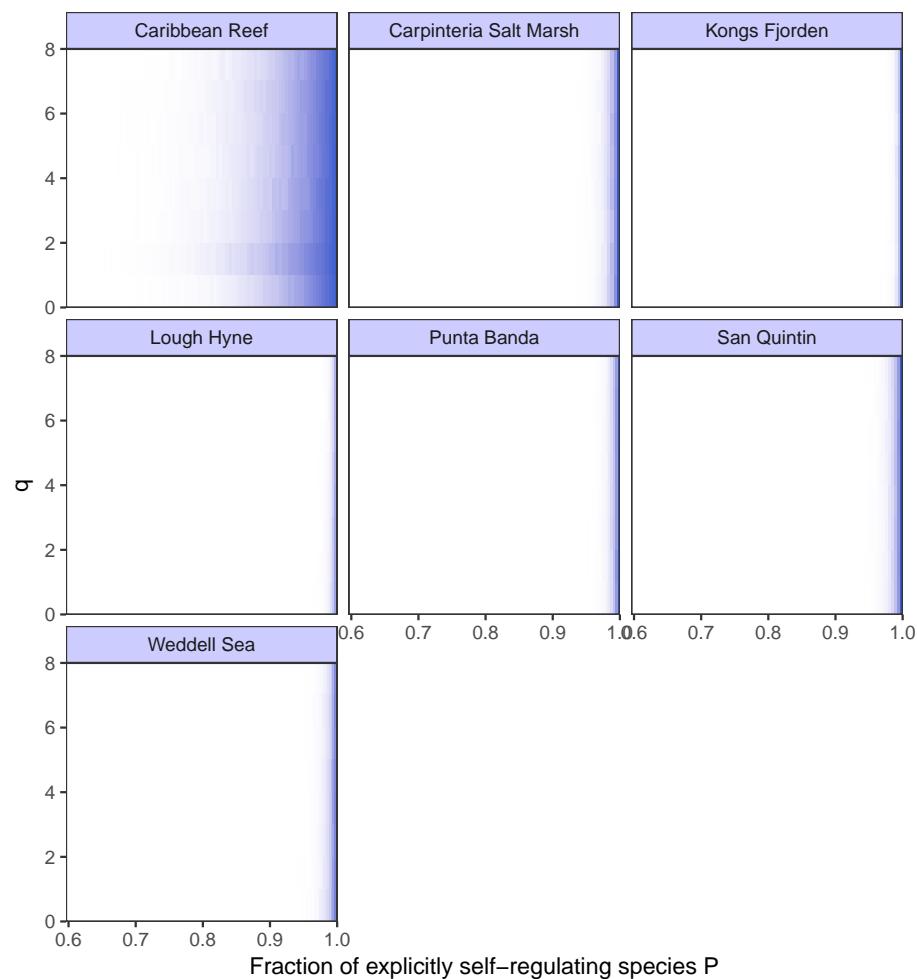
Supplementary Figure 37: As Supplementary Figure 36, except all functional responses are type III ($h = 2$). We see that almost all species must explicitly self-regulate if the communities are to be stable. The Caribbean Reef web is somewhat of an outlier, but even here, more than 80% of species must exhibit direct self-regulation.

## 8.2   The allometric model of Schneider et al. (2016)

Somewhat different conclusions emerge from the allometric food web model of Schneider et al. (2016). In this model, basal species are first generated, which achieve population growth by consuming a number of abiotic nutrients. Their body masses are drawn from either a lognormal or a uniform distribution. Then, a number of consumer species are generated, their body masses determined in the same way. A consumer species eats any other species (basal or itself a consumer) at an efficiency determined by an energetic optimum curve: feeding is maximal on species whose body mass is energetically optimal compared to the consumer's body mass, with the efficiency of consumption declining for both smaller and larger prey. After having determined the link strengths between species this way, population dynamics proceeds via a set of dynamical equations (Eqs. 1-8 in Schneider et al. 2016).

We have followed the model and parameterization of Schneider et al. (2016) exactly, by compiling and running the source code `pdef_dynamics_2.4.c` implementing their model (code found at https://github.com/fdschneider/schneider_et_al_2016_animaldiversity). We have changed only four things. First, we have used ten abiotic nutrients instead of just two—this gives more opportunities to basal species to segregate in resource use and therefore coexist. Second, we have chosen the number of basal and consumer species to conform to the numbers observed in the Weddell Sea food web in Table 3 (149 basal and 209 consumer species). We have attempted to use the actual body mass data for the species in Weddell Sea as well, but this resulted in the code failing (it could not produce an acceptable adjacency matrix). We therefore simply used the same random biomass generation method that was already implemented in the code. Third, we set the Hill exponents in the functional responses either all to 1 (type II response) or 2 (type III response). Fourth, the predator interference parameters were all set to zero at first, since these would introduce direct self-regulation, but we are interested only in the effects of nonlinear functional responses. Later we reintroduced these parameters for comparison, exactly as they were in the original code.

Looking at the fraction of species surviving by the end of the simulation in 100 replicate runs with interference parameters set to zero (Supplementary Figure 38), we see that type II responses are unable to stabilize the communities. However, for type III responses, typically more than half the species are retained, and more importantly, there are some outlying cases where almost all species persist. It would not be appropriate to expect the model to lead to the persistence of all species simultaneously. After all, some of the empirically observed species may not actually be stably persisting in the system either. The fact that the model sometimes leads to the persistence of almost all species already demonstrates that nonlinear functional responses alone are capable of stabilizing large networks—even if such an outcome is not the most typical one.

For comparison, we performed the same simulations but with the predator interference parameters intact (Supplementary Figure 39). Qualitatively, we find the same result as before, but quantitatively a higher fraction of the simulations lead to almost all of the species persisting under type III functional responses. Predator interference may justly be considered a source of direct self-regulation, and this has lead to a higher fraction of species persisting, as expected.

In summary, while the first model in Section 8.1 is one in which the networks can only be stabilized if almost all species exhibit explicit self-regulation, in the second model nonlinear functional responses alone are capable of stabilizing. Such an outcome is not the most typical one, but still is a possibility. This supports the weak assertion that nonlinear responses alone may be insufficient to stabilize large networks (it may be debated just how typical such an outcome is), but disproves the strong assertion that they could never do so.
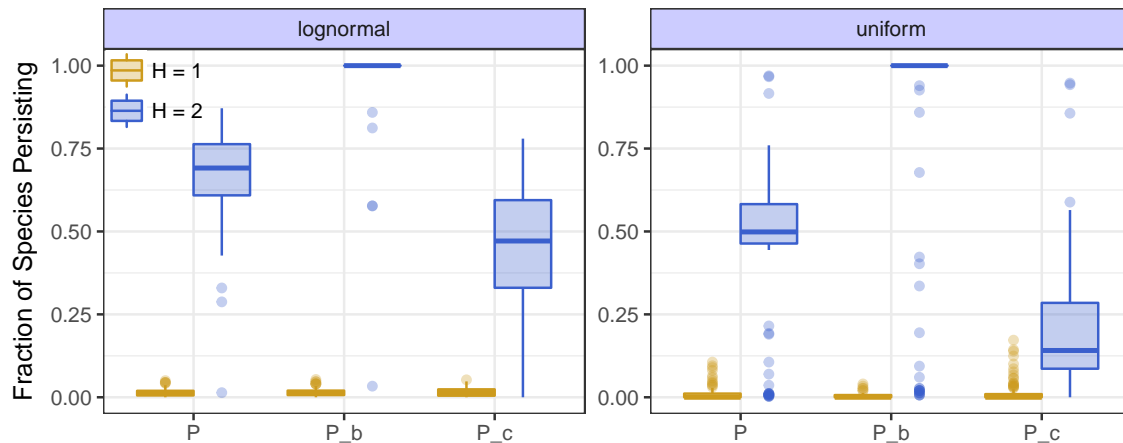
Supplementary Figure 38: Box plots summarizing simulation results for the fraction of species persisting in the model of Schneider et al. (2016). Each box plot summarizes 100 runs. The two panels show results depending on whether species' body masses were drawn from a lognormal (left panel) or a uniform (right panel) distribution. Yellow boxes show results with type II, blue boxes with type III functional responses. In each panel, results are broken down as follows: P refers to the total fraction of surviving species; P_b is the fraction of surviving basal species; and P_c is the fraction of surviving consumers (all species except the basal ones). For type III responses, the mean total fraction of persisting species is either 67% (lognormally distributed body masses) or 46% (uniformly distributed body masses). Box plot guide: median (lines), 25% to 75% quartiles (boxes), ranges (whiskers), outliers (points; defined as falling outside 1.5 times the interquartile range of the box).
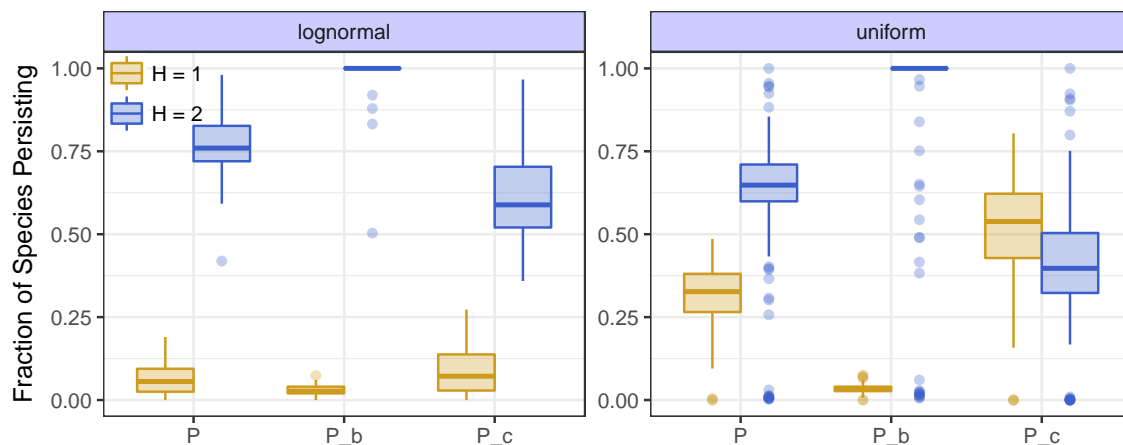
Supplementary Figure 39: As Supplementary Figure 38, but with nonzero interference parameters. The qualitative result is the same as before, but the mean fraction of persisting species with type III functional responses has increased to 77% (lognormally distributed body masses) and 63% (uniform body masses). Also, there is a higher fraction of cases with almost all species persisting than before.

References

Allesina, S., Grilli, J., Barabás, G., Tang, S., Aljadeff, J., Maritan, A., 2015. Predicting the stability of large structured food webs. Nature Communications 6, 7842.

Allesina, S., Tang, S., 2012. Stability criteria for complex ecosystems. Nature 483, 205–208.

Allesina, S., Tang, S., 2015. The stability-complexity relationship at age 40: a random matrix perspective. Population Ecology 57, 63–75.

Arias-Gonzalez, J., Delesalle, B., Salvat, B., Galzin, R., 1997. Trophic functioning of the Tiahura reef sector, Moorea Island, French Polynesia. Coral Reefs 16, 231–246.

Baskerville, E. B., Dobson, A. P., Bedford, T., Allesina, S., Anderson, T. M., Pascual, M., 2011. Spatial guilds in the Serengeti food web revealed by a Bayesian group model. PLoS computational biology 7 (12), e1002321.

Borrelli, J. J., Allesina, S., Amarasekare, P., Arditi, R., Chase, I., Damuth, J., Holt, R. D., Logofet, D. O., Novak, M., Rohr, R. P., Rossberg, A. G., Spencer, M., Tran, K. T., Ginzburg, L. G., 2015. Selection on stability across ecological scales. Trends in Ecology & Evolution 30, 417–425.

Brose, U., Cushing, L., Berlow, E. L., Jonsson, T., Banasek-Richter, C., Bersier, L. F., Blanchard, J. L., et al., 2005. Body sizes of consumers and their resources: Ecological Archives E086-135. Ecology 86 (9), 2545–2545.

Caswell, H., 2001. Matrix population models: Construction, analysis, and interpretation. 2nd edition. Sinauer Associates, Sunderland, Massachusetts, USA.

Christensen, V., Beattie, A., Buchanan, C., Hongguang, M., Martell, S. J. D., Latour, R. J., Preikshot, D., Sigrist M.B., Uphoff, J. H., Walters, C. J., Wood, R. J., Townsend, H., 2009. Fisheries ecosystem model of the Chesapeake Bay: methodology, parameterization, and model exploration. NOAA Technical Memorandum, 1–146.

Cohen, J. E., Briand, F., Newman, C. M., 1990. Community food webs: Data and theory. Springer-Verlag, Berlin, Germany.

Damuth, J., 1981. Population density and body size in mammals. Nature 290, 699–700.

Haerter, J. O., Mitarai, N., Sneppen, K., 2016. Food web assembly rules for generalized Lotka–Volterra equations. PLoS Computational Biology.
URL http://dx.doi.org/10.1371/journal.pcbi.1004727

Hechinger, R. F., Lafferty, K. D., McLaughlin, J. P., et al., 2011. Food webs including parasites, biomass, body sizes, and life stages for three California/Baja California estuaries: Ecological Archives E092-066. Ecology 92, 791–791.

Heymans, J. J., Pitcher, T. J., 2002. In: Pitcher, T. J., Heymans, J. J., Vasconcellos, M. (Eds.), Ecosyst. Model. Newfoundl. time periods 1995, 1985, 1900 1450. Vol. 10. Fisheries Centre Research Reports, pp. 5–71.

Jacob, U., 2005. Trophic dynamics of antarctic shelf ecosystems: food webs and energy flow budgets. Ph.D. thesis, Bremen, Univ., Diss.

Jacob, U., Thierry, A., Brose, U., et al., 2011. The role of body size in complex food webs: A cold case. Advances In Ecological Research 45, 181–223.

Jacquet, C., Moritz, C., Morissette, L., Legagneux, P., Massol, F., Archambault, P., Gravel, D., 2016. No complexity–stability relationship in empirical ecosystems. Nature Communications 7, 12573.

Jorgensen, J., Rossignol, A. M., Puccia, C. J., Levins, R., Rossignol, P. A., 2000. On the variance of eigenvalues of the community matrix: derivation and appraisal. Ecology 81, 2928–2931.

Martinez, N. D., 1991. Artifacts or attributes? Effects of resolution on the Little Rock Lake food web. Ecological Monographs 61, 367–392.

Mouritsen, K. N., Poulin, R., McLaughlin, J. P., Thieltges, D. W., 2011. Food web including metazoan parasites for an intertidal ecosystem in New Zealand: Ecological Archives E092-173. Ecology 92 (10), 2006–2006.

Okey, T., Pugliese, R., 2001. In: Guenette, S., Christensen, V., Pauly, D. (Eds.), Fish. Impacts North Atl. Ecosyst. Model. Anal. Fisheries Centre Research Reports, pp. 167–181.

Opitz, S., 1996. Trophic interactions in Caribbean coral reefs. No. 1085. WorldFish.

O'Rourke, S., Renfrew, D., 2014. Low rank perturbations of large elliptic random matrices. Electronic Journal of Probability 19, 1–65.

Pastur, L. A., 1972. On the spectrum of random matrices. Theoretical and Mathematical Physics 10, 67–74.

Pawar, S., Dell, A. I., Savage, V. M., 2012. Dimensionality of consumer search space drives trophic interaction strengths. Nature 486, 485–489.

Proulx, S. R., Promislow, D. E. L., Phillips, P. C., 2005. Network thinking in ecology and evolution. Trends in Ecology & Evolution 20, 345–353.

Reinschke, K. J., 1988. Multivariable Control — A Graph-theoretic Approach. Lecture Notes in Control and Information Science 108. Springer-Verlag, Berlin, Germany.

Riede, J. O., Brose, U., Ebenman, B., Jacob, U., Thompson, R., Townsend, C. R., Jonsson, T., 2011. Stepping in Elton's footprints: a general scaling model for body masses and trophic levels across ecosystems. Ecology Letters 14, 169–178.

Rogers, T., 2010. Universal sum and product rules for random matrices. Journal of Mathematical Physics 51, 093304.

Schneider, F. D., Brose, U., Rall, B. C., Guill, C., 2016. Animal diversity and ecosystem functioning in dynamic food webs. Nature Communications 7, 12718. URL http://www.nature.com/doifinder/10.1038/ncomms12718

Sommers, H. J., Crisanti, A., Sompolinsky, H., Stein, Y., 1998. Spectrum of large random asymmetric matrices. Physical Review Letters 60, 1895–1898.

Tang, S., Pawar, S., Allesina, S., 2014. Correlation between interaction strengths drives stability in large ecological networks. Ecology Letters 17, 1094–1100.

Thieltges, D. W., Reise, K., Mouritsen, K. N., McLaughlin, J. P., Poulin, R., 2011. Food web including metazoan parasites for a tidal basin in Germany and Denmark: Ecological Archives E092-172. Ecology 92 (10), 2005–2005.

Trites, A. W., Pauly, D., 1998. Estimating mean body masses of marine mammals from maximum body lengths. Canadian Journal of Zoology 76 (5), 886–896.

Walters, C. J., Christensen, V., Martell, S., Kitchell, J. F., 2005. Possible ecosystem impacts of applying MSY policies from single-species assessment. ICES Journal of Marine Science 62, 558–568.

Wigner, E. P., 1958. On the distribution of the roots of certain symmetric matrices. Annals of Mathematics 67, 325–327.

Zander, C. D., Josten, N., Detloff, K. C., Poulin, R., McLaughlin, J. P., Thieltges, D. W., 2011. Food web including metazoan parasites for a brackish shallow water ecosystem in Germany and Denmark: Ecological Archives E092-174. Ecology 92 (10), 2007–2007.